Mon. Not. R. Astron. Soc. **389,** 839–868 (2008) doi:10.1111/j.1365-2966.2008.13594.x

Detecting gravitational wave emission from the known accreting neutron stars

Anna L. Watts,[1,2]★ Badri Krishnan,[3] Lars Bildsten[4] and Bernard F. Schutz[3]

[1]*Max Planck Institut für Astrophysik, Karl-Schwarzschild-Strasse 1, 85741 Garching, Germany*
[2]*Astronomical Institute 'Anton Pannekoek', Kruislaan 403, 1098 SJ Amsterdam, the Netherlands*
[3]*Albert-Einstein-Institut, Max-Planck-Institut für Gravitationsphysik, Am Mühlenberg 1, 14476 Golm, Germany*
[4]*Kavli Institute for Theoretical Physics, Kohn Hall, University of California at Santa Barbara, CA 93106, USA*

Accepted 2008 June 16. Received 2008 June 16; in original form 2008 March 28

ABSTRACT

Detection of gravitational waves from accreting neutron stars (NSs) in our Galaxy, due to ellipticity or internal oscillation, would be a breakthrough in our understanding of compact objects and explain the absence of NSs rotating near the break-up limit. Direct detection, however, poses a formidable challenge. Using the current data available on the properties of the accreting NSs in low-mass X-ray binaries (LMXBs), we quantify the detectability for the known accreting NSs, considering various emission scenarios and taking into account the negative impact of parameter uncertainty on the data analysis process. Only a few of the persistently bright NSs accreting at rates near the Eddington limit are detectable by Advanced LIGO if they are emitting gravitational waves at a rate matching the torque from accretion. A larger fraction of the known population is detectable if the spin and orbital parameters are known in advance, especially with the narrow-band Advanced LIGO. We identify the most promising targets, and list specific actions that would lead to significant improvements in detection probability. These include astronomical observations (especially for unknown orbital periods), improvements in data analysis algorithms and capabilities, and further detector development.

Key words: accretion, accretion discs – gravitational waves – stars: neutron – stars: rotation – X-rays: binaries – X-rays: bursts.

1 INTRODUCTION

A number of interferometric gravitational wave (GW) observatories have been built with the intention of opening a new observational window for studying astrophysical objects. These include the LIGO,[1] GEO,[2] VIRGO[3] and TAMA[4] detectors. The TAMA and LIGO Scientific Collaborations have demonstrated their ability to reach sensitivity goals, take year-long stretches of data with good duty cycles, and analyse the data to set, with confidence, upper limits on the emission from a number of possible sources. At present the large LIGO and VIRGO detectors are performing a significant sensitivity upgrade. This is therefore a good time to carry out a realistic study of the challenges of searching for GWs from one class of sources that future upgrades may render detectable: spinning neutron stars (NSs) in low-mass X-ray binaries (LMXBs).

For the last 10 yr, ever since a paper by one of us (Bildsten 1998) suggested that LMXBs could be steady beacons of GWs, the study of LMXBs (and especially of the source Scorpius X-1) has been one of the scientific goals of the development of detectors with greatly improved sensitivity. Since then, X-ray astronomers have gathered a wealth of new data on these sources, astrophysicists have built better models, and GW scientists have gained considerable experience of their ability to extract weak signals from data streams. It is timely, therefore, to revisit these estimates.

The expectation that LMXBs could be strong steady sources of GWs originates in one of the most important outstanding questions about NSs: why they all spin at frequencies much less than the break-up limit of 1 kHz (Lattimer & Prakash 2007). Simple estimates (Cook, Shapiro & Teukolsky 1994) of the spin-up time-scales for accreting NSs in LMXBs suggest that there should be no difficulty in reaching at least 1 kHz. The fastest rotating accreting pulsar is at 599 Hz (Galloway et al. 2005) and many NSs rotate much more slowly (Chakrabarty et al. 2003). The millisecond radio pulsars, the likely offspring of LMXBs, also spin at slower rates than expected.

★E-mail: a.l.watts@uva.nl
[1] http://www.ligo.caltech.edu.
[2] http://geo600.aei.mpg.de/.
[3] http://wwwcascina.virgo.infn.it.
[4] http://tamago.mtk.nao.ac.jp.

The current record stands at 716 Hz (Hessels et al. 2006) and surveys in nearby globular clusters continue to reveal a paucity of rapid rotators (Ransom et al. 2005; Freire et al. 2008; Hessels et al. 2007). Whether the apparent spin limit is genuine remains to be resolved. Nevertheless, given the current sample, it certainly appears that there is some brake that prevents accreting NSs from reaching the break-up limit.

The candidate mechanisms fall into two main camps. In the first, accretion torques are reduced and eventually balanced by the interaction between the accretion disc and the NS's magnetic field (Ghosh & Lamb 1978; White & Zhang 1997; Andersson et al. 2005). The second possibility, and our focus here, is the loss of angular momentum via the emission of gravitational radiation (Papaloizou & Pringle 1978; Wagoner 1984; Bildsten 1998). There are many conceivable ways for an accreting NS to develop a quadrupolar asymmetry that leads to GW emission: crustal mountains (Bildsten 1998; Ushomirsky, Cutler & Bildsten 2000; Melatos & Payne 2005; Haskell, Jones & Andersson 2006; Payne & Melatos 2006), magnetic deformation (Cutler 2002; Haskell et al. 2008) or internal r-mode oscillations (Bildsten 1998; Andersson, Kokkotas & Stergioulas 1999; Levin 1999; Andersson et al. 2000; Andersson, Jones & Kokkotas 2002; Heyl 2002; Wagoner 2002; Nayyar & Owen 2006; Bondarescu, Teukolsky & Wasserman 2007). The exciting prediction from all GW emission scenarios is the possible direct detection of an accreting NS by a ground-based interferometric GW detector.

Searches for periodic GWs from NSs have already been performed with the LIGO and GEO detectors. These include searches of known radio pulsars (Abbott et al. 2004, 2005b,2007b), assuming the phase of the GW signal to be locked to the known NS rotation and wide parameter surveys for hitherto unknown NSs (Abbott et al. 2005a,2007a, 2008). There have also been searches for GWs from the accreting NS Scorpius X-1. The first (Abbott et al. 2007a) used a coherent statistic on a template grid utilizing 6 h of data (limited by computational requirements) from the second science run of the two LIGO 4-km interferometers, followed by a coincidence analysis between candidates from the two detectors. The second search (Abbott et al. 2007c) used a method of cross-correlating the outputs of the two LIGO 4-km detectors using about 20 d of coincident data taken during the fourth science run. Data from resonant bar detectors have also been used in these searches; see e.g. Astone et al. (2002, 2005) for a blind all-sky search in a narrow frequency band using data from the EXPLORER detector.

These early searches, while so far yielding only upper limits, have served to develop and prove data analysis methods that will be used on data from future, more sensitive searches. The VIRGO detector is approaching its design sensitivity and the LIGO detectors have just completed a full run at their first-stage design sensitivity. An initial upgrade of LIGO is about to commence, followed by a full upgrade to Advanced LIGO[5] in the next decade. VIRGO expects to parallel these developments. These impending improvements in GW sensitivity, coupled with the experience of performing realistic data analysis, make the time right to assess what the relevant accreting NS properties tell us about the ultimate detectability of NS sources.

This paper explains the prospects for detecting GWs from accreting NSs, and identifies the most promising targets. We start in Section 2 with the best case scenario, highlighting the data analysis challenges and the need for detailed information on the accreting NS properties, which are presented in Section 3. Section 4 explains fully the GW search data analysis challenges and the direct consequences of parameter uncertainty on integration times and detection statistics, allowing us to assess future detectability in Section 5. We close in Section 6 by highlighting where progress can be made in the short term on NS source properties, and the implications for current and future GW searches.

2 OVERVIEW AND BEST CASE ESTIMATES

The potential strength of a periodic GW signal at frequency ν from specific LMXBs with accretion rates $\dot{M}$ was estimated by Bildsten (1998) (hereafter B98) in the mountain scenario. In this model a quadrupole moment Q, which is stationary in the rotating frame of the star (a 'mountain'), leads to the emission of GWs with a predominant frequency $\nu = 2\nu_{\rm s}$, $\nu_{\rm s}$ being the spin frequency of the NS. The assumption is that the accretion torque on an NS of mass M and radius R,

$$N_{\rm a} = \dot{M}\,(GMR)^{1/2}\,, \tag{1}$$

is balanced by the GW torque

$$N_{\rm gw} = -\frac{32GQ^2\Omega_{\rm s}^5}{5c^5}, \tag{2}$$

where $\Omega_{\rm s} = 2\pi\nu_{\rm s}$ is the angular frequency of the star. The accretion rate is estimated from the bolometric X-ray flux F by assuming that the luminosity is $L \approx GM\dot{M}/R$, yielding

$$\dot{M} = \frac{4\pi Rd^2F}{GM}, \tag{3}$$

where d is the distance to the source. The predicted GW amplitude h_0 (as defined in Jaranowski, Królak & Schutz (1998))[6] can be written in terms of the GW luminosity, $\dot{E}_{\rm gw} = N_{\rm gw}\Omega_{\rm s}$, as

$$h_0^2 = \frac{5G}{2\pi^2c^3d^2\nu^2}\dot{E}_{\rm gw}. \tag{4}$$

Under the condition of torque balance,

$$h_0 = 3\times10^{-27}F_{-8}^{1/2}\left(\frac{R}{10{\rm km}}\right)^{3/4}\left(\frac{1.4\,{\rm M}_\odot}{M}\right)^{1/4}\left(\frac{1\,{\rm kHz}}{\nu_{\rm s}}\right)^{1/2}, \tag{5}$$

where $F_{-8} = F/10^{-8}\,{\rm erg\,cm^{-2}\,s^{-1}}$. Equation (5) makes it clear that the GW signal strength depends on two observables, the flux on the sky from the LMXB and the NS spin rate (Wagoner 1984; B98). This amplitude is then compared directly to the best case detectable amplitude in a long search, $h_0^{\rm sens}$, which we will derive shortly.

These amplitudes are sufficiently weak that long stretches of data must be folded, using predicted signal templates. This is called matched filtering, and its sensitivity improves with the square root of the observation time, provided that the template manages to keep phase with the real signal to within about one radian over the entire duration. Where spin and orbital parameters are poorly constrained, many templates must therefore be searched. Analysis can become statistically and computationally untenable, and computational loads may limit integration times and thereby detectability. Contrast for example the most recent searches for radio pulsars, where a precise timing ephemeris is available (Abbott et al. 2007b), with searches for the closest accreting NS Scorpius X-1 (Abbott

[5] http://www.ligo.caltech.edu/advLIGO.

[6] Note that flux formulae are often given in terms of an angular and time-averaged amplitude h rather than in terms of h_0. In Owen et al. (1998) and Andersson et al. (1999), for example, the quoted amplitude $h^2 = 2h_0^2/5$.

et al. 2007c). Poor constraints on the spin and orbital parameters for Sco X-1 necessitate multiple templates. This reduces the feasible integration time substantially, resulting in upper limits that are approximately two orders of magnitude larger than those obtained for the best radio pulsar. We begin our discussion there.

2.1 Spin frequencies of accreting neutron stars

The discoveries and studies with the *Rossi X-ray Timing Explorer* (*RXTE*) over the last 10 yr have dramatically improved our understanding of stellar spin rate, ν_s (Strohmayer & Bildsten 2006; van der Klis 2006). Having some constraint on the spin is, as will become clear in later sections, the most important factor determining the feasibility of GW searches. For this reason we concentrate only on sources for which there is some measurement or estimate of ν_s. We now summarize the three relevant categories of accreting NSs: accreting millisecond pulsars, burst oscillation sources, and kilohertz quasi-periodic oscillation (kHz QPO) sources.

The spin is measured directly in the accreting millisecond pulsars, where fixed hotspots, presumably at the magnetic footpoints, are a permanent asymmetry. In 1998 only one such object was known; there are now 10 members of this class, three of which show only intermittent pulsations. The other measures of spin are indirect. Probably the most reliable are burst oscillations, seen during Type I X-ray bursts (when accreted material burns in an unstable thermonuclear flash). In 1998 there were six burst oscillation sources: there are now 12 stars with burst oscillations seen in multiple bursts (including three pulsars), and seven stars with tentative detections.

For the three accreting millisecond pulsars that also show burst oscillations, the burst oscillation frequency is at or very close to the known spin frequency (Chakrabarty et al. 2003; Strohmayer et al. 2003; Altamirano et al. 2008). It would therefore seem reasonable to equate the burst oscillation frequency with the spin frequency for the non-pulsing sources (as was done in B98). The frequency for a given source is highly consistent from burst to burst, implying that there is at least a strong dependence on stellar spin (Strohmayer et al. 1998a; Muno, Özel & Chakrabarty 2002a). The detection of highly coherent oscillations lasting several hundred seconds during a superburst adds further support to this hypothesis (Strohmayer & Markwardt 2002). There are, however, some complicating factors. First, burst oscillations can exhibit frequency drifts of up to a few Hz. Secondly, there are some differences in the properties of the burst oscillations of the non-pulsing LMXBs as compared to the pulsars (see e.g. Watts & Strohmayer 2006), suggesting that the mechanism may differ. In models that involve global modes of the surface layers, for example, the observed frequency would be offset from spin frequency by several Hz (Heyl 2004; Piro & Bildsten 2005).

The third class of sources to be considered are those which exhibit twin kHz QPOs. Early observations suggested that although the frequencies could shift, their separation remained relatively constant, implying a link to stellar spin. We now know that separation varies (often quite substantially) as accretion rate changes, and the cause of the kHz QPOs is still not understood. However, most models still depend in some way on the stellar spin, either directly or via the influence on the space–time in the inner regions of the accretion disc [see van der Klis (2006) for a recent and comprehensive review]. Observations of twin kHz QPOs in two of the accreting millisecond pulsars have done little to resolve the situation: in one case separation is rather close to the spin frequency; in the other it is slightly less than half the spin (Wijnands et al. 2003; Linares et al. 2005). Whether there is any link between kHz QPO separation and stellar spin will doubtless emerge in due course. However, given that most models still predict some relation, we follow B98 and include these stars in our analysis.

2.2 Optimal gravitational wave detection

Before being scaled down for their current sensitivity upgrades, the first generation LIGO interferometers operated for nearly two years at or better than their design sensitivity, by the end of which the first generation Virgo detector was not far behind. The 'Enhanced' LIGO and VIRGO interferometers should begin operation in 2009, and the Advanced LIGO interferometers are now funded and should be operational by 2014. Advanced VIRGO is expected on the same schedule. Beyond this, there are ambitious plans for a third generation Einstein Telescope (ET) in Europe.

The sensitivity of a GW detector is determined by the power spectral density of its instrumental strain noise, normalized to an equivalent GW amplitude $h(t)$. This is just the Fourier power spectrum of $h(t)$ and is called $S_h(\nu)$: the noise power per unit frequency. It is conventional to plot $h(\nu) = [S_h(\nu)]^{1/2}$, which allows comparison of the noise to the signal's amplitude if one knows the signal's bandwidth. The sensitivity curves of current and future detectors are shown in Fig. 1. The design noise curves for initial LIGO, Virgo and ET are taken from analytic models available, for example, in the LIGO software repository.[7] The most recent science runs of the LIGO detectors have in fact reached their design goals over a broad frequency range of interest, above ∼40 Hz. The Enhanced LIGO noise curve in Fig. 1 is a realistic estimate of what can be achieved; thus at low frequencies (below ∼40 Hz), the Enhanced LIGO noise curve lies above the initial LIGO design curve.

The Advanced LIGO detector configurations have not yet been finalized, and we therefore need to consider different possibilities. Advanced LIGO can potentially be operated in a narrow-band mode where sensitivity is gained in a relatively narrow frequency range at the expense of broad-band sensitivity (see e.g. Meers 1988; Buonanno & Chen 2002). This could be particularly relevant for periodic signals where the frequency is well known. The first panel of Fig. 1 shows an example of such a narrow-band noise curve.[8] The noise curve can be tuned to target a broad range of frequencies by changing a number of interferometer parameters, and for our purposes, the value of the noise at the minimum is especially important. Thus, the lower panel of Fig. 1 shows the lower envelope of the narrow-band noise curves above 100 Hz. Between 100 and about 400 Hz, the narrow-band curves are limited by thermal noise, and by quantum noise at higher frequencies.[9] See Section 6.4 for additional discussion. It is important to keep in mind that the narrow-band 'envelope'

[7] http://www.lsc-group.phys.uwm.edu/daswg/projects/lal.html.

[8] The various Advanced LIGO noise curves shown here have been obtained using version 6.2 of the MATLAB script 'Bench'. It is worth mentioning that a newer version of Bench, v7.0, is currently under development which includes an improvement in coating thermal noise; it is probably worth recalculating the Advanced LIGO noise curves once this and later versions become available.

[9] To generate the lower envelope of the narrow-band noise curves, we have used Bench to calculate the narrow-band noise curves for a range of choices for a few interferometer parameters. These parameters are the phase and transmittance of the signal recycling cavity, and the transmittance of the input test mirror and the power recycling mirror. The envelope is then obtained by calculating the convex hull of the minima of the various noise curves.

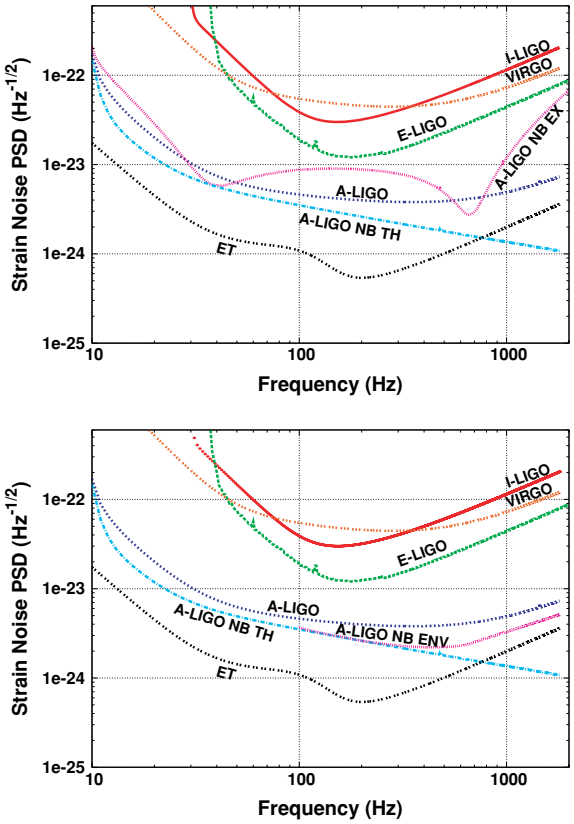

Figure 1. The noise curves for initial LIGO, Virgo, Advanced LIGO and the third generation ET interferometers. The initial, Enhanced and Advanced LIGO curves are labelled 'I-LIGO', 'E-LIGO' and 'A-LIGO', respectively; 'ET' is Einstein Telescope. There are three curves for Advanced LIGO in each panel. The top panel shows a nominal broad-band configuration (the so-called 'zero-detuned' configuration), an example of a narrow-band curve ('A-LIGO NB EX'), and the total thermal noise ('A-LIGO TH'), i.e. the sum of the suspension and mirror thermal noise curves. The lower panel shows the lower envelope of the narrow-band curves ('A-LIGO NB ENV') instead of the narrow-band example. The thermal noise is shown because it is sometimes taken as a theoretical lower bound on the narrow banding for frequencies above, say, 100 Hz; as seen from the lower panel, this is not a good approximation at higher frequencies.

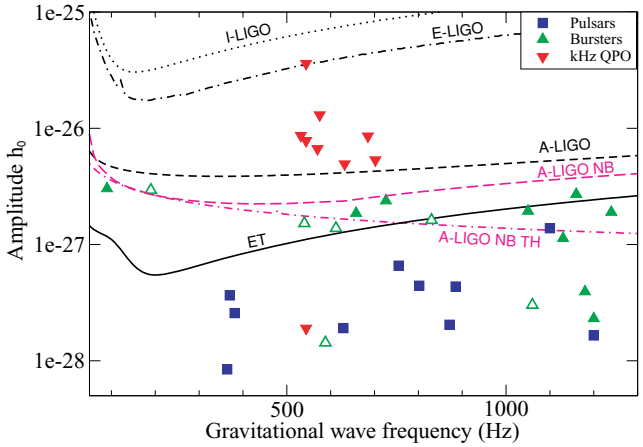

Figure 2. Best case detectability for the mountain scenario for $T_{\rm obs} = 2$ yr, balancing the long-term average flux, and assuming that all parameters are known (single template search). The bursters are divided into two groups: those for which the frequency is confirmed (filled) and those for which the frequency requires confirmation (open), see Section 3. The frequency at which the kHz QPO symbols appear is derived from the centre of the measured range of separations: the predicted amplitude would be higher if the frequency were lower, and vice versa. We show detectability thresholds for initial LIGO (I-LIGO), Enhanced LIGO (E-LIGO), Advanced LIGO (A-LIGO) and the ET. We also show two detectability curves for Advanced LIGO narrow band: the expected envelope for the narrow-band detector that includes all sources of noise (A-LIGO NB), and a curve showing only the thermal noise floor (A-LIGO NB TH).

does not represent any particular interferometer configuration but is rather a superposition of many configurations. It is only useful for targeting narrow-band signals with frequency uncertainties of, say, $\mathcal{O}(10)$ Hz in which case we can choose the appropriate element from the set of configurations used to produce the envelope. Finally, note that possible designs for the third generation detectors are still being explored, and thus the noise curve for the ET is much more preliminary.

To start addressing the question of detecting GWs from LMXBs, we start by asking how strong the signal would need to be for detection if we knew all source parameters to sufficient accuracy that only one template was needed (a coherent fold). Computational cost is no issue, and we can easily integrate for long periods $T_{\rm obs}$. Such a fully coherent search with D detectors of comparable sensitivity is a best case and defines a signal-to-noise ratio (S/N) as $\mathrm{S/N}^2 = h_0^2 T_{\rm obs}\, D/S_{\rm n}$; thus, the S/N squared builds up linearly with the observation time [here $S_{\rm n}(\nu)$ is the power spectral density of the detector noise]. Conversely, for a given choice of S/N threshold for detectability, this leads to a minimum detectable signal amplitude h_0 (following the notation of Jaranowski et al. (1998)):

$$h_0 \approx 11.4\sqrt{\frac{S_{\rm n}}{DT_{\rm obs}}}, \tag{6}$$

which is a useful indicator of the sensitivity of such a search. The factor of 11.4 corresponds to an S/N threshold which would lead to a single trial false alarm rate of 1 per cent and a false dismissal rate of 10 per cent (Abbott et al. 2007a) and a uniform averaging over all possible source orientations and sky positions (Jaranowski et al. 1998).

Fig. 2 compares the predicted and detectable amplitudes for this best case scenario using the long-term flux average derived in Section 3 and summarized in Table 1, and assuming that each NS is in perfect spin balance (so that we can neglect spin derivatives), with GW torque balancing that of accretion. We assume that the spin frequency for the kHz QPO sources lies in the middle of the known range of separations, and take $T_{\rm obs} = 2$ yr as a reference value.

Fig. 2 naively implies that the kHz sources are the most easily detected sources. However, they offer a specific challenge, as we do not know many of their spins or orbital parameters. Detecting the GW signal requires a knowledge of the GW phase evolution which depends crucially on the orbital parameters. Ignorance or inaccurate knowledge of the orbit could then require a search over a significant number of parameters and as we shall see, this can have a dramatic impact on the sensitivity of the GW search. Hence assessing the detectability of GWs requires a more careful description of the mechanics of the GW data analysis process. Most of this paper is therefore focused on clearly assessing the data analysis challenges for present and future generations of GW detectors that takes into account the limitations imposed by incomplete astrophysical knowledge and finite computational resources.

Table 1. Fluxes, distances and outburst properties for transients.

Source	ν_s (Hz)	Distance (kpc)	Long-term flux F_{av} ($\times 10^{-8}$ erg cm^{-2} s^{-1})	Outburst duration (d)	Outburst flux F_{ob} ($\times 10^{-8}$ erg cm^{-2} s^{-1})
Accreting millisecond pulsars					
IGR J00291+5934	598.892 ± 2e−08	5 ± 1	1.8e−03	13	1.6e−01
Aql X-1	550.274 ± 9e−04	4.55 ± 1.35	1.2e−01	45	1.3
SAX J1748.9−2021	442.361 ± 5e−08	8.1 ± 1.3	9.2e−03	61	4.0e−01
XTE J1751−305	435.318 ± 4e−08	9 ± 3[a]	2.0e−03	10	2.9e−01
SAX J1808.4−3658	400.975 ± 6e−09	3.5 ± 0.1	8.6e−03	20	3.5e−01
HETE J1900.1−2455	377.296 ± 5e−09	4.7 ± 0.6	1.8e−02	730	9.0e−02
XTE J1814−338	314.357 ± 1e−09	6.7 ± 2.9	1.3e−03	50	6.9e−02
XTE J1807−294	190.624 ± 8e−08	8.35 ± 3.65[a]	1.4e−03	50	7.2e−02
XTE J0929−314	185.105 ± 9e−09	7.8 ± 4.2[a]	2.7e−03	60	1.0e−01
SWIFT J1756.9−2508	182.066 ± 7e−08	8 ± 4[a]	1.4e−04	13	4.0e−02
Burst oscillation sources					
XTE J1739−285	1122[b]	7.3 ± 3.3[a]	5.9e−03	196	8.2e−02
4U 1608−522	620	4.1 ± 0.4	2.5e−01	100	2.0
SAX J1750.8−2900	601	6.79 ± 0.14	3.5e−03	108	0.12
GRS 1741.9−2853	589	7.2 ± 2.8	1e−02[c]	30[c]	1e−01[c]
4U 1636−536	581	6 ± 0.5	0.47	–	–
X 1658−298	567	12 ± 3	8.0e−02	872	0.77
A 1744−361	530[b]	6 ± 3[a]	5.3e−03	97	0.2
KS 1731−260	524	7.2 ± 1.0	2.2e−01	1886	0.49
4U 0614+09	415[b]	2.5 ± 0.5[a]	1.2e−01	–	–
4U 1728−34	363	5.2 ± 0.5	0.23	–	–
4U 1702−429	329	5.5 ± 0.2	0.13	–	–
MXB 1730−335	306[b]	9.25 ± 2.85	6.4e−02	24	0.59
IGR J17191−2821	294[b]	7.5 ± 3.5[a]	6.6e−04	11	0.26
4U 1916−053	270[b]	8.0 ± 2.2	6.9e−02	–	–
XB 1254−690	95[b]	13 ± 3	9.0e−02	–	–
EXO 0748−676	45	7.4 ± 0.9	4.6e−02	–	–
kHz QPO sources					
Cyg X-2	351 ± 34	10.55 ± 4.45	1.1	–	–
GX 340+0	343 ± 92	9.15 ± 5.15[a]	2.8	–	–
4U 1735−44	316 ± 32	8.5 ± 1.3	8.4e−01	–	–
GX 5−1	288 ± 69	7.85 ± 3.85[a]	5.3	–	–
4U 1820−30	285 ± 65	7.4 ± 0.6	1.4	–	–
Sco X-1	272 ± 40	2.8 ± 0.3	39	–	–
GX 17+2	272 ± 50	11.4 ± 2	1.8	–	–
XTE J2123−058	272 ± 50	9.6 ± 1.3	1.1e−03	53	8.7e−02
GX 349+2	266 ± 13	4 ± 0.4	2.2	–	–

[a]Distance poorly constrained: upper and/or lower limit set arbitrarily. [b]Burst oscillation frequency requires confirmation: tentative detection, or only seen in one burst from this source. [c]No reliable measurement of flux possible for this Galactic Centre source due to field crowding. The values given here are indicative estimates only.

3 ACCRETING NEUTRON STAR PROPERTIES

In this section we summarize our knowledge of the relevant search parameters for all accreting NSs in LMXBs where there is some estimate of the spin: the accreting millisecond pulsars, the burst oscillation sources, and the kHz QPO sources. This sample contains both atoll and Z sources, a classification determined by the spectral and timing properties (Hasinger & van der Klis 1989; Gierliński & Done 2002; Muno, Remillard & Chakrabarty 2002b; van der Klis 2006). As explained in Section 2 we require flux histories, spin frequencies and orbital parameters, some of which are measured, whilst others can only be estimated. We also need to gauge the uncertainty on each quantity. This sets the required search parameter space, and in Section 5 we use this information to compute the number of signal templates required for each source.

This section is rather lengthy, as we give full details of the provenance of all of the values used in our study. There are two main reasons for this: first, to make clear the link between the astronomical observations and the consequences for GW searches. Secondly, many of the values that we derive involve assumptions, or draw on old or uncertain measurements: where this is the case we wanted to make it explicit, in order to drive future astrophysical modelling and observations. The information in this section should also be a useful resource for anyone intending to carry out a search for GWs from these objects, or for future detectability studies. Readers who are not concerned with the details of the source properties and uncertainties can however skip this section, and will find the key results summarized in Tables 1–4.

3.1 Constraining fluxes and accretion rates

The observed flux, F, sets the expected GW signal strength (equation 5). For persistent sources we record only the long-term average flux, F_{av}, whereas for transient sources we also record the outburst

Table 2. Parameter space and template requirements for the accreting millisecond pulsars.

Source	$\nu_s \pm \Delta\nu_s$ (Hz)	N_ν	$P_{orb} \pm \Delta P_{orb}$ (h)	$N_{P_{orb}}$	$a_x \sin i \pm \Delta a_x \sin i$ (light-second)	N_{a_p}	ΔT_{asc} (d)	$N_{T_{asc}}$	$\log_{10}(N_{temp})$	F_{stat}
IGR J00291+5934	598.892 130 53	18	2.456 6922	23	6.4993e−02	1	4e−07	1	2.6	15.9
	± 2e−08	(12)	± 1.7e−06	(15)	± 2e−06	(1)		(1)	(2.2)	(14.7)
Aql X-1	550.2745	7.6e+05	18.9479	1557	2.5	9692	3e−03	1049	15.6	26.6
	± 9e−04	(5.1e+05)	± 2.0e−04	(1038)	± 0.5	(6462)		(700)	(14.9)	(26.0)
SAX J1748.9−2021	442.361 081 18	43	8.765 25	139	0.387 60	1	4e−06	1	3.8	17.1
	± 5e−08	(29)	± 3e−05	(93)	± 4e−05	(1)		(1)	(3.4)	(15.9)
XTE J1751−305	435.317 993 57	34	0.707 0394	11	1.0125e−02	1	4e−7	1	2.5	15.9
	± 4e−08	(23)	± 6e−07	(7)	± 5e−06	(1)		(1)	(2.2)	(14.7)
SAX J1808.4−3658	400.975 210 221	6	2.013 654 711	1	6.028 132e−02	1	1.0e−06	1	0.8	13.2
	± 6e−09	(4)	± 4e−09	(1)	± 2.4e−07	(1)		(1)	(0.6)	(13.2)
HETE J1900.1−2455	377.296 171 971	5	1.387 5717	11	1.841e−02	1	7e−06	1	1.7	14.7
	± 5e−09	(4)	± 1.4e−06	(7)	± 1e−05	(1)		(1)	(1.4)	(13.2)
XTE J1814−338	314.356 108 79	9	4.274 645 250	1	0.390 633	1	9e−07	1	1.0	13.2
	± 1e−08	(7)	± 5.6e−08	(1)	± 9e−06	(1)		(1)	(0.8)	(13.2)
XTE J1807−294	190.623 506 94	68	0.667 8935	1	4.819e−03	1	6e−06	1	1.8	14.7
	± 8e−08	(46)	± 1e−07	(1)	± 4e−06	(1)		(1)	(1.7)	(14.7)
XTE J0929−314	185.105 254 297	9	0.726 3183	4	6.290e−03	1	1e−05	1	1.5	14.7
	± 9e−09	(6)	± 8e−07	(3)	± 9e−06	(1)		(1)	(1.2)	(13.2)
SWIFT J1756.9−2508	182.065 804 253	61	0.911 696	62	5.942e−03	1	6e−05	1	3.6	17.1
	± 7.2e−08	(41)	± 2.3e−05	(42)	± 2.7e−05	(1)		(1)	(3.2)	(15.9)

Note: parameter ranges searched for the pulsars and number of templates resulting for the mountain (r-mode) scenario assuming a coherent fold with $T_{obs} = 2$ yr. For all parameters apart from T_{asc} we give the absolute value as well as the range searched since both quantities affect the number of templates. Note that ΔT_{asc} is the uncertainty on the measurement, so the searched range is twice this value.

flux, F_{ob}. Bolometric outburst fluences have been computed for the accreting millisecond pulsars, but for the majority of sources this is not the case. For the remaining sources we determine F using data from the *RXTE* All Sky Monitor (ASM), which provides a near-continuous history of source activity from 1996 to the present in the 2–10 keV band (Levine et al. 1996). Converting the 2–10 keV flux to a bolometric flux requires detailed spectral modelling. For most burst oscillation sources we use the results of Galloway et al. (2008a): these authors carry out spectral modelling using the pointed *RXTE* PCA data (2.5–25 keV) to estimate bolometric flux. We compare the calculated fluxes to the ASM count rate at the time of the observation to establish this relationship. For the transient sources we only include in our integrated ASM histories the times when the source is in outburst and detectable above a 3σ level. This avoids contamination from other sources in the field which would overestimate the long-term flux. This method of estimating flux history introduces some errors, since spectral shapes (and the correction from 2–10 keV flux to bolometric flux) will change: but it gives a reasonable estimate. This uncertainty should however be borne in mind in Section 6 for those sources that are on the margins of detectability.

We also record position and distance. Source position must be known to a certain degree of precision for the long folds that this type of analysis necessitates (Section 4.1). We have listed the most accurate and up to date position known for the X-ray source or its optical, infrared or radio counterpart. Source distance, which is relevant for the emission modelling in Section 5, can be estimated in several different ways. Only for the closest source in our sample, Sco X-1, can the distance be measured via parallax. For the other sources different methods are used: location of the source in a globular cluster; the presence of radius expansion X-ray bursts (where luminosity reaches the Eddington limit[10]); inferences about mass transfer from the long-term X-ray flux, assuming that the binary orbit evolves due to GW emission; absorption and spectral modelling.

We give details of pulsar frequency, burst oscillation frequency and twin kHz QPO separation, as measured with *RXTE*'s proportional counter array (PCA). For sources with only a burst oscillation frequency, we assume that ν_s lies within ±5 Hz of the burst oscillation frequency ν_b. For the kHz QPO sources we assume that the spin lies within the reported range of kHz QPO separations. We review both of these assumptions in more detail in later sections.

3.2 Orbital uncertainties

We must know (or presume) the orbital parameters in order to fold long stretches of GW data, most importantly, the orbital period P_{orb} and eccentricity, e. We also need a reference time within the orbit. Depending on the original reference we quote either T_{90}, the time of inferior conjunction of the companion star, or T_{asc}, the time of ascending node, when the Doppler-shifted frequency of the NS is at its lowest. Note that $T_{90} = T_{asc} + P_{orb}/4$. The third parameter is the projected semimajor axis of the NS, $a_x \sin i$, which

[10] The Eddington limit depends on the composition. Sometimes composition can be inferred from burst properties, but this is not always the case, leading to additional uncertainty. See also Galloway, Özel & Psaltis (2008b).

Table 3. Parameter space and template requirements for the burst oscillation sources (details as for Table 2).

Source	$\nu_s \pm \Delta\nu_s$ (Hz)	N_ν	$P_{orb} \pm \Delta P_{orb}$ (h)	$N_{P_{orb}}$	$a_x \sin i \pm \Delta a_x \sin i$ (light-second)	N_{a_p}	ΔT_{asc} (d)	$N_{T_{asc}}$	$\log_{10}(N_{temp})$	F_{stat}
XTE J1739−285	1122	4.2e+09	120.1	2.2e+08	11.3	4.1e+05	2.5	1.3e+06	34.4	36.0
	± 5	(2.8e+09)	± 119.9	(1.5e+08)	± 11.3	(2.8e+05)		(8.7e+05)	(33.7)	(36.0)
4U 1608−522	620	4.2e+09	67.5	1.0e+08	6.17	1.3e+05	1.4	3.9e+05	29.1	33.7
	± 5	(2.8e+09)	± 57.5	(6.7e+07)	± 6.17	(8.3e+04)		(2.6+05)	(28.4)	(33.2)
SAX J1750.8−2900	601	4.2e+09	120.1	1.2e+08	11.3	2.2e+05	2.5	7.0e+05	33.6	36.0
	± 5	(2.8e+09)	± 119.9	(7.8e+07)	± 11.3	(1.5e+05)		(4.7e+05)	(32.9)	(35.5)
GRS 1741.9−2853	589	4.2e+09	120.1	1.2e+08	11.3	2.2e+05	2.5	6.8e+05	33.6	36.0
	± 5	(2.8e+09)	± 119.9	(7.7e+07)	± 11.3	(1.5e+05)		(4.6e+05)	(32.9)	(35.5)
4U 1636−536	581	4.2e+09	3.793 1263	238	0.735	1585	2e−3	1112	17.8	27.9
	± 5	(2.8e+09)	± 3.8e−06	(159)	± 8.3e−02	(1057)		(742)	(17.1)	(27.3)
X 1658−298	567	4.2e+09	7.116 109 79	3	1.1	1.7e+04	9.3e−05	41	15.4	26.0
	± 5	(2.8e+09)	± 8e−08	(2)	± 0.9	(1.1e+04)		(27)	(14.7)	(26.0)
A 1744−361	530	4.2e+09	1.62	1.9e+07	0.125	1302	3.4e−02	6817	23.5	30.7
	± 5	(2.8e+09)	± 0.37	(1.3e+07)	± 0.075	(868)		(4545)	(22.8)	(30.7)
KS 1731−260	524	4.2e+09	121	1.0e+08	11.3	1.9e+05	2.5	6.1e+05	31.3	34.6
	± 5	(2.8e+09)	± 119	(6.7e+07)	± 11.3	(1.3e+05)		(4.1e+05)	(30.6)	(34.6)
4U 0614+09	415	4.2e+09	0.29	3.0e+06	7e−03	96	6.1e−03	300	20.2	29.0
	± 5	(2.8e+09)	± 0.04	(2.0e+06)	± 7e−03	(64)		(200)	(19.5)	(28.4)
4U 1728−34	363	4.2e+09	5.1	1.5e+07	0.1	1200	0.1	3770	25.5	31.7
	± 5	(2.8e+09)	± 4.9	(9.7e+06)	± 0.1	(800)		(2513)	(24.8)	(31.7)
4U 1702−429	329	4.2e+09	120.1	6.5e+07	11.3	1.2e+05	2.5	3.8e+05	32.9	35.5
	± 5	(2.8e+09)	± 119.9	(4.3e+07)	± 11.3	(8.2e+04)		(2.6e+05)	(32.2)	(35.1)
MXB 1730−335	306	4.2e+09	120.1	6.0e+07	11.3	1.1e+05	2.5	3.6e+05	32.8	35.5
	± 5	(2.8e+09)	± 119.9	(4.0e+07)	± 11.3	(7.6e+04)		(2.4e+05)	(32.1)	(35.1)
IGR J17191−2821	294	4.2e+09	120.1	5.8e+07	11.3	1.1e+05	2.5	3.4e+05	32.7	35.5
	± 5	(2.8e+09)	± 119.9	(3.9e+07)	± 11.3	(7.3e+04)		(2.3e+05)	(32.0)	(35.1)
4U 1916−053	270	4.2e+09	0.833 514 11	3	1.45e−02	94	1.4e−04	4	12.2	24.0
	± 5	(2.8e+09)	± 2.5e−07	(2)	± 1.05e−02	(63)		(3)	(11.5)	(23.2)
XB 1254−690	95	4.2e+09	3.9334	2606	0.98	390	3e−03	365	17.7	27.9
	± 5	(2.8e+09)	± 2e−04	(1737)	± 0.12	(260)		(243)	(17.0)	(27.3)
EXO 0748−676	45	4.2e+09	3.824 1072	9	0.475	593	1.3e−03	40	14.5	25.3
	± 5	(2.8e+09)	± 2.4e−06	(6)	± 0.365	(395)		(27)	(13.8)	(25.3)

we denote a_p. Depending on the measurement, we may instead quote the amplitude of the projected orbital velocity of the NS, $v_x \sin i$ (referred to as K1 in the optical literature). The two quantities are related by $v_x \sin i = 2\pi\, a_x \sin i / P_{orb}$. The orbital parameters are measured directly for the accreting millisecond pulsars via X-ray timing. The situation is more challenging for the non-pulsing and intermittent sources.

Some high-inclination systems show eclipses in the X-ray light curve, providing both P_{orb} and T_{asc}. There are also systems that show dips rather than full eclipses: the dips occur when the NS is obscured by the bulge where the mass stream from the donor star joins the accretion disc (White & Swank 1982). Dips certainly tell us P_{orb}, and restrict the inclination to lie in the range 60°–75°. What they do not necessarily yield is T_{asc}: in the two systems that show both dips and eclipses, dips occur at various offsets from the eclipse times (Cominsky & Wood 1984; Parmar et al. 1986; Motch et al. 1987; Smale et al. 1992). Detailed modelling is therefore required to determine the relationship between T_{asc} and the dip time T_{dip}. Throughout this section we list the most recent orbital ephemeris for each system. In several cases the ephemerides are sufficiently out of date that we should consider T_{asc} to be totally unconstrained. However, we presume that it would be straightforward to obtain a new ephemeris, with an error no worse that that of the existing measurement. We therefore use all existing measurements in our initial assessment of detectability.

The orbital parameters can also be measured in wavebands other than the X-ray, particularly the optical. A number of systems show photometric variability at the orbital period. Maximum optical light occurs when the NS is at inferior conjunction and we observe reprocessed emission from the heated face of the donor star, yielding both P_{orb} and T_{asc}, but not the projected semimajor axis. An alternative method that can provide all three pieces of information is phase-resolved optical spectroscopy. LMXBs exhibit many emission lines, some from heated face of the donor star (Steeghs & Casares 2002), others from the accretion disc very close to the compact object. By measuring the orbital Doppler shifts of these lines, and using techniques such as Doppler tomography to check the emission location, major progress has been made in computing orbital parameters. Additional constraints on the system are possible (assuming Roche lobe overflow and tidal locking) if one can detect rotational broadening of absorption lines from the donor star (Horne, Wade & Szkody 1986; Casares, Charles & Kuulkers 1998).

Unfortunately, for many of the systems of interest, one or all of the orbital parameters are unknown. We can however still place

Table 4. Parameter space and template requirements for the kHz QPO sources (details as for Table 2).

Source	$\nu_s \pm \Delta\nu_s$ (Hz)	N_ν	$P_{orb} \pm \Delta P_{orb}$ (h)	$N_{P_{orb}}$	$a_x \sin i \pm \Delta a_x \sin i$ (light-second)	N_{a_p}	ΔT_{asc} (d)	$N_{T_{asc}}$	$\log_{10}(N_{temp})$	F_{stat}
Cyg X-2	351	2.8e+10	236.265 600 00	1	13.5	2.0e+04	3.0e−02	3228	18.0	27.9
	± 34	(1.9e+10)	± 8.3e−08	(1)	± 1.6	(1.4e+04)		(2152)	(17.4)	(27.3)
GX 340+0	343	7.6e+10	120.1	8.4e+07	11.3	1.6e+05	2.5	5.0e+05	34.5	36.0
	± 92	(5.1e+10)	± 119.9	(5.6e+07)	± 11.3	(1.1e+05)		(3.3e+05)	(33.8)	(36.0)
4U 1735−44	316	2.7e+10	4.652 0042	177	0.693	7825	3.0e−3	761	19.1	28.4
	± 32	(1.8e+10)	± 7.7e−06	(118)	± 0.693	(5217)		(508)	(18.4)	(27.9)
GX 5−1	288	5.7e+10	120.1	6.9e+07	11.3	1.3e+05	2.5	4.1e+05	34.1	36.0
	± 69	(3.8e+10)	± 119.9	(4.6e+07)	± 11.3	(8.7e+04)		(2.7e+05)	(33.4)	(35.5)
4U 1820−30	285	5.4e+10	0.182 781 083	9	1.35e−02	74	2.2e−04	28	14.5	26.0
	± 65	(3.6e+10)	± 2.8e−08	(6)	± 6.5e−03	(50)		(19)	(13.8)	(25.3)
Sco X-1	272	3.3e+10	18.895 51	58	1.44	1827	3.0e−03	350	17.6	27.9
	± 40	(2.2e+10)	± 2e−05	(39)	± 0.18	(1218)		(234)	(16.9)	(27.3)
GX 17+2	272	4.2e+10	120.1	6.2e+07	11.3	1.2e+05	2.5	3.7e+05	33.8	36.0
	± 50	(2.8e+10)	± 119.9	(4.2e+07)	± 11.3	(7.9e+04)		(2.5e+05)	(33.1)	(35.5)
XTE J2123−058	272	4.2e+10	5.956 833	1657	1.6	3210	1.0e−03	422	19.5	28.4
	± 50	(2.8e+10)	± 5.6e−05	(1105)	± 0.3	(2140)		(281)	(18.8)	(28.4)
GX 349+2	266	1.1e+10	22.5	4.0e+05	3.5	3.2e+04	0.47	1.0e+05	24.8	31.7
	± 13	(7.2e+09)	± 0.1	(2.7e+05)	± 3.5	(2.1e+04)		(6.6e+04)	(24.1)	(31.2)

various constraints on the systems to reduce the number of templates required. For those systems with measured orbital periods, for example, we can assume that the donor star fills its Roche lobe. This fixes $\bar{\rho}_d$, the mean density of the donor star:

$$\bar{\rho}_d \approx 110 \left(\frac{P_{orb}}{1\,h}\right)^{-2} \text{ g cm}^{-3}. \quad (7)$$

The range of donor types with this $\bar{\rho}$ limits the donor mass $M_d = m_d\,M_\odot$. LMXB donors include main-sequence stars, evolved hydrogen-burning stars, helium-burning stars and brown or white dwarfs (Podsiadlowski, Rappaport & Pfahl 2002). For $P_{orb} \gtrsim 10$ h, $\bar{\rho}_d \lesssim 1$g cm^{-3}, the companion must be an evolved hydrogen-burning star such as a subgiant. For ultracompact systems with $P_{orb} \lesssim 80$ min, the companion must be a white dwarf, a helium star, or a highly evolved helium-rich secondary (Rappaport & Joss 1984; Deloye & Bildsten 2003; Nelemans, Jonker & Steeghs 2006). For intermediate orbital periods more options are possible, maximum donor mass being set by the main-sequence star – but evolved, less massive companions or even brown dwarfs may be possible (Tout et al. 1996; Chabrier & Baraffe 2000; Chabrier et al. 2000; Bildsten & Chakrabarty 2001).[11] Additional constraints on donor properties may come from X-ray burst properties or spectral type: more evolved, lower mass donors will have later spectral types than the main-sequence star with the same $\bar{\rho}_d$ (Baraffe & Kolb 2000; Kolb, King & Baraffe 2001). Having finally established the range of likely donor masses, and knowing that the NS mass $M_x = m_x\,M_\odot$ is in the range 1.2–2.4 $M_\odot$ (Lattimer & Prakash 2007), we then estimate $a_x \sin i$ using

$$a_x \sin i = 1.174 \left(\frac{P_{orb}}{1\,h}\right)^{2/3} \frac{m_d}{(m_d + m_x)^{2/3}} \sin i \quad \text{light-second}. \quad (8)$$

[11] Rappaport & Joss (1984) showed that helium-rich donor stars would have higher masses for a given P_{orb} than expected for main-sequence stars. However, the binary evolution simulations of Podsiadlowski et al. (2002) did not generate any such stars at intermediate orbits, so we neglect this possibility unless there is overwhelming evidence for the presence of helium-rich material (from X-ray bursts, for example).

For systems that do not show dips or eclipses ($i \lesssim 60^\circ$), and where there is no other limit on inclination, equation (8) gives only an upper limit. For dipping systems we assume $60^\circ \lesssim i \lesssim 75^\circ$, giving both upper and lower limits. For eclipsing systems an additional constraint comes from the half-angle of the X-ray eclipse θ_x (Bradt & McClintock 1983):

$$\sin i = \frac{1}{\cos\theta_x}\left[1 - \left(0.38 - 0.2 \log\frac{m_x}{m_d}\right)^2\right]^{1/2}. \quad (9)$$

For systems with no measured orbital period, we make the standard LMXB assumption that $m_d/m_x < 0.8$. Time-averaged accretion rate (as estimated from the X-ray flux) can give general constraints if we assume that mass transfer is driven by gravitational radiation: however, magnetic braking may also play a role in mass transfer and the contribution is hard to quantify. The conditions required for the system to be persistent or transient at the inferred accretion rate were also considered (King, Kolb & Burderi 1996; Dubus et al. 1999; in't Zand, Jonker & Markwardt 2007): unfortunately for most of the systems in our study this added very little in the way of tighter constraints. For systems where there are no better constraints on orbital period, we will assume that P_{orb} lies between 10 min and 240 h. The presumed lack of eclipses in such systems sets $i < 60^\circ$, so from equation (8) we obtain an upper limit on $a_x \sin i$ of 22.6 light-second.

3.3 Accreting millisecond pulsars

The 10 accreting millisecond pulsars are the only systems where we clearly know the NS spin frequency ν_s. All are transient, but their pulsation characteristics differ. Seven of these systems, which have short outbursts (weeks) and long periods of quiescence (years), show persistent pulsations throughout their outburst phases. The other three systems are rather different. HETE J1900.1−2455 went into outburst in 2005 and is still active, but only showed pulsations during the first two months of the outburst. The other two systems have shown pulsations only intermittently during outburst. We now

discuss the sources in order of spin frequency, from highest to lowest.

3.3.1 IGR J00291+5934 ($\nu_s = 599$ Hz)

This source was discovered in 2004 during a 13-d outburst with total fluence (0.1–200 keV) 1.8×10^{-3} erg cm^{-2} (Galloway et al. 2005). We assume that this is a typical outburst. The *RXTE* ASM history suggests a recurrence time of 3 yr, giving $F_{\rm av} = 1.8 \times 10^{-11}$ erg cm^{-2} s^{-1}. The most accurate position for the source, given by the optical/near-infrared counterpart, is right ascension (RA) = $00^{\rm h}29^{\rm m}03\overset{\rm s}{.}05 \pm 0\overset{\rm s}{.}01$, declination (Dec.) = $+59^\circ34'18\overset{''}{.}93 \pm 0\overset{''}{.}05$ (Torres et al. 2008). This position accords with the earlier optical position of Fox & Kulkarni (2004) and the *Chandra* X-ray position (Paizis et al. 2005), but is offset by 3.2σ in RA from the radio position (Rupen, Dhawan & Mioduszewski 2004a). Mass transfer arguments suggest a minimum distance of ≈4 kpc (Galloway et al. 2005), and the lack of bursts implies a maximum distance of 6 kpc (Galloway 2006). There have been three studies of the spin and orbital parameters. Galloway et al. (2005) used data from the start of the outburst and the optical position of Fox & Kulkarni (2004). Falanga et al. (2005) and Burderi et al. (2007) used additional data from later in the outburst and the radio position.[12] The studies agree on the orbital parameters: $P_{\rm orb} = 8844.092 \pm 0.006$ s, $T_{90} = 53\,345.187\,5164 \pm 4 \times 10^{-7}$ MJD (TDB), $a_{\rm x} \sin i = 64.993 \pm 0.002$ light-minute (1σ uncertainties; Galloway, private communication), and $e < 2 \times 10^{-4}$ (3σ upper limit). There are however small differences in spin parameters. In our initial assessment of detectability we use the most recent values of Burderi et al. (2007): $\nu_s = 598.892\,130\,53 \pm 2 \times 10^{-8}$ Hz, $\dot{\nu}_s = (8.5 \pm 1.1) \times 10^{-13}$ Hz s^{-1} at epoch MJD 53346.184635 (1σ uncertainties).

3.3.2 Aql X-1 (1908+005) ($\nu_s = 550$ Hz)

Aql X-1 is a transient atoll source with quasi-regular outbursts, ∼10 in the *RXTE* era. Using the spectral modelling of Galloway et al. (2008a) we set 5 ASM cts s^{-1} = 3.1×10^{-9} erg cm^{-2} s^{-1} (bolometric). The long-term average ASM count rate is 1.8 cts s^{-1}, while the average count rate during the bright 45-d outburst of late 2000 was 34 cts s^{-1}. The most recent position, from Very Large Array (VLA) observations of the radio counterpart, is RA = $19^{\rm h}11^{\rm m}16\overset{\rm s}{.}01 \pm 0\overset{\rm s}{.}03$, Dec. = $+00^\circ35'06\overset{''}{.}7 \pm 0\overset{''}{.}3$ (J2000, 1σ error bars) (Rupen et al. 2004b). Galloway et al. (2008a) use PRE bursts to estimate a distance of 3.9 ± 0.7 or 5.0 ± 0.9 kpc depending on composition. Casella et al. (2008) have reported the detection of intermittent accretion-powered pulsations at 550.2745 ± 0.0009 Hz. The orbital period, determined from the optical light curve in outburst, is $P_{\rm orb} = 18.9479 \pm 0.0002$ h (Chevalier & Ilovaisky 1998) (the quiescent period agrees at the 0.02 per cent level). The time of minimum optical light determined by Garcia et al. (1999) gives $T_{90} = 245\,0282.220 \pm 0.003$ HJD. Both time of minimum light and orbital period were confirmed in later analysis by Welsh, Robinson & Young (2000). Cornelisse et al. (2007) attempted to measure the projected orbital velocity of the NS directly using phase-resolved optical spectroscopy: they report a preliminary value of $v_{\rm x} \sin i = 68 \pm 5$ km s^{-1}. Although the fit quality is not good and this result requires confirmation, we will use this value in our preliminary assessment of detectability.

[12] Although an offset position can generate an apparent spin derivative, the offset is not sufficiently large to account for the reported values of $\dot{\nu}_s$.

3.3.3 SAX J1748.9−2021 ($\nu_s = 442$ Hz)

This is a transient source located in the globular cluster NGC 6440, with three outbursts in the *RXTE* era. Using the spectral modelling of Galloway et al. (2008a) we set 13 ASM cts s^{-1} = 5×10^{-9} erg cm^{-2} s^{-1} (bolometric). The long-term average ASM count rate is 0.2 cts s^{-1}, while the average count rate during the bright 60-d outburst of 2005 was 10 cts s^{-1}. The position of the optical counterpart (Verbunt et al. 2000) [which accords with the *Chandra* position of Pooley et al. (2002)] is RA = $17^{\rm h}48^{\rm m}52\overset{\rm s}{.}14$, Dec. = $-20^\circ21'32\overset{''}{.}6$ (J2000), with an error of $0\overset{''}{.}5$. Kuulkers et al. (2003) estimate distance to the cluster as $8.4^{+1.5}_{-1.3}$ kpc, in good agreement with the value of 8.1 ± 1.3 kpc derived from PRE bursts (Galloway et al. 2008a). Altamirano et al. (2008) discovered intermittent accretion-powered pulsations in two outbursts from this source (see also Gavriil et al. 2007). Patruno et al. (2008) have now carried out a detailed phase-connected timing study to determine the spin and orbital parameters. They find $\nu_s = 442.361\,081\,18 \pm 5 \times 10^{-8}$ Hz, $P_{\rm orb} = 8.765\,25 \pm 3 \times 10^{-5}$ h, $T_{\rm asc} = 52191.507190 \pm 4 \times 10^{-6}$ MJD/TDB and $a_{\rm x} \sin i = 0.387\,60 \pm 4 \times 10^{-5}$ light-second, with $e < 1.3 \times 10^{-4}$ (1σ uncertainties and upper limits).

3.3.4 XTE J1751−305 ($\nu_s = 435$ Hz)

The 2004 outburst of this source, which lasted ≈10 d, had total fluence (2–200 keV) $(2.5 \pm 0.5) \times 10^{-3}$ erg cm^{-2} (Markwardt et al. 2002). Assuming that this outburst is typical, the mean recurrence time of 3.8 yr yields $F_{\rm av} = 2 \times 10^{-11}$ erg cm^{-2} s^{-1}. The most accurate position for the source, measured with *Chandra*, is RA = $17^{\rm h}51^{\rm m}13\overset{\rm s}{.}49 \pm 0\overset{\rm s}{.}05$, Dec. = $-30^\circ37'23\overset{''}{.}4 \pm 0\overset{''}{.}6$ (J2000), where the uncertainties are the 90 per cent confidence limits (Markwardt et al. 2002). Mass transfer arguments yield a lower limit on the distance of 6 kpc (Markwardt et al. 2002). The most recent timing study by Papitto et al. (2008), using the *Chandra* position, gives $P_{\rm orb} = 2545.342 \pm 0.002$ s, $T_{\rm asc} = 52368.0129023 \pm 4 \times 10^{-7}$ MJD (TDB), $a_{\rm x} \sin i = 10.125 \pm 0.005$ light-minute, $e < 1.3 \times 10^{-3}$ (90 per cent confidence level uncertainties and upper limits). The spin parameters are $\nu_s = 435.317\,993\,57 \pm 4 \times 10^{-8}$ Hz, and the study also suggests that $\dot{\nu}_s$ may be non-zero.

3.3.5 SAX J1808.4−3658 ($\nu_s = 401$ Hz)

Galloway & Cumming (2006) analyse the five known outbursts from this source, and find a mean outburst fluence of $(6.0 \pm 0.2) \times 10^{-3}$ erg cm^{-2} (0.1–200 keV). In estimating transient GW signal we use an outburst duration of 20 d: we neglect the extended flaring phase often seen at the end of outbursts in this source, since emission during this phase is at a much lower level. Mean recurrence time is 2.2 yr, giving $F_{\rm av} = 8.6 \times 10^{-11}$ erg cm^{-2} s^{-1}. The most recent and precise position, for the optical counterpart, is RA = $18^{\rm h}08^{\rm m}27\overset{\rm s}{.}62$, Dec. = $-36^\circ58'43\overset{''}{.}3$ (J2000), with an uncertainty of $0\overset{''}{.}15$ (Hartman et al. 2008). Galloway & Cumming (2006) have derived a distance of 3.4–3.6 kpc using both mass transfer arguments and burst properties. Using the refined optical position, Hartman et al. (2008) report the following values for the orbital parameters: $P_{\rm orb} = 7249.156\,961 \pm 1.4 \times 10^{-5}$ s at time $T_{\rm asc} = 52499.9602477 \pm 1.0 \times 10^{-6}$ MJD (TDB), $\dot{P}_{\rm orb} = (3.48 \pm 0.12) \times 10^{-12}$ Hz s^{-1}, $a_x \sin i = 60.281\,32 \pm 2.4 \times 10^{-4}$ light-minute (1σ errors). The eccentricity $e < 0.000\,21$ (95 per cent upper limit). The spin rate was tracked across multiple outbursts, and is given relative to a reference frequency $\nu_0 = 400.975\,210$ Hz.

In the 1998 outburst, $\nu_s - \nu_0 = 0.371 \pm 0.018$ μHz, with $\dot{\nu}_s$ in the range $(-7.5, 7.3) \times 10^{-14}$ Hz s^{-1} (95 per cent confidence limits). In the 2000 outburst, $\nu_s - \nu_0 = 0.254 \pm 0.012$ μHz, with $\dot{\nu}_s$ in the range $(-1.1, 4.2) \times 10^{-14}$ Hz s^{-1}. In the 2002 outburst, $\nu_s - \nu_0 = 0.221 \pm 0.006$ μHz, with $\dot{\nu}_s$ in the range $(-1.2, 2.5) \times 10^{-14}$ Hz s^{-1}. In the 2005 outburst, $\nu_s - \nu_0 = 0.190 \pm 0.015$ μHz with $\dot{\nu}_s$ in the range $(-0.5, 2.3) \times 10^{-14}$ Hz s^{-1}. Fitting the frequency evolution across all four outbursts gives $\dot{\nu}_s = (5.6 \pm 2.0) \times 10^{-15}$ Hz s^{-1}. In our initial assessment of detectability, we use the spin solution for the 2002 outburst.

3.3.6 HETE J1900.1−2455 ($\nu_s = 377$ Hz)

This source was first detected in 2005 June, and has remained in outburst ever since (Degenaar et al. 2007). Galloway (2006) and Galloway et al. (2007) report an average (bolometric) outburst flux of $\approx 9 \times 10^{-10}$ erg cm^{-2} s^{-1}. We assume an outburst duration of 2 yr, and (given that no previous outbursts are known) a recurrence time of at least 10 yr (Kaaret et al. 2006), yielding $F_{\rm av} \approx 2 \times 10^{-10}$ erg cm^{-2} s^{-1}. The position of the optical counterpart is RA = 19$^{\rm h}$00$^{\rm m}$08$^{\rm s}$.65, Dec. = −24°55′13″.7 (J2000), with an estimated uncertainty of 0″.2 (Fox 2005). The distance estimated by Galloway et al. (2008a) using *RXTE* observations of radius expansion bursts is 4.7 ± 0.6 kpc. This accords with the earlier estimate of 5 kpc made by Kawai & Suzuki (2005) using HETE burst data. Timing analysis by Kaaret et al. (2006), using *RXTE* data from 2006 June 16 to July 7, resulted in the following orbital parameters: $P_{\rm orb} = 4995.258 \pm 0.005$ s, $T_{90} = 53549.145385 \pm 7 \times 10^{-6}$ MJD (TT), $a_x \sin i = 18.41 \pm 0.01$ light-minute, $e < 0.002$. The spin was $\nu_s = 377.296\,171\,971 \pm 5 \times 10^{-9}$ Hz. All errors and upper limits are 1σ uncertainties. On July 8 there was an apparent jump in spin rate of $\Delta\nu_s/\nu_s \sim 6 \times 10^{-7}$ to $\nu_s = 377.291\,596 \pm 1.6 \times 10^{-5}$ Hz. Thereafter pulsations ceased and spin has not been tracked since despite the fact that the source has remained in outburst (Galloway et al. 2007). In our initial assessment of detectability we do not take into account the apparent jump in spin.

3.3.7 XTE J1814−338 ($\nu_s = 314$ Hz)

This pulsar has had only one outburst in the *RXTE* era, lasting ≈50 d. Galloway (2006) estimate a bolometric outburst fluence of $(3.0 \pm 0.1) \times 10^{-3}$ erg cm^{-2}. Given a recurrence time of at least 7.5 yr, this yields an upper limit on $F_{\rm av}$ of 1.3×10^{-11} erg cm^{-2} s^{-1}. The position derived from X-ray and optical spectroscopy is RA = 18$^{\rm h}$13$^{\rm m}$39$^{\rm s}$.04, Dec. = −33°46′22″.3 (J2000), 90 per cent confidence error circle of 0″.2 (Krauss et al. 2005). These authors use X-ray spectroscopy to infer a minimum distance of 3.8 kpc. The upper limit on the distance, derived from burst properties, is 8.0 ± 1.6 kpc (Strohmayer et al. 2003). Timing analysis by Papitto et al. (2007), using data from the whole 2003 outburst, leads to the following orbital parameters: $P_{\rm orb} = 15\,388.7229 \pm 0.0002$ s, $T_{\rm asc} = 52797.8101698 \pm 9 \times 10^{-7}$ MJD (TDB), $a_x \sin i = 390.633 \pm 0.009$ light-minute, $e < 2.4 \times 10^{-5}$ (3σ upper limit). The associated spin parameters are $\nu_s = 314.356\,108\,79 \pm 1 \times 10^{-8}$ Hz, $\dot{\nu}_s = (-6.7 \pm 0.7) \times 10^{-14}$ Hz s^{-1}. Uncertainties are at the 90 per cent confidence level.

3.3.8 XTE J1807−294 ($\nu_s = 191$ Hz)

There has been only one recorded outburst from this source, for which Galloway (2006) computes a bolometric fluence of $(3.1 \pm 0.2) \times 10^{-3}$ erg cm^{-2}. For a recurrence time of at least 7.1 yr, $F_{\rm av}$ is at most 1.4×10^{-11} erg cm^{-2} s^{-1}. In estimating transient GW signal we use an outburst duration of 50 d, neglecting the prolonged low-flux tail at the end of the outburst. The most accurate position, measured with *Chandra*, is RA = 18$^{\rm h}$06$^{\rm m}$59$^{\rm s}$.8, Dec. = −29° 24′ 30″ (J2000), with an uncertainty due to systematic errors of 1 arcmin (Markwardt, Juda & Swank 2003). Using mass transfer estimates, Galloway (2006) derives a lower limit on the distance of 4.7 kpc. Determination of spin and orbital parameters in this source is complicated by extreme variations in pulse profile. A recent study by Riggio et al. (2007) finds $P_{\rm orb} = 2404.416\,65 \pm 0.000\,40$ s, $a_x \sin i = 4.819 \pm 0.004$ light-minute, $T_{\rm asc} = 52720.675603 \pm 6 \times 10^{-6}$ MJD/TDB and $\nu_s = 190.623\,506\,94 \pm 8 \times 10^{8}$ Hz (1σ uncertainties). The eccentricity $e < 0.0036$ (2σ upper limit). Chou et al. (2008) report similar values apart from for $T_{\rm asc}$, where the values found by the two studies differ by more than the quoted uncertainties. Both Chou et al. (2008) and Riggio et al. (2008) suggest a non-zero $\dot{\nu}_s \sim 10^{-14}$ to 10^{-13} Hz s^{-1} in outburst. In our initial assessment of detectability we use the values and uncertainties of Riggio et al. (2007), although clearly the 'true' uncertainty on $T_{\rm asc}$ is larger.

3.3.9 XTE J0929−314 ($\nu_s = 185$ Hz)

This source has had one outburst in the *RXTE* era, for which Galloway (2006) estimates a bolometric fluence of $(5.4 \pm 0.3) \times 10^{-3}$ erg cm^{-2}. Outburst duration, which we assume to be typical, was ≈60 d. Given a recurrence time of at least 6.3 yr, $F_{\rm av}$ is at most 2.7×10^{-11} erg cm^{-2} s^{-1}. The most accurate position, given by the optical counterpart, is RA = 9$^{\rm h}$29$^{\rm m}$20$^{\rm s}$.19, Dec. = −31°23′03″.2 (J2000) with error circle 0″.1 (Giles et al. 2005). Galloway (2006) uses mass transfer and recurrence time estimates to infer a lower limit to the distance of 3.6 kpc [revising an earlier value of 5 kpc in Galloway et al. (2002)]. Timing analysis by Galloway et al. (2002), using an earlier optical position from Greenhill, Giles & Hill (2002), leads to the following orbital parameters: $P_{\rm orb} = 2614.746 \pm 0.003$ s, $T_{90} = 52405.49434 \pm 1 \times 10^{-5}$ MJD (TDB), $a_x \sin i = 6.290 \pm 0.009$ light-minute. The associated spin parameters are $\nu_s = 185.105\,254\,297 \pm 9 \times 10^{-9}$ Hz, $\dot{\nu}_s = (-9.2 \pm 0.4) \times 10^{-14}$ Hz s^{-1}. All errors are 1σ uncertainties (Galloway, private communication). The eccentricity $e < 0.007$ (2σ limit).

3.3.10 SWIFT J1756.9−2508 ($\nu_s = 182$ Hz)

This source has had one outburst in 2006 lasting 13 d, with total fluence (1–10 000 keV) $(4.5 \pm 0.8) \times 10^{-4}$ erg cm^{-2}. No previous outbursts are known (although there are gaps in coverage), but this suggests a recurrence time of at least 10 yr. The best position for the source, from *Swift*, is RA = 17$^{\rm h}$56$^{\rm m}$57$^{\rm s}$.35, Dec. = −25°06′27″.8 (J2000), with uncertainty 3″.5. The distance is not well constrained, but is thought to be ≈8 kpc. The orbital parameters are $P_{\rm orb} = 3282.104 \pm 0.083$ s, $T_{\rm asc} = 54265.28707 \pm 6 \times 10^{-5}$ MJD (TDB), $a_x \sin i = 5.942 \pm 0.027$ light-minute, $e < 0.026$ (95 per cent upper limit). The spin rate is $\nu_s = 182.065\,804\,253 \pm 7.2 \times 10^{-8}$ Hz, with $\dot{\nu}_s < 1 \times 10^{-12}$ Hz s^{-1}. All errors are 90 per cent confidence; upper limits are 95 per cent confidence. All information on this source is taken from Krimm et al. (2007).

3.4 Burst oscillation sources

We list all sources for which burst oscillations have been reported, in order of decreasing burst oscillation frequency ν_b. For some sources, oscillations have been detected at the same frequency in

multiple bursts: these results can be regarded as secure. In some cases, however, oscillations have only been seen in a single burst. Given the number of NSs whose bursts have now been searched for oscillations (a factor not included in quoted statistical significances), these results should be regarded as tentative until confirmed in a second burst. We include them in our survey (marked with an asterisk) since if they turn out to be promising GW sources this would provide added impetus to confirm or alternatively rule out the candidate burst oscillation detection.

*3.4.1 XTE J1739−285 ($\nu_b = 1122$ Hz)**

This transient atoll source has had four outbursts in the *RXTE* era. Using the spectral modelling of Kaaret et al. (2007) we set 10 ASM cts $s^{-1} = 1.4 \times 10^{-9}$ erg cm^{-2} s^{-1} (2–20 keV) and apply a bolometric correction factor of 1.34 (the average factor found by Galloway et al. (2008a) for burst sources). The long-term average ASM count rate is 0.3 cts s^{-1}, and the average count rate during the bright 200-d outburst of 2005 was 4 cts s^{-1}. The most precise source position, measured by *Chandra*, is RA = $17^h39^m53\overset{s}{.}95$, Dec. = $-28°29'46\overset{''}{.}8$ (J2000), with a 90 per cent error radius of $0\overset{''}{.}6$ (Krauss et al. 2006). The absence of an optical/IR counterpart sets an upper limit on distance of 12 kpc (Torres et al. 2006). The absence of PRE bursts sets a more stringent upper limit of 10.6 kpc (Kaaret et al. 2007). A candidate 1122-Hz burst oscillation was detected in part of one burst recorded by *RXTE* during the 2005 outburst. The orbital parameters of the source are unknown, and there are no measured constraints on the properties of the companion.

3.4.2 4U 1608−522 ($\nu_b = 620$ Hz)

This transient atoll source has had several outbursts during *RXTE*'s lifetime, and seems to be active at a low level (ASM count rate $>3\sigma$) even when not in outburst. Using the spectral modelling of Galloway et al. (2008a) we set 70 ASM cts $s^{-1} = 4.8 \times 10^{-8}$ erg cm^{-2} s^{-1} (bolometric). The long-term average ASM count rate is 3.6 cts s^{-1}, while the average count rate during the bright 100-d outburst in 2005 was 30 cts s^{-1}. The best position, from the optical counterpart, is RA = $16^h08^m52\overset{s}{.}2$, Dec. = $-52°17'43''$ (B1950), with errors of $\pm 0\overset{''}{.}5$ (Grindlay & Liller 1978). No more up to date position is available. Source distance, derived under the assumption that radius expansion bursts reach the Eddington limit for pure helium, is 4.1 ± 0.4 kpc (Galloway et al. 2008a). Burst oscillations at ≈620 Hz have been detected in multiple bursts (Hartman et al. 2003; Galloway et al. 2008a). The last (unsuccessful) search for persistent pulsations from this source, using data from 1989 to 1991, searched only up to 512 Hz (Vaughan et al. 1994). The orbital parameters are not known, although a number of tentative periodicities have been reported (Lochner & Roussel-Dupre 1994; Wachter et al. 2002). The spectral type of the companion is that of a late F/early G type main-sequence companion star, but would also match that of a more evolved K/M type star (Wachter et al. 2002). The mean density range for donors of this type suggests that the orbital period lies in the range 10–125 h. Given that the system is non-eclipsing we assume $i < 60°$ and hence obtain, for the assumed orbital periods, $a_x \sin i < 12.3$ light-second.

3.4.3 SAX J1750.8−2900 ($\nu_b = 601$ Hz)

This weak transient atoll source has had two outbursts in the *RXTE* era. Following the spectral modelling of Galloway et al. (2008a) we set 8 ASM cts $s^{-1} = 3.4 \times 10^{-9}$ erg cm^{-2} s^{-1} (bolometric). The long-term average ASM count rate is 0.08 cts s^{-1}, while the average count rate during the brighter 110-d outburst in 1997 was 2.8 cts s^{-1}. The most precise position, from *BeppoSAX*, is RA = $17^h50^m24^s$, Dec. = $-29°02'18'$ (J2000), with a 99 per cent error radius of $1'$ (Natalucci et al. 1999). The distance, estimated from radius expansion bursts, is 6.79 ± 0.14 kpc (Galloway et al. 2008a). Burst oscillations at 601 Hz have been detected in multiple bursts (Kaaret et al. 2002; Galloway et al. 2008a). The orbital parameters are not known, and there are no observations of the companion star.

3.4.4 GRS 1741.9−2853 (AX J1745.0−2855) ($\nu_b = 589$ Hz)

This is a transient source in the crowded Galactic Centre, with three outbursts in the *RXTE* era. Unfortunately the fact that the field is crowded means that there is no reliable ASM flux history for this source. The most precise position for the source, derived by *Chandra*, is RA = $17h45^m2\overset{s}{.}33$, Dec. = $-28°54'49\overset{''}{.}7$ (J2000), with an uncertainty of $0\overset{''}{.}7$ (Muno, Baganoff & Arabadijs 2003). Analysis of radius expansion bursts suggests a distance 6.0 ± 1.6 kpc (Eddington limit assuming cosmic abundances) or 8 ± 2 kpc (Eddington limit for pure He) (Galloway et al. 2008a). Burst oscillations at 589 Hz have been detected in two bursts (Strohmayer et al. 1997).[13] The orbital parameters are not known, and there is no information on the properties of the companion star.

3.4.5 4U 1636−536 ($\nu_b = 581$ Hz)

This is a persistent atoll source. Using the spectral modelling of Galloway et al. (2008a) we set 18 ASM cts s^{-1} = 8.4 × 10^{-9} erg cm^{-2} s^{-1} (bolometric). The long-term average ASM count rate is 10 cts s^{-1}. The best position for the source, from the optical counterpart V801 Ara, is RA = $16^h36^m56\overset{s}{.}41$, Dec. = $-53°39'18\overset{''}{.}1$ (B1950), with an error circle of less than $1'$ (Bradt & McClintock 1983). No more up to date position is available. The distance, estimated from a large sample of radius expansion bursts, is 6.0 ± 0.5 kpc (Galloway et al. 2006). Burst oscillations at ≈581 Hz have been seen in multiple bursts and a superburst (Strohmayer et al. 1998a; Strohmayer & Markwardt 2002; Galloway et al. 2008a). The most recent unsuccessful search for persistent pulsations, using data from 1987, searched only up to 512 Hz (Vaughan et al. 1994). The latest ephemeris, derived from phase-resolved optical spectroscopy, gives $P_{orb} = 0.158\,046\,93 \pm 1.6 \times 10^{-7}$ d and $T_{90} = 245\,2813.531 \pm 0.002$ HJD (Casares et al. 2006). Augusteijn et al. (1998) set an upper limit on the orbital period derivative of $|P_{orb}/\dot{P}_{orb}| \leq 3 \times 10^5$ yr. No tighter limit has yet been reported. Orbital Doppler shifts on burst oscillations during a superburst lead to limits $90 < v_x \sin i < 113$ km s^{-1}, (Strohmayer & Markwardt 2002; Casares et al. 2006). The quoted range corresponds to varying the reference phase of the ephemeris across the $\pm 1\sigma$ range.

3.4.6 X 1658−298 (MXB 1659−29) ($\nu_b = 567$ Hz)

This transient source, which has eclipses and dips, was active from 1976 to 1979, and then again from 1999 to 2001. Using the spectral modelling of Galloway et al. (2008a) we set 2.4 ASM cts s^{-1} = 6.7 × 10^{-9} erg cm^{-2} s^{-1} (bolometric). Over the most recent outburst, which lasted 870 d, the average ASM count rate

[13] The bursts were originally attributed to a different source, MXB 1743−29, due to source confusion in the crowded field.

was 2.7 cts s^{-1}. Assuming a recurrence time of ≈23 yr, the long-term average ASM count rate is 0.3 cts s^{-1}. The best position for the source, from the optical counterpart V2134 Oph, is RA = $17^h02^m06^s.42$, Dec. = $-29°56'44''.33$ (J2000), with an uncertainty of 0″.1 (Wachter & Smale 1998). Assuming that the bright radius expansion bursts reach the Eddington limit for pure He, Galloway et al. (2008a) derive a distance of 12 ± 3 kpc. Burst oscillations at ≈567 Hz have been detected in multiple bursts (Wijnands, Strohmayer & Franco 2001a). The most up to date X-ray ephemeris, by Oosterbroek et al. (2001), gives $P_{\rm orb} = 0.296\,504\,5746 \pm 3.4 \times 10^{-9}$ d, and $T_{90} = 244\,3059.225\,826 \pm 0.000\,093$ JD/TDB. The projected semimajor axis has not been measured, but we can set bounds on it using the constraints outlined at the start of this section. For the above orbital period, Wachter, Smale & Bailyn (2000) find X-ray eclipse duration half-angles 6°.34 ± 0°.01 [slightly lower than the value reported by Cominsky & Wood (1984)]. We can therefore use equation (9) to restrict $\sin i$. If we assume Roche lobe overflow, then from equation (7) the mean density of the donor star is 2.2 g cm^{-3}, suggesting a main-sequence or evolved companion. Maximum donor mass occurs if the donor is on the main sequence. In this case, maximum $M_{\rm d} = 0.78\,{\rm M}_\odot$ and would be of spectral type K0 (Wachter & Smale 1998). Whilst the data are consistent with this spectral type, there is some indication that the spectral type is later, suggesting a more evolved (lower mass) companion with spectral type perhaps as late as M2 (Wachter et al. 2000). We will therefore adopt a minimum companion mass of $0.1\,{\rm M}_\odot$ (Baraffe & Kolb 2000; Podsiadlowski et al. 2002). For the NS we will consider masses in the range 1.2– $2.4\,{\rm M}_\odot$ (Lattimer & Prakash 2007). These assumptions suggest that $a_{\rm x} \sin i$ lies in the range 0.24–2.03 light-second.

*3.4.7 A 1744−361 ($\nu_{\rm b} = 530$ Hz)**

This transient dipping source has irregular outbursts, three in *RXTE*'s lifetime. Based on the spectral modelling of Bhattacharyya et al. (2006) we set 1.2 ASM cts $s^{-1} = 3 \times 10^{-10}$ erg cm^{-2} s^{-1} (3–14 keV) flux and apply a bolometric correction factor of 1.34 (the mean correction factor for converting 2.5–25 keV flux to bolometric flux found by Galloway et al. (2008a) for other burst sources). The long-term average ASM count rate is 0.16 cts s^{-1}, and during the bright 100-d outburst in 2003 the average count rate was 6 cts s^{-1}. The best position, for the radio counterpart, is RA = $17^h48^m13^s.148 \pm 0^s.014$, Dec. = $-36°07'57''.02 \pm 0''.3$ (J2000) (Rupen, Dhawan & Mioduszewski 2003). This is within the error circle of the *Chandra* position (Torres et al. 2004). The lack of radius expansion in the one burst detected by *RXTE* sets an upper limit on the distance of ≈9 kpc (Bhattacharyya et al. 2006). These authors reported a burst oscillation at ≈530 Hz during the rising phase of the one burst detected by *RXTE*. They also reported a possible orbital period of 97 ± 22 min, traced by dips in the X-ray light curve, (Bhattacharyya et al. 2006). In our initial assessment we will assume that this is indeed the orbital period. In this case the assumption of Roche lobe overflow (equation 7) gives a mean donor density of 28–70 g cm^{-3}, consistent with a main-sequence star or slightly evolved donor. The maximum donor mass (for a star on the main sequence) is $0.22\,{\rm M}_\odot$. For a dipping source we can assume an inclination in the range 60°–75°. For NS masses in the range 1.2–$2.4\,{\rm M}_\odot$ we can therefore set an upper limit on $a_{\rm x} \sin i$ of 0.2 light-second. The minimum donor mass, of $0.07\,{\rm M}_\odot$, is set by the most evolved hydrogen burning star possible. Together with the inclination constraint, this gives a lower limit on $a_{\rm x} \sin i$ of 0.05 light-second.

3.4.8 KS 1731−260 ($\nu_{\rm b} = 524$ Hz)

This transient atoll source was in outburst from 1988 (and possibly earlier) until 2001. Based on the spectral modelling of Galloway et al. (2008a) we set 18 ASM cts $s^{-1} = 9.7 \times 10^{-9}$ erg cm^{-2} s^{-1} (bolometric). The average count rate while the source was still in outburst was 9 cts s^{-1}: the long-term average count rate over the *RXTE* lifetime is 4 cts s^{-1}. The most precise position, for the optical counterpart, is RA = $17^h34^m13^s.47$, Dec. = $-26°05'18''.8$, with an error of 0″.4 (Wijnands et al. 2001b). This is within the error circle of the *Chandra* position (Revnivtsev & Sunyaev 2002). Assuming that the radius expansion bursts reach the limit for pure He, Galloway et al. (2008a) derive a distance of 7.2 ± 1.0 kpc. Burst oscillations at ≈524 Hz have been detected in multiple bursts (Smith, Morgan & Bradt 1997; Muno et al. 2000; Galloway et al. 2008a). The orbital parameters have not been measured. A study of the scatter of asymptotic burst oscillation frequencies by Muno et al. (2000) suggested that $v_{\rm x} \sin i$ might be as high as 340 ± 100 km s^{-1}, but this has not been revisited. Identification of the counterpart was hampered by high reddening along the Galactic plane, but it has now been detected (Mignani et al. 2002). If the companion is on the main sequence, it has to be of spectral type later than F: if it has evolved off the main sequence then it is not a red giant. For this to be the case in a Roche lobe overflowing system we require $P_{\rm orb} >$ 2 h.

*3.4.9 4U 0614+09 ($\nu_{\rm b} = 415$ Hz)**

This is a bursting atoll source, persistent but highly variable. Based on spectral modelling by Ford et al. (2000), we set 9 ASM cts s^{-1} = 3.3×10^{-9} erg cm^{-2} s^{-1} (bolometric). The long-term average ASM count rate is 3.3 cts s^{-1}. The best and most recent position, from a *Spitzer* observation of the IR counterpart, is RA = $6^h17^m07^s.35 \pm 0^s.03$, Dec. = $+09°08'13''.60 \pm 0''.05$ (J2000) (Migliari et al. 2006).[14] Brandt et al. (1992) infer an upper limit on the distance of 3 kpc from an X-ray burst. Strohmayer, Markwardt & Kuulkers (2008) detected burst oscillations at 415 Hz in one burst recorded by the *Swift* Burst Alert Telescope. The orbital parameters are unknown, but this is a candidate ultracompact binary (Juett et al. 2001). Nelemans et al. (2004) have shown that the companion is most likely a C/O white dwarf. Using the white dwarf models of Deloye & Bildsten (2003) this would imply $P_{\rm orb}$ = 15–20 min and hence (assuming that $i < 60°$ due to the lack of dips and eclipses), $a_{\rm x} \sin i \leq 0.014$ light-second.

3.4.10 4U 1728−34 (GX 354+00) ($\nu_{\rm b} = 363$ Hz)

This is a persistent atoll source. Based on the spectral modelling of Galloway et al. (2008a) we set 4 ASM cts $s^{-1} = 1.2 \times 10^{-9}$ erg cm^{-2} s^{-1} (bolometric). The long-term average ASM count rate is 7.3 cts s^{-1}. The most precise position for this source is that of the radio counterpart, RA = $17^h31^m57^s.73 \pm 0^s.02$, Dec. = $-33°50'02''.5 \pm 1''.1$ (J2000), where the errors are 1σ uncertainties (Martí et al. 1998). Assuming that the bright PRE bursts reach the He limit, Galloway et al. (2008a) infer a distance of 5.2 ± 0.5 kpc. Burst oscillations have been detected in multiple bursts at ≈363 Hz (Strohmayer et al. 1996; Galloway et al. 2008a). An unsuccessful search for persistent pulsations using *Ginga* data was carried out

[14] This is consistent with the older position for the optical counterpart V1055 Ori (Bradt & McClintock 1983).

by Vaughan et al. (1994). The orbital parameters are not known, although Strohmayer et al. (1998b) infer $v_x \sin i < 20.7\,\mathrm{km\,s^{-1}}$ from the scatter of asymptotic frequencies of burst oscillations from a series of bursts from 1996 to 1997. We will use this constraint in our initial assessment and use it to estimate $P_{\rm orb}$. If we assume Roche lobe overflow, then we find that a main-sequence or evolved star cannot satisfy the various relations. The companion must be either a white dwarf or a helium star. This is consistent with the properties of the X-ray bursts from this source, which suggest a hydrogen poor donor (Galloway et al. 2008a). We will therefore assume that $P_{\rm orb} < 10$ h.

3.4.11 4U 1702−429 ($\nu_{\rm b} = 329$ Hz)

This is a persistent atoll source. Based on the spectral modelling of Galloway et al. (2008a), we set 2 ASM cts $\mathrm{s^{-1}} = 7.8 \times 10^{-10}\,\mathrm{erg\,cm^{-2}\,s^{-1}}$ (bolometric). The long-term average ASM count rate is 3.2 cts $\mathrm{s^{-1}}$. The best position, measured by *Chandra*, is RA = $17^{\rm h}06^{\rm m}15\overset{\rm s}{.}314$, Dec. = $-43^\circ02'08\overset{''}{.}60$ (J2000), with an uncertainty of $0\overset{''}{.}6$ (Wachter et al. 2005). Assuming that the PRE bursts reach the limit for pure He, Galloway et al. (2008a) derive a distance of 5.5 ± 0.2 kpc. Burst oscillations are detected in multiple bursts at ≈329 Hz (Markwardt, Strohmayer & Swank 1999a; Galloway et al. 2008a). The orbital parameters are not known but there are no dips or eclipses.

*3.4.12 MXB 1730−335 (Rapid Burster) ($\nu_{\rm b} = 306$ Hz)**

The Rapid Burster is a transient globular cluster source with regular outbursts that occur around every 200 d. It is unusual in being the only system to show both Type I and Type II X-ray bursts, the latter being driven by spasmodic accretion. Using the spectral modelling of Galloway et al. (2008a) we set 10 ASM cts $\mathrm{s^{-1}} = 6.7 \times 10^{-9}\,\mathrm{erg\,cm^{-2}\,s^{-1}}$ (bolometric). The long-term average ASM count rate is 1 ct $\mathrm{s^{-1}}$, and during a typical 25-d outburst the average count rate is 8.8 cts $\mathrm{s^{-1}}$. The most accurate position, given by the radio counterpart, is RA = $17^{\rm h}33^{\rm m}24\overset{\rm s}{.}61$, Dec. = $-33^\circ23'19\overset{''}{.}8$ (J2000), with an error of $0\overset{''}{.}1$ (Moore et al. 2000). This is within the error circle of *Chandra* observations (Homer et al. 2001). The distance to the host globular cluster, Liller 1, is $8.8^{+3.3}_{-2.4}$, kpc (Kuulkers et al. 2003). Averaging the burst rise phase of 31 X-ray bursts recorded by *RXTE* revealed a weak candidate burst oscillation frequency of ≈306 Hz (Fox et al. 2001). The orbital parameters are not known, and no optical counterpart has been detected because of crowding in the host globular cluster.

*3.4.13 IGR J17191−2821 ($\nu_{\rm b} = 294$ Hz)**

This transient X-ray source was discovered only recently, with one recorded outburst. The average ASM count rate during the 11-d outburst was 3.7 cts $\mathrm{s^{-1}}$, giving a long-term average count rate during the *RXTE* era of 0.01 cts $\mathrm{s^{-1}}$. Based on Klein-Wolt et al. (2007a) we assume 3.5 ASM cts $\mathrm{s^{-1}} = 1.2 \times 10^{-9}\,\mathrm{erg\,cm^{-2}\,s^{-1}}$ (2–10 keV), and apply a bolometric correction factor of 2. The most precise position for the source, from *Swift*, is RA = $259\overset{\circ}{.}813\,06$, Dec. = $-28\overset{\circ}{.}299\,19$ (J2000), with an accuracy of $4'$ (Klein-Wolt et al. 2007b). Burst oscillations at ≈294 Hz have been detected in one burst (Markwardt et al. 2007). The peak flux of the X-ray bursts sets an upper limit to the distance of ∼11 kpc (Markwardt et al. 2007). Orbital parameters are not yet known, and there is no information on the companion.

*3.4.14 4U 1916−053 ($\nu_{\rm b} = 270$ Hz)**

This is a persistent source in an ultracompact binary with an H-poor donor star. Following the spectral modelling of Galloway et al. (2008a) we set 0.5 ASM cts $\mathrm{s^{-1}} = 2.7 \times 10^{-10}\,\mathrm{erg\,cm^{-2}\,s^{-1}}$ (bolometric). The long-term average ASM count rate is 1.3 cts $\mathrm{s^{-1}}$. The most recent position, given by *Chandra*, is RA = $19^{\rm h}18^{\rm m}47\overset{\rm s}{.}871$, Dec. = $-05^\circ14'17\overset{''}{.}09$ (J2000), with an error $0\overset{''}{.}6$ (Iaria et al. 2006).[15] Galloway et al. (2008a) derive a distance of 8.9 ± 1.3 or 6.8 ± 1.0 kpc, depending on composition, from PRE bursts. Burst oscillations at ≈270 Hz have been detected in one X-ray burst (Galloway et al. 2001). The orbital period has been the subject of much debate in the literature, due in part to differences between the X-ray and orbital periods determined by dipping and photometry, respectively. The most recent papers on this topic seem to resolve the issue (Chou, Grindlay & Bloser 2001; Retter et al. 2002) by determining that the system displays superhumps rather than being a hierarchical triple. Chou et al. (2001) use X-ray dip times to derive $P_{\rm orb} = 3000.6508 \pm 0.0009$ s (in agreement with the value of $P_{\rm orb} = 3000.6452 \pm 0.0043$ s reported by Wen et al. (2006) using the *RXTE* All Sky Monitor), with $\dot{P}_{\rm orb} < 2.06 \times 10^{-11}$ (2σ upper limit). The X-ray dip ephemeris is $T_{\rm dip} = 50123.00944 \pm 1.4 \times 10^{-4}$ MJD. Whilst it is not entirely clear how the dip time relates to T_{90} we will assume in our initial analysis that this could be determined, and use the uncertainty in $T_{\rm dip}$ as an estimate of the uncertainty in T_{90}. The projected semimajor axis has not been measured, but we can impose some constraints. For the known orbital period, the assumption of Roche lobe overflow (equation 7) gives the mean mass of the donor as 158 g $\mathrm{cm^{-3}}$, implying a dwarf companion. X-ray burst properties imply a helium-rich donor. Optical spectroscopy shows large amounts of N, suggesting that the companion is a helium white dwarf rather than a helium star or an evolved secondary (Nelemans et al. 2006). Using the models of Deloye & Bildsten (2003) this implies a companion mass in the range 0.008–0.03 $\mathrm{M_\odot}$ (depending on core temperature). For dips we expect an inclination in the range 60°–75°. If we assume that the NS mass is in the range 1.2– 2.4 $\mathrm{M_\odot}$, equation (8) implies that $a_x \sin i$ must lie in the range 4–25 light-minute.

*3.4.15 XB 1254−690 ($\nu_{\rm b} = 95$ Hz)**

This source is persistent, at a steady level, with dips. Galloway et al. (2008a) carry out spectral modelling and find a persistent flux level of $9 \times 10^{-10}\,\mathrm{erg\,cm^{-2}\,s^{-1}}$ (bolometric). The *Chandra* position reported by Iaria et al. (2007) is RA = $12^{\rm h}57^{\rm m}37\overset{\rm s}{.}153$, Dec. = $-69^\circ17'18\overset{''}{.}98$, with a 90 per cent uncertainty radius of $0\overset{''}{.}6$.[16] Radius expansion in the precursor to a superburst leads to a distance estimate of 13 ± 3 kpc (in't Zand et al. 2003). Bhattacharyya (2007) reported tentative evidence of a burst oscillation at 95 Hz in one burst from this source. Motch et al. (1987) used optical photometry to find $P_{\rm orb} = 3.9334 \pm 0.0002$ h. This accords with the period of 3.88 ± 0.15 h derived from the X-ray light curve (Courvoisier et al. 1986), although the X-ray dips are not always present (Smale & Wachter 1999). Barnes et al. (2007) have recently updated the ephemeris derived by Motch et al. (1987) and report an X-ray dip

[15] This position has a substantial offset in declination from the optical counterpart (V1405 Aql) reported by (Gottwald et al. 1991), with RA = $19^{\rm h}18^{\rm m}47\overset{\rm s}{.}91$, Dec. = $-05^\circ14'08\overset{''}{.}7$ (J2000).

[16] This position is 2 arcsec away from the older optical counterpart position reported by Bradt & McClintock (1983).

time $T_{\rm dip} = 245\,3151.647 \pm 0.003$. Motch et al. (1987) showed that the X-ray dips in this source occurred at phase 0.84 (with zero at optical minimum), so they therefore derive $T_0 = {\rm JD}\ 245\,3151.509 \pm 0.003$. Barnes et al. (2007) have used phase-resolved spectroscopy of the He II λ4686 emission line (thought to be emitted in the inner accretion disc, close to the compact object) to estimate the velocity of the compact object, and find a velocity semi-amplitude $v_{\rm x} \sin i = 130 \pm 16\,{\rm km\,s^{-1}}$. Only the lower portion of this range is consistent with a main-sequence or undermassive companion star: however, we will use this value in our initial assessment of detectability.

3.4.16 EXO 0748−676 ($\nu_{\rm b} = 45$ Hz)

This system, which shows both dips and eclipses, has been persistently active since 1985. Based on the spectral modelling of Galloway et al. (2008a), we set 0.6 ASM cts $s^{-1} = 3.6 \times 10^{-10}\,{\rm erg\,cm^{-2}\,s^{-1}}$ (bolometric). The long-term average count rate is 0.76 cts s^{-1}. The best position, for the optical counterpart UY Volantis, is RA = $7^{\rm h}48^{\rm m}25\overset{\rm s}{.}0 \pm 0\overset{\rm s}{.}1$, Dec. = $-67^\circ 37' 31\overset{''}{.}7 \pm 0\overset{''}{.}7$ (B1950) (Wade et al. 1985). No more up to date position is available. The detection of PRE bursts that seem to be He-rich implies a distance of 7.4 ± 0.9 kpc (Galloway et al. 2008a). Villarreal & Strohmayer (2004) discovered burst oscillations at 45 Hz by averaging together spectra from 38 separate bursts detected between 1996 and early 2003. Timing of the eclipses constrains the orbital parameters. Attempts to compute an orbital ephemeris, however, have been complicated. The most recent study by Wolff et al. (2002) finds a large apparent period change of 8 ms over the period 1985–2000 – much larger than expected from orbital models – and intrinsic jitter that cannot be explained by any simple ephemeris. The reason for this variability has yet to be resolved, and it is not clear whether this represents genuine evolution in the binary period or not. Wolff et al. (2002) consider various models in their analysis, with orbital periods $P_{\rm orb} = 0.159\,3378 \pm 1 \times 10^{-7}$ d, mid-eclipse times $T_{90} = 46111.0739 \pm 0.0013$ MJD/TDB, and $|\dot{P}_{\rm orb}| \lesssim 10^{-11}$. More recent analysis by Wen et al. (2006), using ASM data, finds $P_{\rm orb} = 0.159\,3375 \pm 6 \times 10^{-7}$ d. The projected semimajor axis has not been measured directly, but can be constrained. Wolff et al. (2002) find eclipse durations 497.5 ± 6 s, which gives an eclipse half-angle $\theta_x = 6\overset{\circ}{.}543 \pm 0\overset{\circ}{.}015$. This constrains the inclination via equation (9). Roche lobe overflow (equation 7) implies a mean density for the donor star of 7.5 g cm^{-3}, suggesting a main-sequence or evolved companion. Maximum donor mass corresponds to a main-sequence donor, with $M_{\rm d} = 0.42\,{\rm M}_\odot$. Donor mass can be lower if the companion is evolved, so following Hynes et al. (2006) we take a minimum plausible companion mass of $0.07\,{\rm M}_\odot$. For the NS we consider masses in the range 1.2–2.4 $\rm M_\odot$. This implies that $a_{\rm x} \sin i$ lies in the range 0.11–0.84 light-second.

3.5 Kilohertz QPO sources

These remain the most difficult sources, because of the uncertainty in the precise relationship between kHz QPO separation (which varies) and spin frequency. Sources where a wide range of accretion rates have been sampled show variation, those where only a few accretion rates have been sampled (including the pulsars that have kHz QPOs) do not. To gauge the uncertainty, consider the kHz QPO separations recorded for those sources where we have either a spin frequency or a burst oscillation frequency, illustrated in Fig. 3.

(i) Aql X-1: 550-Hz intermittent pulsar, twin kHz QPO separation 278 ± 18 Hz (Barret, Boutelier & Miller 2008).

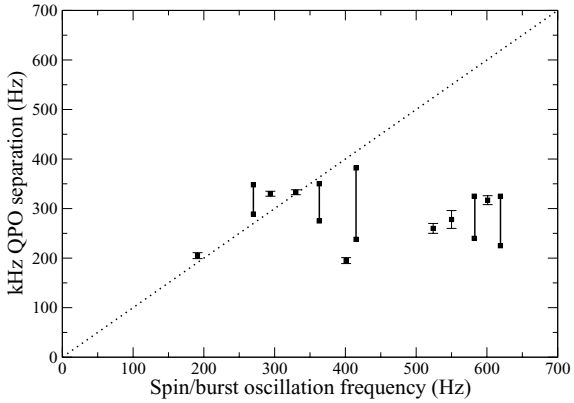

Figure 3. A comparison of twin kHz QPO separation and spin frequency or burst oscillation frequency for those sources that show both phenomena. The dotted line indicates equality of the two measures. For some objects kHz QPO separation is consistent with being constant: these are shown as single points with error bars. Note however that this may be due to poor sampling of source states. For five objects kHz QPO separation varies: these are shown as two points with a line indicating the range.

(ii) SAX J1808.4−3658: 401-Hz pulsar. Twin kHz QPOs observed once during the 2002 outburst. Wijnands et al. (2003) report a separation of 195 ± 6 Hz, later analysis by van Straaten, van der Klis & Wijnands (2005) using a different fitting technique gives a separation of 182 ± 8 Hz.

(iii) XTE J1807−294: 191-Hz pulsar. Twin kHz QPOs detected on several occasions during the 2003 outburst. The measured separations were consistent with the spin frequency, although the weighted average separation of 205 ± 6 Hz exceeds the spin at the 2.3σ level (Linares et al. 2005).

(iv) 4U 1608−522: 619-Hz burst oscillations. Twin kHz QPOs observed in the 1996 and 1998 outbursts, separations in the range 225–325 Hz (Méndez et al. 1998a,b).

(v) SAX J1750.8−2980: 601-Hz burst oscillations. Tentative detection of twin kHz QPOs with a separation of 317 ± 9 Hz (Kaaret et al. 2002).

(vi) 4U 1636−536: 582-Hz burst oscillations. Twin kHz QPOs detected on multiple occasions, with separations varying from 240 to 325 Hz (Wijnands et al. 1997a; Méndez, van der Klis & van Paradijs 1998c; Jonker, Méndez & van der Klis 2002a; di Salvo, Méndez & van der Klis 2003; Barret, Olive & Miller 2005).

(vii) KS 1731−260: 524-Hz burst oscillations. Twin kHz QPOs with separation 260.3 ± 9.6 Hz seen in one observation (Wijnands & van der Klis 1997).

(viii) 4U 0614+09: 415-Hz burst oscillations. Twin kHz QPOs have been seen on several occasions (Ford et al. 1997; van Straaten et al. 2000, 2002). Separations vary from 238 ± 7 to 382 ± 7 Hz (perhaps even as low as 213 ± 9 Hz although this figure is tentative).

(ix) 4U 1728−34: 363-Hz burst oscillations. Twin kHz QPOs detected on multiple occasions, with separations in the range 275–350 Hz (Strohmayer et al. 1996; Méndez & van der Klis 1999; di Salvo et al. 2001; Migliari et al. 2003).

(x) 4U 1702−429: 330-Hz burst oscillations. Twin kHz QPOs detected once in 1997, with a separation of 333 ± 5 Hz (Markwardt et al. 1999a).

(xi) IGR J17191−2821: 294-Hz burst oscillations. Twin kHz QPOs with separation 330 Hz (Klein-Wolt et al. 2007c).

(xii) 4U 1916−053: 270-Hz burst oscillations. Twin kHz QPOs detected several times in 1996. Separation was consistent with being

constant at 348 ± 12 Hz on four occasions; on the fifth it was 289 ± 5 Hz (Boirin et al. 2000).

It is far from clear that there is a direct (or indeed any) relationship between kHz QPO separation and spin, particularly for the high frequency sources. See Yin et al. (2007) and Méndez & Belloni (2007) for an extended discussion of this issue.

We now summarize the properties for the kHz QPO sources. Note that we exclude from our data set the peculiar X-ray binary Cir X-1 (1516−559), since it is not clear that our accretion torque model applies. Although this source has twin kHz QPOs (Boutloukos et al. 2006), it is thought to be a high-mass X-ray binary (Jonker et al. 2007) with a highly eccentric orbit (Murdin et al. 1980; Oosterbroek et al. 1995) where accretion disc formation is only sporadic (Johnston, Fender & Wu 1999; Johnston et al. 2001).

3.5.1 Cyg X-2 (2142+380)

This is a persistent Z source that has X-ray bursts. Galloway et al. (2008a) carried out spectral modelling and found that the long-term average flux is 1.1×10^{-8} erg cm^{-2} s^{-1}. The best position for this source, from the optical counterpart, is RA = $21^{\rm h}42^{\rm m}36\overset{\rm s}{.}91$, Dec. = $+38^\circ05'27\overset{''}{.}9$, with an accuracy of $0\overset{''}{.}5$ (B1950) (Giacconi et al. 1967; Bradt & McClintock 1983). No more up to date high-precision position is available. Galloway et al. (2008a) use the PRE bursts to estimate a distance of 10 ± 2 or 14 ± 3 kpc depending on composition. However, optical observations suggest a distance of only 7.2 ± 1.1 kpc (Orosz & Kuulkers 1999). Wijnands et al. (1998a) detected twin kHz QPOs in *RXTE* data from a few hours on 1997 July 2, when the source was on the horizontal branch. Peak separation was 346 ± 29 Hz. Kuznetsov (2002) reanalysed the same data and found a separation of 366 ± 18 Hz. Unsuccessful searches for persistent pulsations were carried out using *Ginga* data from 1987 to 1989 (Wood et al. 1991; Vaughan et al. 1994). Kuulkers, van der Klis & van Paradijs (1995) set upper limits on the presence of burst oscillations for frequencies below 256 Hz using *EXOSAT* data from 1983 to 1985, and Smale (1998) set upper limits on burst oscillations in the 200–600 Hz range for one burst observed with *RXTE*. The binary orbit can be constrained by optical observations of the companion star V1341 Cyg. The most recent spectroscopic observations, by Casares et al. (1998) give $P_{\rm orb}$ = 9.8444 ± 0.0003 d, T_{90} = 244 9339.50 ± 0.03 HJD, and e = 0.024 ± 0.015 (consistent at the 2σ level with being zero, which we assume in our initial analysis). Error bars are 1σ uncertainties. By measuring the projected velocity of the secondary star and its rotational broadening, then assuming tidal locking and Roche lobe overflow, they infer $v_{\rm x} \sin i = 29.9 \pm 3.6$ km s^{-1}. We use this value in our initial assessment of detectability.

3.5.2 GX 340+0 (1642−455)

This is a persistent Z source that has not shown X-ray bursts. Based on spectral modelling by Ford et al. (2000) we set 25 ASM cts s^{-1} = 2.3×10^{-8} erg cm^{-2} s^{-1} (bolometric). The long-term average count rate is 30 cts s^{-1}. The best position, given by the radio counterpart, is RA = $16^{\rm h}45^{\rm m}44\overset{\rm s}{.}60 \pm 0\overset{\rm s}{.}02$, Dec. = $-45^\circ37'53\overset{''}{.}6 \pm 0\overset{''}{.}3$ (J2000) (Penninx et al. 1993). Christian & Swank (1997) use Einstein observations to establish an upper limit on the distance of 11 ± 3.3 kpc.[17] Twin kHz QPOs have been detected in *RXTE* data from 1997 to 1998, with separations in the range 275 ± 24 to 413 ± 21 Hz (Jonker et al. 1998, 2000). However, for the sample as a whole, the separation is formally consistent with being constant at 339 ± 8 Hz. Unsuccessful searches for persistent pulsations have been carried out using *Ginga* data (Wood et al. 1991; Vaughan et al. 1994). The orbital parameters are not known.

3.5.3 4U 1735−44

This is a bright persistent atoll source that has both bursts and superbursts. Using the spectral modelling of Galloway et al. (2008a) we set 18 ASM cts s^{-1} = 9.1×10^{-9} erg cm^{-2} s^{-1} (bolometric). The long-term average count rate is 14 cts s^{-1}. The best position, for the optical counterpart V926 Sco, is RA = $17^{\rm h}35^{\rm m}19\overset{\rm s}{.}28$, Dec. = $-44^\circ25'20\overset{''}{.}3$, uncertainty $<1'$ (Bradt & McClintock 1983). No more up to date position is available. The distance inferred from the radius expansion bursts (assuming He limit) is 8.5 ± 1.3 kpc (Galloway et al. 2008a). Twin kHz QPOs were seen in *RXTE* observations on 1998 May 30–31. Peak separation varied from 296 ± 12 to 341 ± 7 Hz, inconsistent at the 3.1σ level with being constant (Ford et al. 1998). Jongert & van der Klis (1996) placed upper limits on the presence of burst oscillations (up to 256 Hz) using *EXOSAT* data: no figures have been reported for the *RXTE* burst sample. The orbital parameters can be constrained by optical observations. Casares et al. (2006) report a recent spectroscopic ephemeris, with $P_{\rm orb}$ = 0.193 833 51 ± 3.2×10^{-7} d, in agreement with the most recent photometric ephemeris (Augusteijn et al. 1998). The time of inferior conjunction of the donor star T_{90} = 245 2813.495 ± 0.003 HJD. Further measurements and source modelling suggest that velocity semi-amplitude of the donor star is in the range 215–381 km s^{-1}, with a mass ratio $m_{\rm d}/m_{\rm x}$ in the range 0.05–0.41. This would suggest $v_{\rm x} \sin i < 156$ km s^{-1} and we use this limit in our initial estimate of detectability.

3.5.4 GX 5−1 (1758−250)

This is a persistent non-bursting Z source, located in the highly absorbed Galactic bulge region. Based on spectral modelling by Ford et al. (2000), we set 50 ASM cts s^{-1} = 3.8×10^{-8} erg cm^{-2} s^{-1} (bolometric). The long-term average ASM count rate is 70 cts s^{-1}. The best position, for the radio counterpart, is RA = $18^{\rm h}01^{\rm m}08\overset{\rm s}{.}233$, Dec. = $-25^\circ04'42\overset{''}{.}044$ (J2000), positional uncertainty $0\overset{''}{.}040$ (Berendsen et al. 2000). Distance to this source is poorly constrained, although Christian & Swank (1997) give an upper limit of 9 ± 2.7 kpc.[18] Twin kHz QPOs have been reported in *RXTE* observations from 1996 to 2000 (Wijnands et al. 1998b; Jonker et al. 2002b). Peak separation is not constant, but varies from 232 ± 13 to 344 ± 12 Hz. Unsuccessful searches for persistent pulsations were carried out using *Ginga* data from 1987 (Wood et al. 1991; Vaughan et al. 1994). The orbital parameters are unknown.

3.5.5 4U 1820−30

This is a persistent bursting atoll source with regular dipping cycles. Using the spectral modelling of Galloway et al. (2008a) we set 32 ASM cts s^{-1} = 2.1×10^{-8} erg cm^{-2} s^{-1} (bolometric). The long-term average ASM count rate is 20.6 cts s^{-1}. The best position,

[17] Ford et al. (2000) quote a lower distance for this source, but the value given does not tally with that in the original reference that they cite.

[18] The distance of 6.4 ± 0.6 kpc derived by Penninx (1989), cited incorrectly as 9.2 ± 0.7 kpc by Fender & Hendry (2000), Migliari & Fender (2006) is highly model dependent.

from *Hubble Space Telescope* observations of the optical counterpart, is RA = $18^{\rm h}23^{\rm m}40\overset{\rm s}{.}453 \pm 0\overset{\rm s}{.}012$, Dec. = $-30^\circ21'40\overset{''}{.}08 \pm 0\overset{''}{.}15$ (J2000, 1σ errors), (Sosin & King 1995).[19] The source is located in the globular cluster NGC 6624, and optical observations imply a cluster distance of 7.6 ± 0.4 kpc (Heasley et al. 2000). The distance estimated from X-ray bursts is ≈6.6 kpc (Vacca, Lewin & van Paradijs 1986; Kuulkers et al. 2003). Twin kHz QPOs have been detected by *RXTE* on several occasions (Smale, Zhang & White 1997; Zhang et al. 1998a; Altamirano et al. 2005). Measured separations vary in the range 220–350 Hz, although the uncertainties are such that the separation is consistent with being constant at ≈275 Hz. Dib et al. (2005) have placed extremely stringent limits on the presence of persistent pulsations up to 2000 Hz using archival *RXTE* data, for all $a_{\rm x} \sin i < 16.8$ light-minute (superceding earlier work by Wood et al. (1991) and Vaughan et al. (1994)). Jongert & van der Klis (1996) placed upper limits on the presence of burst oscillations up to 256 Hz for *EXOSAT* bursts. The most up to date X-ray ephemeris, using all data from Ariel 5, *Ginga* and *RXTE*, gives $P_{\rm orb} = 685.0119 \pm 1.02 \times 10^{-4}$ s, $\dot{P}_{\rm orb} = (-7.54 \pm 3.21) \times 10^{-13}{\rm ss}^{-1}$, and the time of maximum X-ray light is 244 2803.635 64 $\pm$ 2.2 $\times$ 10^{-4} HJD (Chou & Grindlay 2001). Noting that an ephemeris of similar accuracy can also be derived from ultraviolet (UV) data (Anderson et al. 1997), we will assume that the reference time could if required be related to a known phase in the orbit. There is also a superorbital periodicity of ≈176 d, most likely due to perturbations of the orbital eccentricity (up to $e = 0.004$ by a third member of the system (Chou & Grindlay 2001; Zdziarski, Wen & Gierliński 2007), but we neglect this in our initial assessment. The projected semimajor axis has not been measured, but can be constrained. The assumption of Roche lobe overflow (equation 7) gives a mean donor density of 3300 g cm^{-3}, implying a white dwarf companion. The donor must also be helium-rich to explain the X-ray burst properties. Helium white dwarf models of Deloye & Bildsten (2003) suggest a donor mass in the range 0.07– 0.08 $M_\odot$ (depending on temperature). Anderson et al. (1997) inferred an inclination in the range 35°–50° from observations of the UV counterpart. Ballantyne & Strohmayer (2004), analysing superburst data, inferred a slightly lower value, so we will consider a minimum inclination of 30°. Then for NS masses in the range 1.2– 2.4 $M_\odot$ we predict $a_{\rm x} \sin i$ in the range 7–20 light-minute. Recent modelling by Zdziarski et al. (2007) suggests that the superorbital variability may eventually pose even tighter constraints on the system.

3.5.6 Sco X-1 (1617−155)

This is the closest accreting NS in our study, and is a persistent Z source. Using the spectral modelling of Ford et al. (2000) we set 920 ASM cts s^{-1} = 4×10^{-7} erg cm^{-2} s^{-1} (bolometric). The long-term average ASM count rate is 892 cts s^{-1}. The most accurate position for the source, given by VLBA measurements, is RA = $16^{\rm h}19^{\rm m}55\overset{\rm s}{.}0850$, Dec. = $-15^\circ38'24\overset{''}{.}9$, with an uncertainty of $0\overset{''}{.}5$ (Bradshaw, Fomalont & Geldzahler 1999). The source has also has a measurable proper motion, which we neglect in this initial analysis (Bradshaw et al. 1999). The distance, measured by parallax, is 2.8 ± 0.3 kpc (Bradshaw et al. 1999). Twin kHz QPOs are observed, with separations in the range 240–310 Hz (van der Klis et al. 1996, 1997; Méndez & van der Klis 2000). There have been unsuccessful searches for persistent pulsations up to 256 Hz using *EXOSAT* (Middleditch & Priedhorsky 1986) and up to 512 Hz using *Ginga* data (Wood et al. 1991; Hertz et al. 1992; Vaughan et al. 1994). Photometric observations of the optical counterpart V818 Sco imply an orbital period of 68 023.84 $\pm$ 0.08 s (Gottlieb, Wright & Liller 1975), although analysis of *RXTE* ASM data by Vanderlinde, Levine & Rappaport (2003) suggests that the true period could in fact be slightly longer, at 68 170 s. Analysis by Steeghs & Casares (2002) indicates $v_{\rm x} \sin i = 40 \pm 5$ km s^{-1}. Assuming the orbital period of Gottlieb et al. (1975), Steeghs & Casares (2002) derive an ephemeris with $T_{90} = 245\,1358.568 \pm 0.003$ HJD.[20]

3.5.7 GX 17+2 (1813−140)

This is a persistent Z source with X-ray bursts. Using the spectral modelling of Galloway et al. (2008a) we set 40 ASM cts s^{-1} = 1.6×10^{-8} erg cm^{-2} s^{-1} (bolometric). The long-term average ASM count rate is 45 cts s^{-1}. The most accurate position, from VLA observations of the radio counterpart, is RA = $18^{\rm h}16^{\rm m}1\overset{\rm s}{.}389 \pm 0\overset{''}{.}06$, Dec. = $-14^\circ02'10\overset{''}{.}62 \pm 0\overset{''}{.}04$ (J2000), 1σ uncertainties in position (Deutsch et al. 1999). This is within the *Chandra* error circle for the X-ray position (Callanan et al. 2002). Analysis of X-ray bursts suggests a distance of either 9.8 ± 0.4 or 12.8 ± 0.6 kpc (Galloway et al. 2008a). However, there are questions over how to correct for the super-Eddington persistent flux, and the true distance could be lower (Kuulkers et al. 2002). Twin kHz QPOs have been observed on multiple occasions (Wijnands et al. 1997b; Homan et al. 2002). Separation, which varies from 239 ± 17 to 308 ± 14 Hz, is not constant at the 97 per cent confidence level. Upper limits on the presence of persistent pulsations in *Ginga* data were reported by Wood et al. (1991) and Vaughan et al. (1994). Upper limits on the presence of burst oscillations in *EXOSAT* and *RXTE* data have been reported by Kuulkers et al. (1997) and Kuulkers et al. (2002). The orbital parameters are not known.

3.5.8 XTE J2123−058

This is a transient bursting atoll source in the Galactic halo, with one recorded outburst in 1998. Using the spectral modelling of Galloway et al. (2008a) we set 6.4 ASM cts s^{-1} = 2.1×10^{-9} erg cm^{-2} s^{-1} (bolometric). The average ASM count rate over the 50-d outburst was 2.7 cts s^{-1}, yielding a long-term average count rate over *RXTE*'s lifetime of 0.03 cts s^{-1}. The most accurate position, as measured by *Chandra*, is RA = $21^{\rm h}23^{\rm m}14\overset{\rm s}{.}54$, Dec. = $-05^\circ47'53\overset{''}{.}2$ (J2000, uncertainty $0\overset{''}{.}6$) (Tomsick et al. 2004). Tomsick et al. (2001) infer a distance of 8.5 ± 2.5 kpc, consistent with the distance of 9.6 ± 1.3 kpc inferred by Casares et al. (2002). Twin kHz QPOs were detected during one observation, with separations in the range 255 ± 14 to 276 ± 9 Hz (Homan et al. 1999; Tomsick et al. 1999). Casares et al. (2002) use spectroscopic and photometric measurements to derive $P_{\rm orb} = 21\,447.6 \pm 0.2$ s (1σ errors). Tomsick et al. (2002), however, derive $P_{\rm orb} = 21\,442.3 \pm 1.8$ (1σ errors). This discrepancy, and results from earlier photometric measurements by Tomsick et al. (1999) and Zurita et al. (2000), have yet to be resolved. The most recent time of minimum optical light $T_{90} = 245\,1779.652 \pm 0.001$

[19] Obtaining a more accurate radio position is complicated by the presence of a nearby pulsar (Migliari et al. 2004).

[20] Abbott et al. (2007a) use a slightly larger uncertainty on T_{90} in their searches for GWs from Sco X-1, to account for the time elapsed since the Steeghs & Casares (2002) measurement. For consistency with the rest of our analysis we use the smaller uncertainty, assuming that the measurement could be redone today to the same level of accuracy.

HJD. The projected velocity $v_x \sin i$ is also constrained. Casares et al. (2002) attempt to measure this directly, and find $v_x \sin i = 140 \pm 27\,\mathrm{km\,s^{-1}}$. Tomsick et al. (2001, 2002) measure the projected orbital velocity and rotational velocity of the companion. Assuming a Roche lobe filling and tidally locked companion they infer the mass ratio, and hence a projected orbital velocity for the NS of $v_x \sin i = 110^{+54}_{-36}\,\mathrm{km\,s^{-1}}$. Shahbaz et al. (2003) use the projected orbital velocity of the companion measured by Casares et al. (2002) and use more sophisticated models of the system to give the mass ratio. The resulting projected orbital velocity is $v_x \sin i = 103^{+46}_{-7}\,\mathrm{km\,s^{-1}}$ (90 per cent confidence). In our initial analysis, however, we use the direct measurement by Casares et al. (2002).

3.5.9 GX 349+2 (1702−363, Sco X-2)

This persistent Z source does not show X-ray bursts. Using the modelling of Zhang, Strohmayer & Swank (1998b), we set 43 ASM cts $\mathrm{s^{-1}} = 1.4 \times 10^{-8}\,\mathrm{erg\,cm^{-2}\,s^{-1}}$ (2–10 keV). There is no detailed spectral modelling available for this source, so we adopt a bolometric correction factor of 2. The long-term average ASM count rate is 50.2 cts $\mathrm{s^{-1}}$. The best position, from VLA measurements of the radio counterpart, is RA = $17^{\mathrm{h}}02^{\mathrm{m}}22\overset{\mathrm{s}}{.}93$, Dec. = $-36^\circ 21' 20\overset{''}{.}3$ (B1950, accuracy $0\overset{''}{.}5$) (Cooke & Ponman 1991). Iaria et al. (2004) infer a distance of 3.6–4.4 kpc from *BeppoSAX* observations. Twin kHz QPOs were detected by *RXTE* in 1998 January, with a separation of 266 ± 13 Hz (Zhang et al. 1998b), confirmed by O'Neill et al. (2002). The source has however rarely been observed in the state where kHz QPOs are prevalent. A search for persistent pulsations in *Ginga* data from 1989 was unsuccessful (Vaughan et al. 1994). The binary period, measured using optical photometry and spectroscopy, has been the subject of some debate (Southwell, Casares & Charles 1996; Wachter & Margon 1996; Barziv et al. 1997), but is now established as $P_{\mathrm{orb}} = 22.5 \pm 0.1$ h (1σ error) (Wachter 1997). The other binary parameters have not been measured, although we can constrain $a_x \sin i$. The assumption of Roche lobe overflow (equation 7) gives a mean donor density 0.2 g $\mathrm{cm^{-3}}$, which requires a donor that has evolved off the main sequence. In the absence of better constraints we will assume a mass ratio $m_d/m_x < 0.8$. For the range of NS masses considered (1.2–2.4 $\mathrm{M_\odot}$) this implies $a_x \sin i < 7$ light-second.

4 SEARCHING WITH PARAMETER UNCERTAINTIES

Let us summarize briefly the GW emission from an NS in a binary system. We assume that the centre of mass of the binary is not accelerating in the solar system barycentre (SSB) frame. The timing model for the arrival times of the wavefronts of the GW is taken to be the usual one (Taylor & Weisberg 1989). Let T be the arrival time of the wave at the SSB, τ the proper time of emission in the rest frame of the NS and t the time in the rest frame of the GW detector. The quantities T and τ are related by

$$T - T_0 = \tau + \Delta_R + \Delta_E + \Delta_S, \tag{10}$$

where Δ_R is the Roemer time delay accounting for the light travel time across the binary, Δ_E and Δ_S are, respectively, the orbital Einstein and Shapiro time delays in the binary, and T_0 is a reference time. There are no additional timing delays due to dispersion. It turns out that, for our purposes, the Roemer delay is the most significant contribution. If $\boldsymbol{r}$ is the vector joining the centre of mass of the binary system with the NS, and $\boldsymbol{n}$ is the unit vector pointing from the SSB to the source, then

$$\Delta_R = -\frac{\boldsymbol{r}\cdot\boldsymbol{n}}{c}. \tag{11}$$

There is then a similar relation between T and the arrival time t at the earth based detector, and we assume that this can be corrected for since the sky position is known.

In the models that we are considering, the intrinsic GW frequency ν depends on the spin frequency ν_s. The phase of the GW at the SSB is

$$\phi(t) = \Phi_0 + \Phi(t), \tag{12}$$

where

$$\Phi(T) = 2\pi\nu\left[T - \frac{\boldsymbol{n}\cdot\boldsymbol{r}(T)}{c}\right]. \tag{13}$$

Inclusion of frequency derivatives in this phase model is straightforward, and we do not write it down explicitly. Since the GW amplitudes are expected to be very weak and the output of the GW detectors dominated by noise, knowledge of the waveform, especially its phase, is crucial for detection.

The phase $\Phi(t)$ depends on the orbital parameters introduced in Section 3.2: P_{orb}, $\dot{P}_{\mathrm{orb}}$, T_{asc}, $a_x \sin i$ and e. In addition, there are two parameters specifying the orientation of the orbital plane: the inclination angle ι and the argument of periapsis ω. Of these seven parameters, only six are required to define the phase model because of the projection along the line of sight $\boldsymbol{n}$; see Dhurandhar & Vecchio (2001) for further details. Taking the spin frequency ν_s and its time derivative $\dot{\nu}_s$ into account, we therefore have a total of eight parameters which determine the frequency evolution of the signal: (ν_s, $\dot{\nu}_s$, $a_x \sin i$, e, P_{orb}, $\dot{P}_{\mathrm{orb}}$, T_{asc}, ω).

This is clearly a very large parameter space, and a search over all these parameters using a sufficiently large data volume will be a big data analysis challenge. Let us therefore make some simplifying assumptions: $\dot{\nu}_s = 0$, $\dot{P}_{\mathrm{orb}} = 0$ and $e = 0$; i.e. we assume an NS spin perfectly balanced between accretion and gravitational radiation, and a circular orbit which does not decay appreciably over the course of the observation time. These assumptions may not hold for the sources and for the large observation times that we are considering, and an actual search might very well have to take some or all of these effects into account. However, for assessing the detection prospects as we want to do here, this simplification is useful, since adding the extra parameters will further increase the number of templates. For some of the more promising sources at or near the detection threshold, these assumptions will need to be revisited in greater detail. Some of these extra parameters may need to included, and the resulting search might again become computationally difficult; this will be studied in greater detail in future work.

In the case when the orbit is circular ($e = 0$), which we shall assume in the rest of this paper, the argument of periapsis and the initial orbital phase combine additively into a single parameter so that we are left with only four search parameters: $\boldsymbol{\lambda} = (\nu_s, a_x \sin i, P_{\mathrm{orb}}, T_{\mathrm{asc}})$; we shall denote the components of $\boldsymbol{\lambda}$ by λ^i with $i = 0, \ldots, 3$.

4.1 Template counting

To determine the computational cost involved in searching the parameter space described above, we need to calculate the number of templates required. A calculation of the required number of templates to search a portion of the parameter space is based on demanding a certain maximum mismatch between the templates at

neighbouring points in parameter space. This also guarantees that the true signal will not have more than the given mismatch to at least one of the search templates. The mismatch between waveform templates is measured simply as the fractional loss in the S/N when one waveform is filtered (folded) by the other. This fractional loss can be regarded as a distance measure between points in parameter space, and this leads naturally to the definition of a parameter space metric g_{ij} (Sathyaprakash & Dhurandhar 1991, 1994; Owen 1996; Prix 2007b). Using the metric, we write the proper distance squared (the 'mismatch') between two infinitesimally separated parameter space points as

$$m = g_{ij} \mathrm{d}\lambda^i \mathrm{d}\lambda^j. \tag{14}$$

The size of the parameter space is then given by the volume measure determined by the metric in the usual way. Then, assuming that we cover this parameter space by a lattice grid, the number of templates is the total parameter space volume divided by the volume of each unit cell which makes up the lattice.

The optimal choice of the lattice is determined by a solution to the so-called sphere-covering problem (Prix 2007a). For our purposes, we shall use a simple cubic grid, and there are two reasons why it is acceptable to use this approximation. First, the dimensionality of the reduced parameter space that we are looking at is low enough that the improvement in the template placement efficiency is not more than a factor of about 2 or 3 (Prix 2007a). Furthermore, this improvement in the efficiency does not actually lead to a corresponding factor of 2–3 improvement in the sensitivity; the gain in the coherent integration time afforded by this improvement is much smaller because the computational cost typically scales as a large power of the coherent integration time. Finally, the size of each unit cell is chosen based on the fractional loss in S/N, i.e. the mismatch m, that we are willing to tolerate; we shall use a reference value of $m = 30$ per cent in this paper.

The first detailed study of the parameter space metric for an NS in a binary orbit was carried out in Dhurandhar & Vecchio (2001) for a coherent matched filter search. The search for gravitational radiation from Sco X-1 reported in Abbott et al. (2007a) was the first and so far, only application of this paper. The aim of this section is mainly to collect some template counting equations for later use. These equations can all be derived in a more or less straightforward manner from the results of Dhurandhar & Vecchio (2001). The main difference is that Dhurandhar & Vecchio (2001) use notation and variables targeted towards GW data analysis, while here we choose to use notation more familiar to an astronomy/astrophysics audience.

The first issue is the number of parameters which must be searched. Let us denote by $\Delta\lambda^i = \lambda^i_{\max} - \lambda^i_{\min}$ the uncertainty in λ^i from astronomical observations; we assume the region to be rectangular. Since the proper length of the line in the λ^i direction is $\int_{\lambda^i_{\min}}^{\lambda^i_{\max}} \sqrt{g_{ii}} \mathrm{d}\lambda^i$, a useful upper bound on this proper length is to use the maximum value of g_{ii}, i.e. $(g^{\max}_{ii})^{1/2}\Delta\lambda^i$. This proper distance can then be compared with our reference mismatch m, and we get a measure of the number of templates required in the λ^i direction:

$$N_{\lambda^i} = \Delta\lambda^i \sqrt{\frac{g^{\max}_{ii}}{m}}. \tag{15}$$

If $N_{\lambda^i} < 1$, it indicates that the λ^i direction can be covered by just a single template, and the effective dimensionality of our parameter space is reduced by 1. The number of templates for the frequency is

$$N_\nu = \Delta\nu \frac{\pi T_{\mathrm{obs}}}{\sqrt{3m}}. \tag{16}$$

The uncertainty $\Delta\nu$ relates directly to the uncertainty in spin $\Delta\nu_{\mathrm{s}}$. We shall ignore the correlations of ν with the other parameters; this approximation will suffice for our purposes. For the other directions, the expressions for N_{λ^i} have simple expressions in two regimes: $T_{\mathrm{obs}} \ll P_{\mathrm{orb}}$ and $T_{\mathrm{obs}} \gg P_{\mathrm{orb}}$.

In the limit of large observation times, $T_{\mathrm{obs}} \gg P_{\mathrm{orb}}$, we have

$$N_{a_{\mathrm{p}}} = \Delta a_{\mathrm{p}} \frac{\sqrt{2}\pi\nu_{\max}}{\sqrt{m}}, \tag{17}$$

$$N_{T_{\mathrm{asc}}} = \Delta T_{\mathrm{asc}} \frac{\sqrt{8}\pi^2 a_{\mathrm{p}}^{\max}\nu_{\max}}{P_{\mathrm{orb}}^{\min}\sqrt{m}}, \tag{18}$$

$$N_{P_{\mathrm{orb}}} = \Delta P_{\mathrm{orb}} \frac{\sqrt{8}\pi^2 a_{\mathrm{p}}^{\max}\nu_{\max}T_{\mathrm{obs}}}{\sqrt{3m}\left(P_{\mathrm{orb}}^{\min}\right)^2}. \tag{19}$$

In the other limiting case $T_{\mathrm{obs}} \ll P_{\mathrm{orb}}$, we get

$$N_{a_{\mathrm{p}}} = \Delta a_{\mathrm{p}} \frac{2\pi^3\nu_{\max}T_{\mathrm{obs}}^2}{\sqrt{45m}\left(P_{\mathrm{orb}}^{\min}\right)^2}, \tag{20}$$

$$N_{T_{\mathrm{asc}}} = \Delta T_{\mathrm{asc}} \frac{8\pi^5 a_{\mathrm{p}}\nu_{\max}T_{\mathrm{obs}}^3}{\sqrt{175m}\left(P_{\mathrm{orb}}^{\min}\right)^4}, \tag{21}$$

$$N_{P_{\mathrm{orb}}} = \Delta P_{\mathrm{orb}} \frac{4\pi^3 a_{\mathrm{p}}\nu_{\max}T_{\mathrm{obs}}^2}{\sqrt{45m}\left(P_{\mathrm{orb}}^{\min}\right)^3}. \tag{22}$$

For a search over all three parameters at once, the total number of templates in $(a_{\mathrm{p}}, P_{\mathrm{orb}}, T_{\mathrm{asc}})$ space is, for $T_{\mathrm{obs}} \gg P_{\mathrm{orb}}$,

$$N_{a_{\mathrm{p}}P_{\mathrm{orb}}T_{\mathrm{asc}}} = \frac{\pi^5\nu_{\max}^3 T_{\mathrm{obs}}}{\sqrt{8m^3}} \Delta\left[a_{\mathrm{p}}^3\right] \Delta\left[P_{\mathrm{orb}}^{-2}\right] \Delta[T_{\mathrm{asc}}], \tag{23}$$

while for $T_{\mathrm{obs}} \ll P_{\mathrm{orb}}$ it is

$$N_{a_{\mathrm{p}}P_{\mathrm{orb}}T_{\mathrm{asc}}} = \frac{\sqrt{48}\pi^{13}\nu_{\max}^3 T_{\mathrm{obs}}^9}{\sqrt{7027\,611\,500m^3}} \Delta\left[a_{\mathrm{p}}^3\right] \Delta\left[P_{\mathrm{orb}}^{-10}\right] \Delta[T_{\mathrm{asc}}]. \tag{24}$$

Note that $N_{a_{\mathrm{p}}} N_{P_{\mathrm{orb}}} N_{T_{\mathrm{asc}}} \neq N_{a_{\mathrm{p}}P_{\mathrm{orb}}T_{\mathrm{asc}}}$. This happens because the correlations between the different parameters (i.e. the off-diagonal terms in the metric) can be very important, especially for short observation times.

Similarly, we shall require the equations in the case when one of the coordinates can be ignored and the search can be performed in a two-dimensional subspace. The equations for $T_{\mathrm{obs}} \gg P_{\mathrm{orb}}$ are

$$N_{a_{\mathrm{p}}T_{\mathrm{asc}}} = \frac{\pi^3\nu_{\max}^2}{P_{\mathrm{orb}}m} \Delta\left[a_{\mathrm{p}}^2\right] \Delta[T_{\mathrm{asc}}], \tag{25}$$

$$N_{P_{\mathrm{orb}}T_{\mathrm{asc}}} = \frac{\pi^4 (a_{\mathrm{p}}^{\max})^2\nu_{\max}^2 T_{\mathrm{obs}}}{m\sqrt{3}} \Delta\left[P_{\mathrm{orb}}^{-2}\right] \Delta[T_{\mathrm{asc}}], \tag{26}$$

$$N_{a_{\mathrm{p}}P_{\mathrm{orb}}} = \frac{\pi^3\nu_{\max}^2 T_{\mathrm{obs}}}{m\sqrt{3}} \Delta\left[a_{\mathrm{p}}^2\right] \Delta\left[P_{\mathrm{orb}}^{-1}\right]. \tag{27}$$

Finally, for $T_{\mathrm{obs}} \ll P_{\mathrm{orb}}$ we get

$$N_{a_{\mathrm{p}}T_{\mathrm{asc}}} = \frac{2\pi^8\nu_{\max}^2 T_{\mathrm{obs}}^5}{45\sqrt{35}m P_{\mathrm{orb}}^6} \Delta\left[a_{\mathrm{p}}^2\right] \Delta[T_{\mathrm{asc}}], \tag{28}$$

$$N_{P_{\mathrm{orb}}T_{\mathrm{asc}}} = \frac{4\pi^8\nu_{\max}^2 T_{\mathrm{obs}}^5 (a_{\mathrm{p}}^{\max})^2}{135\sqrt{35}m} \Delta\left[P_{\mathrm{orb}}^{-6}\right] \Delta[T_{\mathrm{asc}}], \tag{29}$$

$$N_{a_{\mathrm{p}}P_{\mathrm{orb}}} = \frac{8\pi^8\nu_{\max}^2 T_{\mathrm{obs}}^6}{2835\sqrt{5}m} \Delta[P_{\mathrm{orb}}^{-6}] \Delta\left[a_{\mathrm{p}}^2\right]. \tag{30}$$

We take the total number of templates to be N_ν (if it exceeds unity) multiplied by the number of templates in (a_p, P_{orb}, T_{asc}) space.

While these equations might not seem very illuminating, two important features are worth remembering. First, and probably most importantly, the scaling of the number of templates with T_{obs} is very different in the two regimes $T_{obs} \ll P_{orb}$ and $T_{obs} \gg P_{orb}$. For example, in equations (23) and (24), the scaling is $\mathcal{O}(T_{obs})$ when $T_{obs} \gg P_{orb}$, while it is $\mathcal{O}(T_{obs}^9)$ for small T_{obs}. This will have important consequences for GW data analysis, as we shall see later. Secondly, computational cost issues become more important at higher frequencies and for tighter orbits, because the number of templates typically increases when ν_{max} increases or P_{orb} decreases.

Finally, we say a few words about the positional accuracy required for the GW searches. We do not wish to consider searches over sky position, and thus it is important to know the position sufficiently accurately beforehand. The periodic wave searches get their sky position information from the Doppler pattern of the frequency evolution. The sky position accuracy $\Delta\theta$ depends strongly on the coherent observation time T_{coh}. For short observation times ($\ll$1 yr) $\Delta\theta$ increases as roughly $\mathcal{O}(T_{obs}^2)$ or $\mathcal{O}(T_{obs}^3)$ (Brady et al. 1998; Prix 2007b). This increase in the sky-resolution eventually saturates when T_{coh} becomes comparable to a year. The ultimate limit on $\Delta\theta$ is the diffraction limit, with Earth's orbit being the aperture size. Thus, the smallest error box for position will be $\Delta\theta \sim \lambda_{gw}/1$ au where λ_{gw} is the wavelength of the GW. This corresponds to about 8 arcsec at 50 Hz and it is inversely proportional to frequency; this requirement is easily met for all the sources we are considering. It might in fact be possible to use a sky position mismatch as a veto to rule out potential candidates. For a candidate with given values of the frequency and orbital parameters, we could calculate the detection statistic at mismatched sky positions and verify that the S/N does decrease as expected. The work of Prix & Itoh (2005) [see also appendix A of Krishnan et al. (2004)] which studies correlations in frequency and sky position mismatch might be useful for this purpose.

5 FUTURE DETECTABILITY

5.1 Best case detectability for various emission models

We will start by looking at the best case scenarios for detection, and ask what would happen if we knew all of the parameters to sufficient accuracy that we only had to search one template for each source, using the flux information collected in Section 3 and summarized in Table 1. In this case computational cost is not an issue, and we can integrate for long periods. We will assume that the system is in perfect spin balance (so that we can neglect spin derivatives), and that GW torques are the only negative torques operating in the system. This means that we neglect any possible spin-down effects due to the interaction of the NS magnetosphere with the accretion disc, or any magnetic dipole spin-down.

In Section 2 we gave an overview of the spin balance model and calculated the best case detectability assuming GW emission due to a 'mountain', balancing the long-term average flux. The results were shown in Fig. 2. We also however need to consider whether the quadrupole Q required for spin balance is feasible:

$$Q = 7.4 \times 10^{35} \mathrm{g\,cm^2} \left(\frac{R_{10}^3}{M_{1.4}}\right)^{1/4} d_{kpc} F_{-8}^{1/2} \left(\frac{1\,\mathrm{kHz}}{\nu_s}\right)^{5/2}, \qquad (31)$$

where $d_{kpc} = d/(1\,\mathrm{kpc})$. Fig. 4 shows the required quadrupole (scaled by $10^{45}\,\mathrm{g\,cm^2}$, the approximate moment of inertia of an NS), assuming the long-term average flux. We also show the maximum sustainable quadrupole for an accreted crust computed by Haskell et al. (2006) [note that these authors compute $Q_{22} = (15/8\pi)^{1/2}Q$]. The values required for the slower spinning bursters are at the upper boundary of what is thought to be feasible, and if the spin of the kHz QPO sources is slower than the measured separations, the required quadrupole may exceed this value. However, magnetic confinement could support larger quadrupoles (Melatos & Payne 2005; Payne & Melatos 2006).

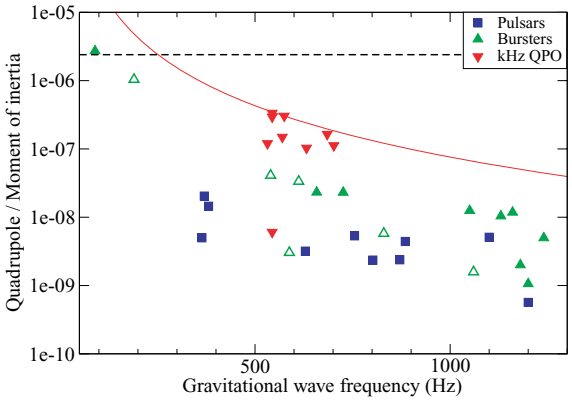

Figure 4. The quadrupole Q required for spin balance in the mountain scenario given the long-term average flux. Q is scaled by $10^{45}\,\mathrm{g\,cm^2}$ (the approximate moment of inertia of an NS). The frequency at which the kHz QPO symbols appear is the centre of the measured range of separations. The solid line illustrates how the requisite Q would vary for Sco X-1 if this is not the spin frequency. The dashed line shows the maximum feasible non-magnetic quadrupole calculated by Haskell et al. (2006). The uncertainty in the inferred quadrupole is not shown, but can be substantial since it depends on the distance to the star (see Table 1).

It is clear from Fig. 2 that if the kHz QPO sources do have spins in the range inferred from the kHz QPO separation (or higher) then Sco X-1 is the only source that is in principle marginally detectable by Enhanced LIGO. Predicted amplitude would of course rise if the spin frequency were substantially lower, and if this were the case both Sco X-1 and GX 5−1 could be within detectable range for Enhanced LIGO (although the inferred quadrupole would be large, approaching the maximum thought possible).

For Advanced LIGO, several of the kHz QPO sources are in principle detectable for a single template search in the broad-band configuration. Two of the burst oscillation sources (XB 1254−690 and 4U 1728−34) are also marginally detectable within the given narrow-band envelope. Several other burst oscillation sources might be detectable if it were possible to push the narrow-band envelope further down towards the thermal noise floor. If the proposed ET reaches its design specification, several more of the burst and kHz QPO sources might be reachable, although the pulsars remain undetectable.

One of the major uncertainties in our modelling is the response to variations in accretion rate. In order to gauge this effect we therefore consider an alternative model for the transients, one in which the GW torque balances the accretion torque in outburst. This assumes that the GW emission mechanism responds very rapidly to the accretion. Although response time-scales are not well studied, this scenario is not unreasonable – an accretion-induced mountain or unstable oscillation, for example, may well grow during outburst and decay during quiescence. Fig. 5 compares the best case detectability for the transients if we balance the outburst flux rather than the

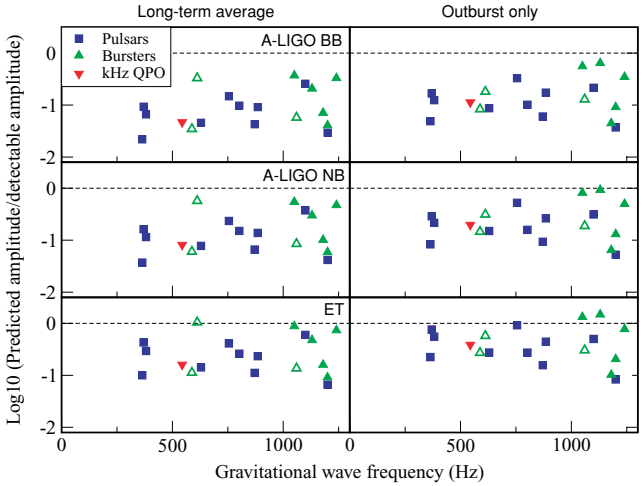

Figure 5. Best case detectability (single template) for the transients, in the mountain scenario. The left-hand panels show the detectability if GW emission balances the long-term average accretion rate, for $T_{\rm obs} = 2$ yr. The right-hand panels show the detectability if we if we consider the quadrupole necessary to balance the accretion torque during outburst. $T_{\rm obs}$ for each source is now either the outburst duration or the maximum integration time (2 yr), whichever is longer. In order to compare sources with different integration times, we show $\log_{10}$ of the ratio of the predicted to the detectable amplitude. The three rows are for different detector configurations: top – Advanced LIGO broad-band; middle – Advanced LIGO narrow-band envelope; bottom – ET.

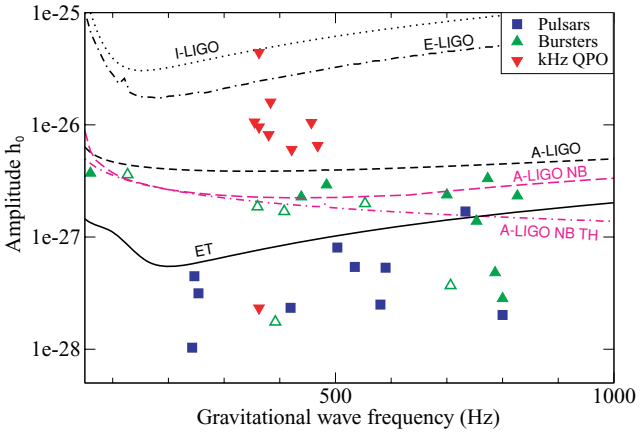

Figure 6. Best case detectability (single template search) using the long-term average flux, for the r-mode scenario. Symbols and lines are as for Fig. 2.

long-term average flux (Table 1). The integration time in outburst is taken to be either the typical outburst duration, or the maximum integration time, whichever is larger. The required quadrupoles are all below the Haskell et al. (2006) limit. Many of the sources show an improvement: the reduction in $T_{\rm obs}$ is more than compensated for by the increase in flux. The burst oscillation sources X 1658−298 and KS 1731−260, for example, which are undetectable if we consider time-averaged flux, lie within this scenario on or just above the Advanced LIGO narrow-band envelope. The intermittent pulsar HETE J1900.1−2455 also becomes a more promising source for the ET. Further theoretical consideration should clearly be given to the issue of torque response time-scales.

We also consider the situation that would result if the accretion torque is balanced by spin-down due to an internal r-mode rather than a mountain. We first make the assumption that the star has a spin rate and temperature such that it can sustain an unstable r-mode (so that it lies in the 'r-mode instability window', see Andersson & Kokkotas 2001). This assumption may not be warranted, particularly for some of the more slowly rotating stars. We also assume that the r-mode amplitude is steady: r-mode unstable stars may well experience duty cycles with short-lived periods of strong spin-down (Levin 1999; Andersson et al. 2000; Heyl 2002; Kinney & Mendell 2003), but there are some scenarios in which r-mode emission may be persistent (Andersson et al. 2002; Wagoner 2002; Nayyar & Owen 2006; Bondarescu et al. 2007). The GW torque associated with the dominant $l = m = 2$ r-mode (l and m being the standard angular quantum numbers) is

$$N_{\rm gw} = -3\tilde{J}\Omega_{\rm s}\alpha^2 M R^2/\tau_{\rm g} \tag{32}$$

(Andersson & Kokkotas 2001). The frequency of the emitted gravitational radiation is not a harmonic of the spin frequency: for the $l = m = 2$ r mode it is 4/3 times the spin frequency.[21] The quantity α is the mode amplitude. For an $n = 1$ polytrope model of the NS, $\tilde{J} = 1.635 \times 10^{-2}$ and the radiation reaction time-scale $\tau_{\rm g}$ is given by

$$\tau_{\rm g} = 47 M_{1.4}^{-1} R_{10}^{-4} \left(\frac{1\ {\rm kHz}}{\nu_{\rm s}}\right)^6 {\rm s} \tag{33}$$

(Andersson & Kokkotas 2001). The associated luminosity is $\dot{E}_{\rm gw} = N_{\rm gw}\omega_m/m$, where $\omega_m = \omega_{\rm gw}$ is the angular frequency of the mode. Assuming spin balance, $N_{\rm a} = N_{\rm gw}$, the resulting GW amplitude is

$$h_0 = 3.7 \times 10^{-27} \left(\frac{R_{10}^3}{M_{1.4}}\right)^{1/4} F_{-8}^{1/2} \left(\frac{1\ {\rm kHz}}{\nu_{\rm s}}\right)^{1/2}. \tag{34}$$

In Fig. 6 we compare the predicted and detectable amplitudes for the r-mode scenario for $T_{\rm obs} = 2$ yr.

We now consider whether the required r-mode amplitude is feasible. Assuming spin balance, the mode amplitude is

$$\alpha = 6.9 \times 10^{-8} \left(M_{1.4}^5 R_{10}^9\right)^{-1/4} d_{\rm kpc} F_{-8}^{1/2} \left(\frac{1\ {\rm kHz}}{\nu_{\rm s}}\right)^{7/2}. \tag{35}$$

Fig. 7 shows the amplitude required for spin balance for each source for the long-term average flux. The required amplitudes should be compared to the maximum saturation amplitude $\alpha_{\rm s}$ computed by Arras et al. (2003):

$$\alpha_{\rm s} \approx 8 \times 10^{-3} \left(\frac{\nu_{\rm s}}{1\ {\rm kHz}}\right)^{5/2}. \tag{36}$$

The values required for the two slowest spinning bursters exceed the amplitude limit, as would the kHz QPO sources if the spin is much slower than the measured separations. However, for all other sources the required amplitude is below the Arras et al. (2003) limit. The GW frequency is lower within the r-mode scenario than in the mountain scenario. Spin balance therefore requires a higher GW amplitude, making the r-mode emission model rather more optimistic. For Advanced LIGO many of the kHz QPO sources lie above the broad-band noise curve. Two of the burst oscillation sources with reasonable values of α, 4U 1636−536 and 4U

[21] We assume that this calculation of the relationship between mode frequency and spin is exact. In practice there is some theoretical uncertainty, which would further increase the number of templates to be searched.

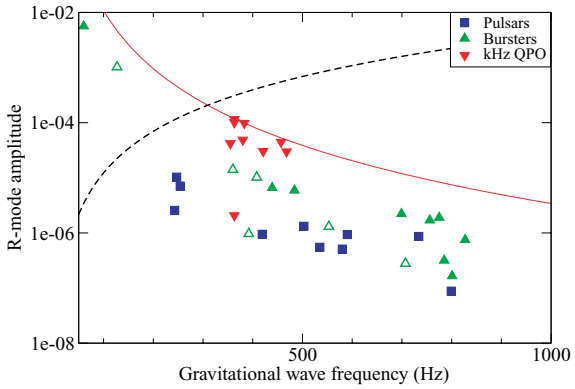

Figure 7. The r-mode amplitude α required for spin balance in the r-mode scenario, using the long-term average flux for all sources (persistent and transient). The dashed line shows the maximum (saturation) amplitude calculated by Arras et al. (2003). The uncertainty in the inferred amplitude is not shown, but can be substantial since it depends on the distance to the star. The solid line indicates the r-mode amplitude that would be required for Sco X-1 if the spin frequency differs from that inferred from kHz QPO separation.

1728−34, sit well above the Advanced LIGO narrow-band envelope, while 4U 1702−429 and KS 1731−260 lie on the curve (XB 1254−690, which would also be marginal for the narrow-band configuration, has an unfeasibly high α). For the ET, however, these sources are well above the noise curve, and the intermittent pulsar Aql X-1 is also marginally detectable.

If we consider the transient scenario (balancing outburst torque rather than time-averaged torque) the r-mode model also makes rather more optimistic predictions than the mountain model. Three burst oscillation sources that are marginally detectable at best when balancing long-term flux now come within range of Advanced LIGO's narrow-band configuration: XB 1658−298, KS 1731−260 and 4U 1608−522. By the time we reach the sensitivity of the ET the intermittent pulsar HETE J1900.1−2455 may also be detectable in outburst.

5.2 Data analysis techniques

We consider two kinds of searches over our parameter space [either of these methods can also be used as parts of an optimized multistage hierarchical scheme (Brady & Creighton 2000; Cutler, Gholami & Krishnan 2005; Meinshausen, Bickel & Rice 2007)].

(i) A full coherent matched-filter search using all available data, possibly from multiple detectors. This involves a demodulation of the data for a given parameter space point using the so-called $\mathcal{F}$ statistic; details can be found in (Jaranowski et al. 1998; Cutler & Schutz 2005). Such a coherent demodulation statistic can be augmented by the technique of combining sidebands as described in Messenger & Woan (2007) [adapted from similar techniques used in radio pulsar searches, Ransom, Cordes & Eikenberry (2003)].

(ii) A power folding method where the available data are broken up into smaller segments (often called 'stacks' in the GW literature); the duration of each stack is $T_{\rm coh}$ and $N_{\rm stacks}$ denotes the number of stacks. If there were no gaps in the data, we would have $T_{\rm obs} = N_{\rm stacks} T_{\rm coh}$, but duty factors of ∼80 per cent are more likely. Each segment is coherently demodulated using (i) and excess power from each segment is combined without maintaining phase coherence. Examples of such power folding methods are: (1) stack-slide (Brady & Creighton 2000) where the relevant statistic is simply a weighted sum of $\mathcal{F}$ statistic values (at the appropriate frequency bins)

$$\rho = \sum_{k=1}^{N_{\rm stacks}} w_k \mathcal{F}_{(k)}, \tag{37}$$

or (2) the Hough transform method (Krishnan et al. 2004) where one adds weighted binary number counts

$$\rho = \sum_{k=1}^{N_{\rm stacks}} w_k n_{(k)}, \tag{38}$$

where $n_{(k)}$ is either 0 or 1 depending on whether the $\mathcal{F}$ exceeds a certain threshold. In each case, the weights w_k are chosen to optimize the sensitivity.

For both (i) and (ii), the computational cost is proportional to the total number of templates $N_{\rm temp}$ and to the amount of data available. Thus, for (i), it is approximately $A T_{\rm obs} N_{\rm coh}$ for some constant A, while for (ii) it is proportional to $N_{\rm stacks}\ T_{\rm coh}\ N_{\rm temp}$. The precise value of the sensitivity of these searches clearly depends on the details of the analysis method and software, and the quality of data, such as the duty cycle of the detector (which might reduce the amount of data actually available), the presence of noise artefacts such as spectral disturbances, uncertainties in the calibration of the detector, and so on. It is thus not possible to estimate the sensitivity to better than, say, ∼5–10 per cent without actually carrying out the search, and it is in fact even pointless to try and do so in this paper. It is of course possible to get semirealistic estimates and this is what we shall do, but these uncertainties should always be kept in mind.

Starting with the statistical factor, note that if the threshold corresponding to a single trial false alarm rate is α, the probability that the threshold is crossed at least once in $N_{\rm trials}$ independent trials is $\mathrm{FA} = 1 - (1-\alpha)^{N_{\rm trials}} \approx \alpha N_{\rm trials}$ when $\alpha\ N_{\rm trials} \ll 1$ (Jaranowski et al. 1998). So we choose $\alpha = \mathrm{FA}/N_{\rm trials}$ to ensure that the total false alarm probability is FA. We equate the number of trials with the total number of templates that must be searched. Strictly speaking, this is not true because the different templates are not completely independent. This is usually not a significant effect as long as the mismatch m used to construct the template bank is not too small; we shall use a reference value of $m = 0.3$. To make matters more complicated, while there are reliable calculations for the template counting for (i) as presented in Section 4.1, there are as yet no reliable estimates for (ii). We shall therefore consider only the number of templates in each coherent segment. Fortunately, the dependence of the statistical factor is not very steep (in fact slower than logarithmic) with the number of trials, so this does not make a significant difference to our results.

Some details of the statistical calculation are in order. The choice of α determines the thresholds for both the coherent $\mathcal{F}$ statistic search and the semicoherent search. The exact relation is however different. The $\mathcal{F}$ statistic follows a χ^2 distribution with four degrees of freedom (it is actually $2\mathcal{F}$ which is χ^2 distributed). For the semicoherent statistic ρ is, to a reasonable approximation, simply Gaussian (assuming $N_{\rm stacks}$ to be sufficiently large); it is actually χ^2 with $4N_{\rm stacks}$ degrees of freedom. The assumption of Gaussianity may be questionable here because we are after all dealing with the tail of the distribution, and the central limit theorem may not be reliable especially when $N_{\rm stacks}$ is not particularly large. A further complication arises when ρ is not simply a sum of the $\mathcal{F}$ statistic values but is perhaps a Hough statistic (Krishnan et al. 2004) when the distribution of ρ is closer to a binomial (which can also be approximated by a Gaussian). We shall nevertheless assume Gaussianity for our purposes and leave a more detailed study for future

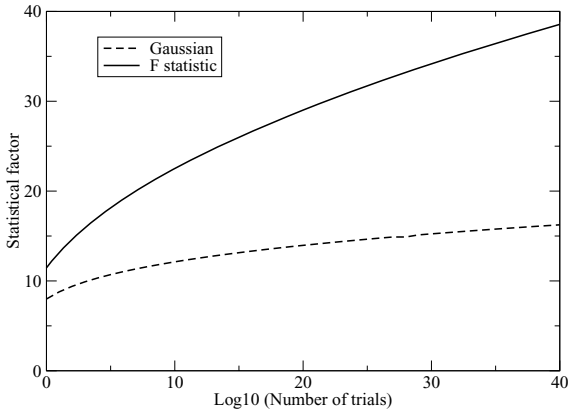

Figure 8. Dependence on the number of independent trials (templates) of the statistical factor $F_{\rm stat}$ that appears in the detectability equation (40). Note that $F_{\rm stat} = 11.4$ when $N_{\rm trials} = 1$ which reproduces equation (6).

work. The relations between α and the corresponding threshold $\mathcal{F}_{\rm th}$ and $\rho_{\rm th}$ are then different in the two cases:

$$\alpha = (1 + \mathcal{F}_{\rm th})e^{-\mathcal{F}_{\rm th}}, \qquad \alpha = \frac{1}{2}{\rm erfc}\left(\frac{\rho_{\rm th}}{\sqrt{2}\sigma}\right), \tag{39}$$

where erfc is the complementary error function, and σ is the standard deviation of ρ. In the presence of a signal with amplitude h_0, the mean values of $\mathcal{F}$ and ρ are increased by an amount proportional to S/N^2, and thus to h_0^2. Taking a fixed value of the false dismissal rate β determines the minimum value of h_0 needed to exceed the thresholds $\rho_{\rm th}$ and $\mathcal{F}_{\rm th}$; we shall always take $\beta = 0.1$ as the reference value. Folding in a uniform averaging over all possible pulsar orientations along with the statistical factor in a single parameter $F_{\rm stat}$, we get the following expression for the sensitivity

$$h_0^{\rm sens} \approx \frac{F_{\rm stat}}{N_{\rm stacks}^{1/4}}\sqrt{\frac{S_h}{DT_{\rm coh}}}, \tag{40}$$

where $F_{\rm stat}$ varies with the number of trials required, as shown in Fig. 8. This factor was also discussed in Abbott et al. (2007a) and Abbott et al. (2005a) which are examples of (i) and (ii), respectively. In each case, $F_{\rm stat}$ increases slower than logarithmically with $N_{\rm trials}$, and the statistical factor is worse for the χ^2 distribution as expected because it is not as sharply peaked as the Gaussian. Finally, it is perhaps worth mentioning that averaging over the pulsar orientation $\cos\iota$ may not always be appropriate, especially if there happen to be independent estimates of the NS orientation. If the value of $\cos\iota$ happens to be anywhere in the top $(1-p)$th percentile of a uniform distribution (i.e. if we average over all $|\cos\iota| \geq p$), then

$$F_{\rm stat} \rightarrow \frac{F_{\rm stat}}{\sqrt{1 + 11(p+p^2)/16 + (p^3+p^4)/16}}. \tag{41}$$

So for example, if $p = 0.9$, we get $F_{\rm stat} \rightarrow {\rm F_{stat}}/1.5$. This could be important for sources which happen to be near the detection threshold.

So far we have incorporated the statistical and geometrical factors in equation (40). For template bank based searches, the sensitivity is further degraded because of the discreteness of the template grid. For a template bank created with a maximum mismatch of m, assuming a cubic grid, the average degradation in the S/N is $(1 - m/3)$. This corresponds to a degradation of $\sqrt{1 - m/3}$ in h_0 which is $\approx$0.95 for $m = 0.3$.

The next question we need to address is the computational cost and whether it is necessary or worthwhile to do the semicoherent search (ii). Clearly, for a given amount of data while we ideally want to make the coherent integration time $T_{\rm coh}$ as large as possible, and the number of segments $N_{\rm stacks}$ correspondingly small, the choice of these parameters is dictated by the computational cost. This computational burden is in fact, by far, what limits the search sensitivity. (As we just saw, $F_{\rm stat}$ has a very weak dependence on the number of templates; we need to change the number of templates by orders of magnitude before it has an appreciable effect.) The bigger effect of reducing the number of templates by better astrophysical modelling or observations is that it allows us to have a larger coherent integration time $T_{\rm coh}$.

For a given source, we would first like to know if a semicoherent search would be useful. The obvious answer is: whenever computational cost is an issue, but a more quantitative answer is also easy to get. Let us compare the sensitivities of (i) and (ii) for a given computational cost. Let us assume that the cost for the coherent analysis scales as a power of $T_{\rm obs}$: $C_{\rm coh} = AT_{\rm obs}^k$ for some constants A and k. So if we assume a fixed value of the computational cost C_0, then $T_{\rm obs} = (C_0/A)^{1/k}$. Thus, the sensitivity is $h_0^{\rm coh} \propto T_{\rm obs}^{-1/2} = (C_0/A)^{-1/2k}$. For a semicoherent search on the other hand, we have $C_0 \approx AN_{\rm stacks}\,T_{\rm coh}^k$ (this is true if the cost of combining the different stacks is negligible). In this case we get $T_{\rm coh} = (C_0/AN_{\rm stacks})^{1/k}$. Using $h_0^{\rm semicoh} \propto N^{-1/4}\,T_{\rm coh}^{-1/2}$ we get

$$\frac{h_0^{\rm semicoh}}{h_0^{\rm coh}} = N_{\rm stacks}^{(2-k)/4k}. \tag{42}$$

This tells us that a semicoherent search is not effective (i.e. $h_0^{\rm semicoh} > h_0^{\rm coh}$) for $k \leq 2$, and it gets more and more effective for larger k (this conclusion is robust: it is not affected by the approximation of neglecting the cost of the semicoherent step).

In our present case, recall from equations (17)–(28) that we have very different scalings in the regimes $T_{\rm obs} \gg P_{\rm orb}$ and $T_{\rm obs} \ll P_{\rm orb}$. So, for binary systems for which the parameters have been sufficiently constrained astronomically and we can afford large integration times, we shall assume that we are better off doing a simple coherent search. For others, a semicoherent strategy has a much larger impact.[22] For each potential source, our strategy is to first estimate the number of templates that are required for a coherent search. With reasonable estimates of available computational resources, and assuming $T_{\rm obs} = 2$ yr, this determines the maximum coherent integration time $T_{\rm coh}$ that can be analysed. If $T_{\rm coh}$ is not much smaller than $P_{\rm orb}$, then by the previous argument we assume that the gain in using a semicoherent search is not significant, and we restrict ourselves to a pure coherent search. On the other hand, if this $T_{\rm coh}$ does turn out to be much less than $P_{\rm orb}$, then we consider a semicoherent search and estimate $T_{\rm coh}$ and $N_{\rm stacks}$ (assuming here the cost of the semicoherent step to be comparable to the coherent step). Equation (40) then yields an estimate of the search sensitivity $h_0^{\rm sens}$ for each potential source. We take the statistical factor $F_{\rm stat}$ in equation (40) using just the number of templates in the coherent step. There is as yet no systematic study of the semicoherent metric for binary systems, and this estimate should be updated as soon as these calculations are available. We expect that this approximation will not make a qualitative difference to our final results because of the weak dependence of $F_{\rm stat}$ on the number of templates, but this needs to be verified. In the previous section, we estimated the GW

[22] Semicoherent searches might start becoming more important as soon as we need to start including other parameters, especially frequency derivatives and $\dot{P}_{\rm orb}$.

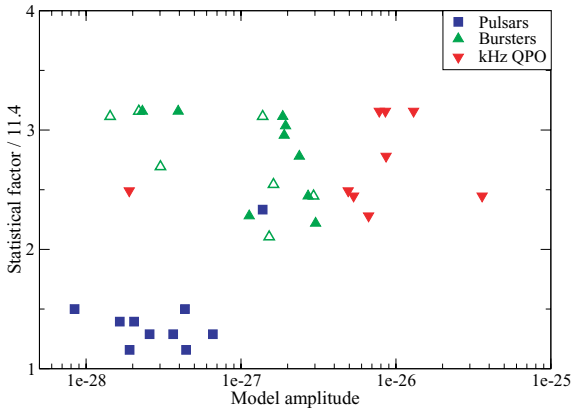

Figure 9. The factor by which $F_{\rm stat}$ increases over the single template value ($F_{\rm stat} = 11.4$) plotted against the predicted amplitude for the mountain scenario (equation 5). The brightest and most promising sources are the most poorly constrained, and this is reflected in the effect on $F_{\rm stat}$. The difference in $F_{\rm stat}$ between the two strongest sources, Sco X-1 and GX 5−1, is primarily due to the fact that Sco X-1 has much better orbital constraints.

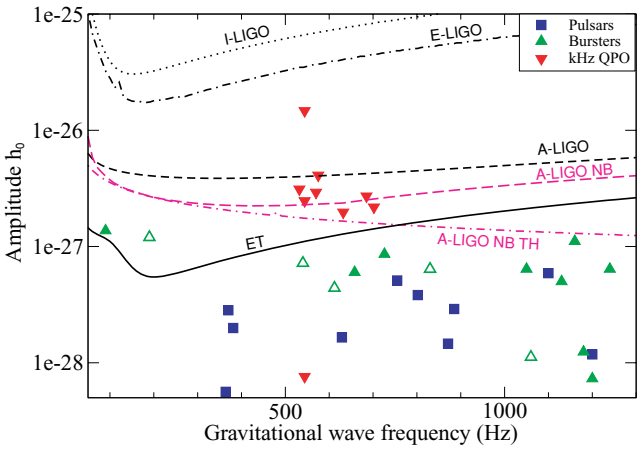

Figure 10. Effect on detectability for the mountain scenario (assuming long-term average flux and a coherent fold with $T_{\rm obs} = 2$ yr), taking into account the effect on $F_{\rm stat}$ associated with the fact that $N_{\rm temp} > 1$. Compare to the best case detectability shown in Fig. 2. As in Fig. 2, the noise curves are computed assuming $F_{\rm stat} = 11.4$ (the single template value), but we have scaled the predicted amplitudes to reflect the fact that $F_{\rm stat}$ is larger. Although this is not strictly 'correct' (it is the thresholds that should move, not the predicted amplitudes) this is a useful way to visualize the impact. See the text for more details.

amplitude $h_0^{\rm exp}$ from each source, and the ratio $h_0^{\rm exp}/h_0^{\rm sens}$ can be a useful 'detectability' ranking for each source.

In the cases when $P_{\rm orb}$ is essentially unknown, the ranges of $T_{\rm asc}$ and $a_{\rm x} \sin i$ that we have chosen depend on $P_{\rm orb}$. This means that the parameter space region is not rectangular and thus the template counting equations of Section 4.1 will overestimate the number of templates significantly, though not by orders of magnitude.

5.3 Numbers of templates

We can now compute the effect on our searches of parameter uncertainty. We will start by considering the effect on the statistical factor $F_{\rm stat}$, neglecting computational cost issues. In other words, we assume that it is feasible to do a coherent fold. In Tables 2–4 we summarize the parameter ranges assumed for the pulsars, bursters and kHz QPO sources, respectively. The tables show the associated N_{λ^i} for each parameter (for $T_{\rm obs} = 2$ yr), the resulting total number of templates that must be searched $N_{\rm temp}$, and the effect on $F_{\rm stat}$. Fig. 9 shows the change in the statistical factor for each source.

In Fig. 2, where we showed results for a single template search, each source had $F_{\rm stat} = 11.4$. This meant that we could plot a single detectability threshold curve for each detector. When each source has a different $F_{\rm stat}$, however, the detectability threshold curves differ for each source. One way of comparing detectability for sources with different noise threshold curves is to plot the ratio of emitted to detectable amplitude: this is the approach that we took for the transients (Fig. 5), and that we will adopt when we come to consider computational cost. What we can also do, however, to see the effect, is to scale the predicted amplitude h_0 by $11.4/F_{\rm stat}$. Predicted amplitude does not really change, of course, but it is a useful way of visualizing the impact of the statistical factor.

Fig. 10 shows the impact on the mountain scenario: it should be compared to Fig. 2. Only for the most tightly constrained pulsars is detectability largely unchanged: for the majority of sources the detectable amplitude falls by a factor of 2–3 compared to a single template search. Although this does not sound like a great deal, it is sufficient to push all sources except Sco X-1 below the detection threshold for Advanced LIGO broad-band.[23] The effect on the r-mode scenario, summarized in Tables 2–4, is slightly less severe, leaving Sco X-1, GX 5−1, GX 349+2 and 4U 1820−30 above the detection threshold for Advanced LIGO broad-band. The situation is better for the narrow-band configuration: although none of the burst oscillation sources remain within range (for any of the emission scenarios considered), several of the kHz QPO sources are still viable. The spins for these sources are poorly constrained. However, the anticipated narrow-band configurations (see top panel of Fig. 1) have a reasonably broad bandwidth, leaving ample scope for searches.

We can now take the final step and look at the impact of computational constraints on searches involving multiple templates. The available computational power sets the length of data $T_{\rm obs}$ that can feasibly be analysed within a given amount of time. In Table 5 we summarize the impact in the situation where we assume a maximum analysis time of 2 yr, assuming that for Advanced LIGO we have computational power 50 times greater than that currently available within the LIGO Scientific Collaboration, while for the ET we assume 100 times more computing than at present. These assumptions are, of course, arbitrary, since the computing power that can be applied to future searches depends not just on technology (e.g. Moore's law) but also on improvements in data analysis techniques, and of course also on how much money is spent on computing by future projects. We have taken numbers we feel are defensible, but they may turn out to be conservative, especially for the ET.

For the pulsars, computing constraints have little effect on the detectability of the sources; however, these are not likely to be detectable in any case. But for the bursters and the kHz QPO sources, computational constraints lead to a major reduction in the $T_{\rm obs}$ that it is feasible to analyse. For many sources we have to resort to a semicoherent search, as a coherent fold is no longer possible.

[23] Sco5 X-1 would also be marginal for Enhanced LIGO, over a restricted frequency range.

Table 5. Computational cost effects for future performance scenarios.

Source	ν (Hz)	× 50 improvement		× 100 improvement		$T_{\rm decoh}$ (yr)
		$N_{\rm stacks}$	$T_{\rm obs}$ (d)	$N_{\rm stacks}$	$T_{\rm obs}$ (d)	
Accreting millisecond pulsars						
IGR J00291+5934	599	1 (1)	730 (730)	1 (1)	730 (730)	1.26
Aql X-1	550	1 (1)	512 (730)	1 (1)	645 (730)	0.17
SAX J1748.9−2021	442	1 (1)	730 (730)	1 (1)	730 (730)	0.35
XTE J1751−305	435	1 (1)	730 (730)	1 (1)	730 (730)	0.67
SAX J1808.4−3658	401	1 (1)	730 (730)	1 (1)	730 (730)	0.82
HETE J1900.1−2455	377	1 (1)	730 (730)	1 (1)	730 (730)	0.43
XTE J1814−338	314	1 (1)	730 (730)	1 (1)	730 (730)	1.12
XTE J1807−294	191	1 (1)	730 (730)	1 (1)	730 (730)	0.86
XTE J0929−314	185	1 (1)	730 (730)	1 (1)	730 (730)	0.66
SWIFT J1756.9−2508	182	1 (1)	730 (730)	1 (1)	730 (730)	2.81
Burst oscillation sources						
XTE J1739−285	1122	1.5e+05 (1.5e+05)	0.1 (0.1)	1.5e+05 (1.5e+05)	0.1 (0.1)	0.48
4U 1608−522	620	8372 (7209)	3.1 (3.6)	7865 (6655)	3.3 (3.9)	0.13
SAX J1750.8−2900	601	1.5e+05 (1.5e+05)	0.1 (0.1)	1.5e+05 (7.3e+04)	0.1 (0.2)	0.67
GRS 1741.9−2853	589	1.5e+05 (1.5e+05)	0.1 (0.1)	1.5e+05 (7.3e+04)	0.1 (0.2)	0.37
4U 1636−536	581	1 (1)	98 (167)	1 (1)	123 (211)	0.07
X 1658−298	567	1 (1)	611 (730)	1 (1)	730 (730)	0.08
A 1744−361	530	1 (1)	1.2 (2.1)	1 (1)	1.5 (2.6)	0.61
KS 1731−260	524	2.4e+04 (2.1e+04)	0.6 (0.7)	2.4e+04 (2.1e+04)	0.6 (0.7)	0.08
4U 0614+09	415	1 (1)	14.9 (25.6)	1 (1)	18.8 (32.3)	0.31
4U 1728−34	363	9.6e+04 (8.2e+04)	3.6 (4.2)	9.1e+04 (7.7e+04)	3.8 (4.5)	0.11
4U 1702−429	329	1.5e+05 (7.3e+04)	0.1 (0.2)	7.3e+04 (7.3e+04)	0.2 (0.2)	0.14
MXB 1730−335	306	7.3e+04 (7.3e+04)	0.2 (0.2)	7.3e+04 (7.3e+04)	0.2 (0.2)	0.11
IGR J17191−2821	294	7.3e+04 (7.3e+04)	0.2 (0.2)	7.3e+04 (7.3e+04)	0.2 (0.2)	1.39
4U 1916−053	270	1 (1)	730 (730)	1 (1)	730 (730)	0.13
XB 1254−690	95	1 (1)	102 (175)	1 (1)	128 (220)	0.07
EXO 0748−676	45	1 (1)	730 (730)	1 (1)	730 (730)	0.17
kHz QPO sources						
Cyg X-2	351	123 (1)	60 (51)	1 (1)	40 (73)	0.02
GX 340+0	343	1.5e+05 (7.3e+04)	0.1 (0.2)	1.5e+05 (7.3e+04)	0.1 (0.2)	0.02
4U 1735−44	316	1 (1)	35 (61)	1 (1)	44 (76)	0.03
GX 5−1	288	1.5e+05 (7.3e+04)	0.1 (0.2)	1.5e+05 (7.3e+04)	0.1 (0.2)	0.01
4U 1820−30	285	1 (1)	730 (730)	1 (1)	730 (730)	0.03
Sco X-1	272	1 (1)	110 (188)	1 (1)	138 (237)	0.02
GX 17+2	272	7.3e+04 (7.3e+04)	0.2 (0.2)	7.3e+04 (7.3e+04)	0.2 (0.2)	0.02
XTE J2123−058	272	1 (1)	26 (44)	1 (1)	33 (56)	0.85
GX 349+2	266	1908 (1625)	41 (48)	1781 (1514)	44 (51)	0.05

Note: Computational cost effects on data analysis, assuming a 50 or 100 times improvement in computational power over current capabilities, for the mountain (r-mode) scenario. Where $N_{\rm stacks} = 1$, the fold is coherent and $T_{\rm obs}$ is the maximum feasible quantity of data that can be folded. Where $N_{\rm stacks} > 1$, the fold is semicoherent and $T_{\rm obs}$ is the length of each individual data segment. The assumed spin frequency is given for each source to assist in cross-referencing this table with the figures. We also give the decoherence time $T_{\rm decoh}$, as defined in Section 6.

Figs 11 and 12 show the effects on detectability for the mountain and r-mode scenarios, respectively, taking into account both the change in $F_{\rm stat}$ and the reduced observation times for our assumed computing power.

The additional impact of computational limitation is substantial. For Advanced LIGO's broad-band configuration, only Sco X-1 and 4U 1820−30 (the latter in the r-mode scenario) remain above the detectability threshold. These two sources are also the only two left above the narrow-band envelope threshold, although there are other sources just below the envelope that might be detectable if the narrow-band configuration were able to push closer to the thermal noise floor. Parameter uncertainty clearly poses a major problem, even for stars where we have some indication of the spin rate.[24] If the parameter space volume can be reduced, however, then the statistical and computational restrictions will have less impact. In the following section we will examine this in more detail and consider how best to solve it.

[24] This problem is of course even more pronounced for the accreting NSs where we have no indication of spin rate.

6 DISCUSSION

6.1 Current and future prospects

It is clear from Section 5 that the detection of GWs from accreting NSs is a difficult task. The X-ray bright kHz QPO sources suffer from parameter uncertainty, forcing us to look in addition at the much weaker but better constrained burst oscillation sources. The best constrained sources, the accreting millisecond pulsars, are expected to emit at such a low level that they are unlikely to be detectable by second generation detectors. This is particularly

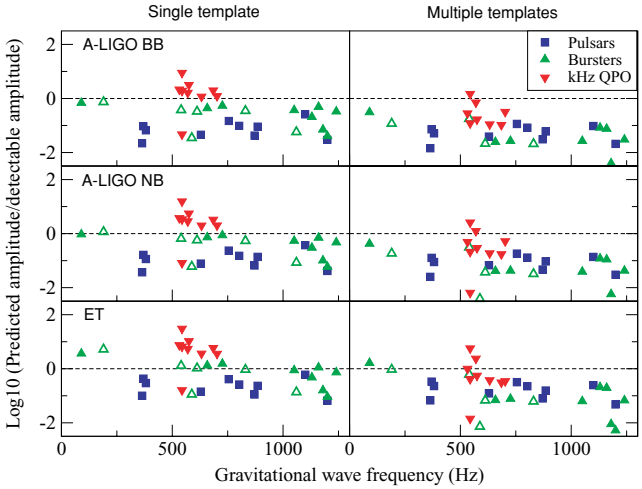

Figure 11. Detectability for the mountain scenario (long-term average flux, maximum $T_{\rm obs} = 2$ yr), taking into account computational limitations as well as the effect on $F_{\rm stat}$. The computational cost of searching multiple templates affects the feasible integration time and the choice of coherent/semicoherent search technique (Table 5). In order to compare detectability for sources with different integration times we plot $\log_{10}$ of the ratio of predicted to detectable amplitude. The three rows are for different detector configurations: Top – Advanced LIGO broad-band; middle – Advanced LIGO narrow-band envelope; bottom – ET. The left-hand panels show detectability for the best case (single template) search, as in Fig. 2; the right-hand panels show the situation after including the statistical and computational limitation. For Advanced LIGO we assume a 50-fold increase in computational efficiency as compared to the current situation; for the ET we assume a 100-fold increase. In both cases we assume a maximum analysis time of 2 yr.

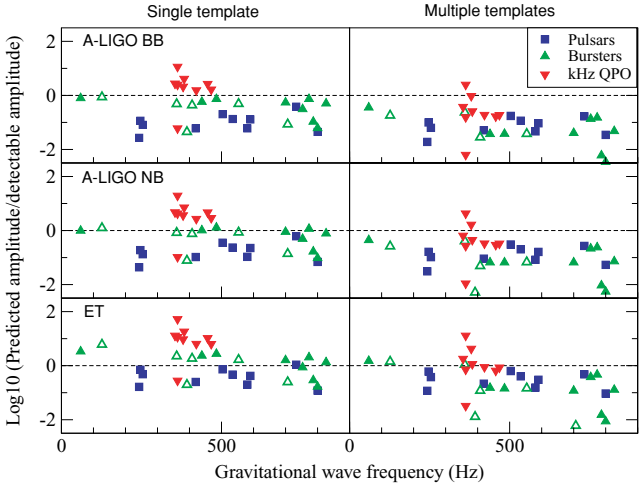

Figure 12. As Fig. 11 but for the r-mode scenario.

depressing since our calculations have been carried out within the context of a fairly optimistic modelling and analysis scenario. We have not as yet considered any additional sources of spin-down, and have also neglected physically reasonable complications such as spin variability which would increase the number of templates still further. Spin variability would of course also lead to decoherence of the signal for sources where we cannot track the spin, reducing integration times to the decoherence time $T_{\rm decoh}$, defined by

$$T_{\rm decoh}^2 \dot{\nu}_{\rm s} = 1. \qquad (43)$$

One can get some idea of the worst case scenario by calculating the $\dot{\nu}_{\rm s}$ that would result if the source were spinning up at the maximal rate due to the accretion torque (equation 1). The results are given in Table 5: for the bright kHz sources this worst case decoherence time could be $\sim$1 week, and this is something that will need to be considered in future studies of detectability.

In order to improve prospects for those sources that are in principle detectable, we clearly need to find ways of improving source constraints and removing computational limitations. In the sections that follow we detail the actions that would lead to the biggest improvements.

6.2 Astronomical observations

The major obstacle to detection by the current and imminent generation of detectors is clearly parameter uncertainty, with spin uncertainty having the largest impact (see Tables 2–4). Astronomical observations might help to constrain source properties.

The single most valuable thing that could be done to improve the current situation is to determine more precisely the NS spin in the bright kHz QPO and burst sources. A substantial archive of high time resolution X-ray data exists for many of these sources from *RXTE* and its predecessors. However, the only deep search for pulsations in the literature is that carried out by Dib et al. (2005) for 4U 1820−30. Serious consideration should be given to carrying out similar analysis for all of the kHz QPO and burst sources, most particularly Sco X-1. Thorough searches for intermittent pulsations, such as those carried out by Casella et al. (2008) and Altamirano et al. (2008), would also be worthwhile.

It may also be possible to find burst oscillations in the kHz QPO sources: five of the sources that we have analysed are known to burst. If a sufficient archive of bursts can be built up from these sources burst oscillations may well be detected either in individual bursts or by stacking power spectra from multiple bursts (the technique used to find weak burst oscillations from EXO 0748−676 (Villarreal & Strohmayer 2004). We also need to verify the burst oscillation frequencies for the seven sources with tentative or single burst detections, in particular the four that are above the detection threshold for some of the scenarios that we have examined: XB 1254−690, 4U 1916−053, MXB 1730−335 and 4U 0614+09.

Identifying the orbital period can also make a substantial difference to the number of templates searched. Consider for example the difference between the two kHz QPO sources Sco X-1 and GX 5−1. Both are expected to be strong emitters, but Sco X-1 suffers much less from parameter uncertainty than GX 5−1 because the former has a well constrained orbital period. Three of the most promising kHz QPO sources have no orbital constraints (GX 340+0, GX 5−1 and GX 17+2), while a fourth (GX 349+2) has only a relatively weak constraint. Several of the most promising burst oscillation sources also fall into this category: attention should focus on 4U 1608−522, KS 1731−260, 4U 1728−34, 4U 1702−429 and MXB 1730−335, sources that could be detectable in some scenarios. Immense progress has been made in recent years in constraining orbital parameters for LMXBs using optical/IR observations, particularly with the Bowen technique of spectroscopy. Identification of counterparts is often difficult, but there would be a substantial payoff in terms of GW detection prospects.

6.3 Astrophysical modelling issues

Both burst oscillation frequency and kHz QPO frequency are proxy measures for the stellar spin rate. The precise link to spin for each

measure is not clear because in neither case do we understand the mechanism. Astrophysical modelling to pin down the cause of the two phenomena could therefore shed light on the reliability and accuracy of the spin proxy.

Several models have been suggested for burst oscillations. These include global oscillations of the surface layers of the NS, large-scale drifting vortices excited by the passage of the flame fronts, or hotspots linked in some way to persistent pulsations. All of the models have shortcomings, and progress towards understanding this phenomenon has to some degree stalled. The situation for the kHz QPOs is however even worse. There are several models, summarized in detail in van der Klis (2006). All involve either orbital motions of material within the disc or disc oscillations, and many also require some mechanism to select preferred radii within the disc. Developing testable predictions that would distinguish between the different models, however, is very difficult. A substantial body of data exists within the *RXTE* archive to test models if such predictions can be made. The identification of a robust link between kHz QPO frequency and stellar spin would have a major impact in reducing parameter uncertainty for the most promising sources for Advanced LIGO.

6.4 Data analysis and detector issues

In the absence of computational limitations, even taking into account the effect on statistics, there would be up to eight sources potentially detectable by Advanced LIGO (Fig. 10). We therefore need to improve the data analysis tools used for the searches. We need significant improvements in all relevant aspects of the data analysis pipelines: accelerating existing software through improvements to both software algorithms and computer hardware, and also developing other data analysis techniques. The software algorithms being used in the LIGO data analysis software have improved continually over the years since the first LSC publication on periodic waves in 2003; we expect these improvements to continue. It is possible that we may get an improvement of more than an order of magnitude in existing codes over the next several years. The improvements in computer hardware, even just following Moore's law, will yield an additional factor of about 16 in the next 8 yr, i.e. by the time we expect Advanced LIGO to be operating. Furthermore, computing platforms like Einstein@Home allow us to increase the total number of computers available to do the analysis. On top of this, it might also be possible to use special purpose hardware for the periodic wave searches. Most of the analysis involves a large number of relatively simple operations, and it might be quite feasible to design chips which are efficient for these particular calculations. An example of these are the GRAPE special-purpose computers which have proven to be extremely useful in astrophysical N-body simulations (Makino & Taiji 1995) and in molecular dynamics calculations in condensed matter physics. It is hard to anticipate these developments, but an improvement of four or five orders of magnitude in effective computing power might be feasible.

Apart from these technical improvements, it is also possible to develop new analysis methods. A good example of this is the cross-correlation method used in the Sco X-1 search (Abbott et al. 2007c). This was neither a matched filter nor a standard time-frequency semicoherent search. It was instead based on aperture synthesis, i.e. the fact that we have multiple detectors in operation, and that they all see essentially the same GW signal at any given time. This method has so far mostly been used in the stochastic background searches, and is now being adapted to the periodic wave searches (Dhurandhar et al. 2008). Apart from the computational efficiency, this method is also relatively insensitive to the uncertainty in the signal model caused, e.g. by pulsar glitches (though this leads to a correspondingly greater computational cost in any follow-ups that must be done for verifying a detection and for parameter estimation). Further searches using this method, in combination with the other methods discussed in this paper seem to be quite promising, especially given that by the time of Advanced LIGO there will be a third interferometer of comparable sensitivity in Virgo.

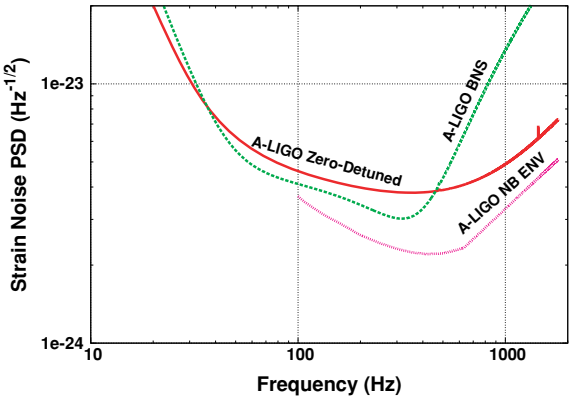

Figure 13. Some possible Advanced LIGO configurations. See text for discussion.

In the near term while these improvements are in progress, it seems reasonable to search for some of the brighter sources such as Sco X-1 not at the frequency implied by the kHz QPOs, but rather at lower frequencies corresponding to the sweet spot of the detectors. Not only are the instruments more sensitive at these frequencies, but this is computationally easier and is astrophysically well motivated if the link between the kHz QPO and the spin frequency is not validated.

We conclude this section with a brief discussion of possible Advanced LIGO configurations and some of its implications for our purposes. Fig. 13 shows noise curves for three cases: an example broad-band configuration with some tuning of the signal recycling cavity optimized for binary neutron star (BNS) inspirals, the envelope of possible narrow-band configurations, and the zero-detuned broad-band configuration. The zero-detuned curve and the narrow-band envelope are the same as in Fig. 1. The BNS curve is relevant because BNS inspirals will be among the key targets for Advanced LIGO and the detector might possibly be operated in this configuration for significant durations. Thus, while BNS signals are not our concern in this paper, it is important to consider the impact of this configuration for our purposes. It is obvious that the BNS curve affects us adversely above $\sim$500 Hz which, as we see from Fig. 2 is precisely where the kHz QPO sources are expected to lie.

These curves highlight the importance of spin measurements. For all potential sources with frequencies between, say, 150 and 2000 Hz, the narrow banding gains us no more than a factor of 2. The best case for narrow banding is then a compelling source whose frequency is very well known and is within this range and is not detectable by the broad-band curve. The other possibility is to employ the zero-detuned noise curve for detection and then use the narrow-band curve as a follow-up to confirm detection or to increase S/N for extracting better astrophysical information. Given the present uncertainties in the spin frequency, this latter possibility seems to be the best option for detecting periodic waves from LMXBs. This conclusion could change if there turn out to be significant improvements in the narrow-band noise curves.

6.5 Conclusions

We have shown that GW observations of accreting NSs will be challenging. It is therefore worthwhile considering what is to be gained from such an effort: what new information GW observations will bring to the study of these sources.

The input from electromagnetic observations that is required for these searches is primarily on kinematical parameters like spin rates and orbital ephemerides. The GWs that are generated carry information on the orientation and dynamics of the NS and its interaction with the accretion disc. The elliptical polarization of the GWs, which will emerge from analysis of the detected signal, determines the orientation of the NS spin axis. The degree of alignment of this with the inferred disc orientation, especially for the slower spinning (presumably younger) systems, will constrain models of binary evolution and the formation of the NS.

In systems where observations and modelling constrain the NS spin to a relatively narrow range, the GW frequency will determine whether the r-mode or mountain scenario, or indeed some other scenario, is the appropriate one. The GW amplitude will then determine the degree of mass asymmetry (mountains) or the size of the velocity field (r-modes). In both cases this will open for the first time a wealth of opportunities for studying the physics of NS interiors.

For all detected systems, the measured GW amplitude and frequency will tell us how much angular momentum is being carried away in GWs; by measuring or limiting the rate of change of the GW frequency we can then infer the rate at which angular momentum is being accreted from the disc. This will be an important constraint on models of the disc and the NS magnetic field.

Clearly, if GW searches turn up signals in unexpected places in parameter space, this will challenge prevailing models for these systems. For example, if the GW frequency equals the X-ray pulsation frequency instead of twice or four-thirds its value, then this might imply that the pulsation frequency is actually twice the true spin frequency.

Even in the worst case, where a sufficiently sensitive search fails to detect GWs at the expected amplitude, the negative result could eliminate the GW option for spin balance and demonstrate that this somehow resulted from a propeller-type torque from the NS's magnetic field. Of course, one would have to have confidence that the GWs were not coming out at a different frequency, so the search would have to include that as a parameter.

The additional astronomical input that could make the difference between detecting and not detecting GWs could come from a variety of observations. Clearly, long-term X-ray timing is highly desirable, and here it is disappointing that the future of *RXTE* is limited and no X-ray mission with comparable capabilities seems to be planned for the period before Advanced LIGO comes online. Thorough exploitation of the *RXTE* data archive is therefore especially important. On the other hand, sensitive radio observations of X-ray systems in quiescence may provide unexpected information, and this will be easier with arrays like the Square Kilometre Array and its pathfinders.

ACKNOWLEDGMENTS

We would like to thank Alan Levine for advice on ASM count rates, Jake Hartman for advice on the effects of positional uncertainty on pulsar timing, Reinhard Prix for help with the computational cost estimates, Alberto Vecchio and Chris Messenger for discussions regarding the parameter space metric and Maria Alessandra Papa, Mike Landry and Graham Woan for useful comments on a draft of this paper. We are grateful to Rana Adhikari, Peter Fritschel, Gregg Harry, Bangalore Sathyaprakash, David Shoemaker, Kentaro Somiya and Ken Strain for pointing us to Bench and for valuable discussions related to the Advanced LIGO noise spectrum. We thank Rana Adhikari also for providing us with the Enhanced LIGO noise curve. ALW would like to thank the Kavli Institute for Theoretical Physics for hospitality during a KITP/MPA postdoctoral exchange visit, when this work was started. BK is grateful to the LSC continuous waves data analysis group for valuable discussions. LB acknowledges support from the National Science Foundation via grants PHY 05-51164 and AST 07-07633. BK and BFS acknowledge the support of the DFG's special research centre SFB/Transregio 7 'Gravitational Wave Astronomy'.

REFERENCES

Abbott B. et al., 2004, Phys. Rev. D, 69, 182004
Abbott B. et al., 2005a, Phys. Rev. D, 72, 102004
Abbott B. et al., 2005b, Phys. Rev. Lett. 94, 181103
Abbott B. et al., 2007a, Phys. Rev. D, 76, 082001
Abbott B. et al., 2007b, Phys. Rev. D, 76, 042001
Abbott B. et al., 2007c, Phys. Rev. D, 76, 082003
Abbott B. et al., 2008, Phys. Rev. D, 77, 022001
Altamirano D., van der Klis M., Méndez M., Migliari S., Jonker P. G., Tiengo A., Zhang W., 2005, ApJ, 633, 358
Altamirano D., Casella P., Patruno A., Wijnands R., van der Klis M., 2008, ApJ, 674, L45
Andersson N., Kokkotas K. D., 2001, Int. J. Mod. Phys., 10, 381
Andersson N., Kokkotas K. D., Stergioulas N., 1999, ApJ, 516, 307
Andersson N., Jones D. I., Kokkotas K. D., Stergioulas N., 2000, ApJ, 534, L75
Andersson N., Jones D. I., Kokkotas K. D., 2002, MNRAS, 337, 1224
Andersson N., Glampedakis K., Haskell B., Watts A. L., 2005, MNRAS, 361, 1153
Anderson S. F., Margon B., Deutsch E. W., Downes R. A., Allen R. G., 1997, ApJ, 482, L69
Arras P., Flanagan E. E., Morsink S. M., Schenk A. K., Teukolsky S. A., Wasserman I., 2003, ApJ, 591, 1129
Astone P., Borkowski K. M., Jaranowski P., Królak A., 2002, Phys. Rev. D, 65, 042003
Astone P. et al., 2005, Class. Quantum Gravity, 22, S1243
Augusteijn T., van der Hooft F., de Jong J. A., van Kerkwijk M. H., van Paradijs J., 1998, A&A, 332, 561
Ballantyne D. R., Strohmayer T. E., 2004, ApJ, 602, L105
Baraffe I., Kolb U., 2000, MNRAS, 318, 354
Barnes A. D., Casares J., Cornelisse R., Charles P. A., Steeghs D., Hynes R. I., O'Brien K., 2007, MNRAS, 380, 1182
Barret D., Olive J.-F., Miller M. C., 2005, MNRAS, 361, 855
Barret D., Boutelier M., Miller M. C., 2008, MNRAS, 384, 1519
Barziv O., Kuulkers E., Méndez M., van der Hooft F., Groot P. J., van der Klis M., Kemper C., van Paradijs J., 1997, A&A, 325, 1035
Berendsen S. G. H., Fender R., Kuulkers E., Heise K., van der Klis M., 2000, MNRAS, 318, 599
Bhattacharyya S., 2007, MNRAS, 377, 198
Bhattacharyya S., Strohmayer T. E., Markwardt C. B., Swank J. H., 2006, ApJ, 639, L31
Bildsten L., 1998, ApJ, 501, L89 (B98)
Bildsten L., Chakrabarty D., 2001, ApJ, 557, 292
Boirin L., Barret D., Olive J., Bloser P., Grindlay J., 2000, A&A, 361, 121
Bondarescu R., Teukolsky S. A., Wasserman I., 2007, Phys. Rev. D, 76, 64019
Boutloukos S., van der Klis M., Altamirano D., Klein-Wolt M., Wijnands R., Jonker P. G., Fender R. P., 2006, ApJ, 653, 1435
Bradshaw C. F., Fomalont E. B., Geldzahler B. J., 1999, ApJ, 512, 121
Bradt H. V. D., McClintock J. E., 1983, ARA&A, 21, 13

Brady P. R., Creighton T., 2000, Phys. Rev. D, 61, 082001
Brady P. R., Creighton T., Cutler C., Schutz B., 1998, Phys. Rev. D, 57, 1
Brandt S., Castro-Tirado A. J., Lund N., Dremin V., Lapshov I., Sunyaev R. A., 1992, A&A, 262, L15
Buonanno A., Chen, Y., 2002, Phys. Rev. D, 65, 042001
Burderi L. et al., 2007, ApJ, 657, 961
Callanan P. J. et al., 2002, ApJ, 574, L143
Casares J., Charles P., Kuulkers E., 1998, ApJ, 493, L39
Casares J., Dubus G., Shahbaz T., Zurita C., Charles P. A., 2002, MNRAS, 329, 29
Casares J., Cornelisse R., Steeghs D., Charles P. A., Hynes R. I., O'Brien K., Strohmayer T. E., 2006, MNRAS, 373, 1235
Casella P., Altamirano D., Patruno A., Wijnands R., van der Klis M., 2008, ApJ, 674, L41
Chabrier G., Baraffe I., 2000, ARA&A, 38, 337
Chabrier G., Baraffe I., Allard F., Hauschildt P., 2000, ApJ, 542, 464
Chakrabarty D., Morgan E., Muno M., Galloway D., Wijnands R., van der Klis M., Markwardt C., 2003, Nat, 424, 42
Chevalier C., Ilovaisky S. A., 1998, IAU Circ., 6806
Chou Y., Grindlay J. E., 2001, ApJ, 563, 934
Chou Y., Grindlay J. E., Bloser P. F., 2001, ApJ, 549, 1144
Chou Y., Chung Y., Hu C. P., Yang T. C., 2008, ApJ, 678, 1316
Christian D. J., Swank J. H., 1997, ApJS, 109, 177
Cook G. B., Shapiro S. L., Teukolsky S. A., 1994, ApJ, 423, L117
Cooke B. A., Ponman T. J., 1991, A&A, 244, 358
Cominsky L. R., Wood K. S., 1984, ApJ, 283, 765
Cornelisse R., Casares J., Steeghs D., Barnes A. D., Charles P. A., Hynes R. I., O'Brien K., 2007, MNRAS, 375, 1463
Courvoisier T. J.-L., Parmar A. N., Peacock A., Pakull M., 1986, ApJ, 309, 265
Cutler C., 2002, Phys. Rev. D., 66, 084025
Cutler C., Schutz B. F., 2005, Phys. Rev. D, 72, 063006
Cutler C., Gholami I., Krishnan B., 2005, Phys. Rev. D, 72, 042004
Degenaar N. et al., 2007, ATel, 1106
Deloye C. J., Bildsten L., 2003, ApJ, 598, 1217
Deutsch E. W., Margon B., Anderson S. F., Wachter S., Goss W. M., 1999, ApJ, 524, 406
Dhurandhar S. V., Vecchio A., 2001, Phys. Rev. D, 63, 122001
Dhurandhar S. V., Krishnan B., Mukhopadhyay H., Whelan J., 2008, Phys. Rev. D, 77, 082001
di Salvo T., Méndez M., van der Klis M., Ford E., Robba N. R., 2001, ApJ, 546, 1107
di Salvo T., Méndez M., van der Klis M., 2003, A&A, 406, 177
Dib R., Ransom S. M., Ray P. S., Kaspi V. M., Archibald A. M., 2005, ApJ, 626, 333
Dubus G., Lasota J.-P., Hameury J.-M., Charles P., 1999, MNRAS, 303, 139
Falanga M. et al., 2005, A&A, 444, 15
Fender R. P., Hendry M. A., 2000, MNRAS, 317, 1
Ford E. et al., 1997, ApJ, 475, L123
Ford E. C., van der Klis M., van Paradijs J., Méndez M., Wijnands R., Kaaret P., 1998, ApJ, 508, L155
Ford E. C., van der Klis M., Méndez M., Wijnands R., Homan J., Jonker P. G., van Paradijs J., 2000, ApJ, 537, 368
Fox D. B., 2005, ATel, 526, 1
Fox D. B., Kulkarni S. R., 2004, ATel, 354
Fox D. W. et al., 2001, MNRAS, 321, 776
Freire P. C. C., Ransom S. M., Begin S., Stairs I. H., Hessels J. W. T., Frey L. H., Camilo F., 2008, ApJ, 675, 670
Galloway D. K., 2006, in D'Amico F., Braga J., Rothschild R., eds, AIP Conf. Proc., Vol. 840, The Transient Milky Way: A Perspective for MIRAX. Am. Inst. Phys., New York, p. 50
Galloway D. K., Cumming A., 2006, ApJ, 652, 559
Galloway D., Chakrabarty D., Muno M., Savov P., 2001, ApJ, 549, L85
Galloway D., Chakrabary D., Morgan E. H., Remillard R. A., 2002, ApJ, 576, L137
Galloway D. K., Markwardt C. B., Morgan E. H., Chakrabarty D., Strohmayer T. E., 2005, ApJ, 622, L45
Galloway D. K., Psaltis D., Muno M. P., Chakrabarty D., 2006, ApJ, 639, 1033
Galloway D. K., Morgan E. H., Krauss M. I., Kaaret P., Chakrabarty D., 2007, ApJ, 654, L73
Galloway D. K., Muno M. P., Hartman J. M., Savov P., Psaltis D., Chakrabarty D., 2008a, ApJS, in press (astro-ph/0608259)
Galloway D. K., Özel F., Psaltis D., 2008b, MNRAS, 387, 268
Garcia M. R., Callanan P. J., McCarthy J., Eriksen K., Hjellming R. M., 1999, ApJ, 518, 422
Gavriil F. P., Strohmayer T. E., Swank J. H., Markwardt C. B., 2007, ApJ, 669, L29
Ghosh P., Lamb F., 1978, ApJ, 223, L83
Giacconi R., Gorenstein P., Gursky H., Usher P. D., Waters J. R., Sandage A., Osmer P., Peach J. V., 1967, ApJ, 148, L129
Gierliński M., Done C., 2002, MNRAS, 331, L47
Gierliński M., Poutanen J., 2005, MNRAS, 343, 1301
Gierliński M., Done C., Barret D., 2002, MNRAS, 331, 141
Giles A., Hill K., Strohmayer T., Cummings N., 2002, ApJ, 568, 279
Giles A. B., Greenhill J. G., Hill K. M., Sanders E., 2005, MNRAS, 361, 1180
Gottlieb E. W., Wright E. L., Liller W., 1975, ApJ, 195, L33
Gottwald M., Steinle H., Pietsch W., Graswer U., 1991, A&AS, 89, 367
Greenhill J. G., Giles A. B., Hill K. M., 2002, IAU Circ., 7889, 1
Grindlay J. G., Liller W., 1978, ApJ, 220, L127
Hartman J., Chakrabarty D., Galloway D., Muno M., Savov P., Méndez M., van Straaten S., di Salvo T., 2003, BAAS, 35, 865
Hartman J. et al., 2008, ApJ, 675, 1468
Hasinger G., van der Klis M., 1989, A&A, 225, 79
Haskell B., Jones D. I., Andersson N., 2006, MNRAS, 373, 1423
Haskell B., Samuelsson L., Glampedakis K., Andersson N., 2008, MNRAS, 385, 531
Heasley J. N., Janes K. A., Zinn R., Demarque P., da Costa G. S., Christian C. A., 2000, AJ, 120, 879
Hertz P., Vaughan B., Wood K. S., Norris J. P., Mitsuda K., Michelson P. F., Dotani T., 1992, ApJ, 396, 201
Hessels J. W. T., Ransom S. M., Stairs I. H., Freire P. C. C., Kaspi V. M., Camilo F., 2006, Sci, 311, 1901
Hessels J. W. T., Ransom S. M., Stairs I. H., Kaspi V. M., Freire P. C. C., 2007, ApJ, 670, 363
Heyl J., 2002, ApJ, 574, L57
Heyl J. S., 2004, ApJ, 600, 939
Homan J., Méndez M., Wijnands R., van der Klis M., van Paradijs J., 1999, ApJ, 513, L119
Homan J., van der Klis M., Jonker P., Wijnands R., Kuulkers E., Méndez M., Lewin W., 2002, ApJ, 568, 878
Homer L., Deutsch E. W., Anderson S. F., Margon B., 2001, AJ, 122, 2627
Horne K., Wade R. A., Szkody P., 1986, MNRAS, 219, 791
Hynes R. I., Horne K., O'Brien K., Haswell C. A., Robinson E. L., King A. R., Charles P. A., Pearson K. J., 2006, ApJ, 648, 1156
Iaria R., di Salvo T., Robba N. R., Burderi L., Stella L., Frontera F., van der Klis M., 2004, ApJ, 600, 358
Iaria R., di Salvo T., Lavagetto G., Robba N. R., Burderi L., 2006, ApJ, 647, 1341
Iaria R., di Salvo T., Lavagetto G., d'Aí A., Robba N. R., 2007, A&A, 464, 291
in't Zand J. J. M., Kuulkers E., Verbunt F., Heise J., Cornelisse R., 2003, A&A, 411, L487
in't Zand J. J. M., Jonker P. G., Markwardt C. B., 2007, A&A, 465, 953
Jaranowski P., Królak A., Schutz B. F., 1998, Phys. Rev. D, 58, 063001
Johnston H. M., Fender R., Wu K., 1999, MNRAS, 308, 415
Johnston H. M., Wu K., Fender R., Cullen J. G., 2001, MNRAS, 328, 1193
Jongert H. C., van der Klis M., 1996, A&A, 310, 474
Jonker P. G., Wijnands R., van der Klis M., Psaltis D., Kuulkers E., Lamb F. K., 1998, ApJ, 499, L191
Jonker P. et al., 2000, ApJ, 537, 374
Jonker P., Méndez M., van der Klis M., 2002a, MNRAS, 336, L1
Jonker P., van der Klis M., Homan J., Méndez M., Lewin W., Wijnands R., Zhang W., 2002b, MNRAS, 333, 665

Jonker P. G., Nelemans G., Bassa C. G., 2007, MNRAS, 374, 999
Juett A. M., Psaltis D., Chakrabarty D., 2001, ApJ, 560, L59
Kaaret P., in't Zand J., Heise J., Tomsick J., 2002, ApJ, 575, 1018
Kaaret P., Morgan E. H., Vanderspek R., Tomsick J., 2006, ApJ, 638, 963
Kaaret P. et al., 2007, ApJ, 657, L97
Kawai N., Suzuki M., 2005, ATel, 534
King A. R., Kolb U., Burderi L., 1996, ApJ, 464, L127
Kinney J. B., Mendell G., 2003, Phys. Rev. D, 67, 024032
Klein-Wolt M., Wijnands R., Swank J. H., Markwardt C. B., 2007a, ATel, 1065
Klein-Wolt M., Maitra D., Wijnands R., Swank J. H., Markwardt C. B., Bailyn C., 2007b, ATel, 1070
Klein-Wolt M., Wijnands R., Swank J. H., Markwardt C. B., 2007c, ATel, 1075
Kolb U., King A. R., Baraffe I., 2001, MNRAS, 321, 544
Krauss M. I. et al., 2005, ApJ, 627, 910
Krauss M. I., Juett A. M., Chakrabarty D., Jonker P. G., Markwardt C. B., 2006, ATel, 777
Krimm H. A. et al., 2007, ApJ, 668, L147
Krishnan B., Sintes A. M., Papa M. A., Schutz B. F., Frasca S., Palomba C., 2004, Phys. Rev. D, 70, 082001
Kuulkers E., van der Klis M., van Paradijs J., 1995, ApJ, 450, 748
Kuulkers E., van der Klis O. T., van Paradijs J., Lewin W. H. G., 1997, MNRAS, 287, 495
Kuulkers E., Homan J., van der Klis M., Lewin W. H. G., Méndez M., 2002, A&A, 382, 947
Kuulkers E., den Hartog P. R., in't Zand J. J. M., Verbunt F. W. M., Harris W. E., Cocchi M., 2003, A&A, 399, 663
Kuznetsov S. I., 2002, Astron. Lett., 28, 73
Lattimer J. M., Prakash M., 2007, Phys. Rep., 442, 109
Levin Y., 1999, ApJ, 517, 328
Levine A. M., Bradt H., Cui W., Jernigan J. G., Morgan E. H., Remillard R., Shirey R. E., Smith D. A., 1996, ApJ, 469, L33
Linares M., van der Klis M., Altamirano D., Markwardt C. B., 2005, ApJ, 634, 1250
Lochner J. C., Roussel-Dupre D., 1994, ApJ, 435, 840
Makino J., Taiji M., 1995, Proc. 1995 ACM/IEEE Conference on Supercomputing, 63
Markwardt C., Strohmayer T., Swank J., 1999a, ApJ, 512, L125
Markwardt C. B., Marshall F. E., Swank J. H., Cui W., 1999b, IAU Circ., 7300, 1
Markwardt C., Swank J., Strohmayer T., in't Zand M., Marshall F., 2002, ApJ, 575, L21
Markwardt C., Juda M., Swank J., 2003, IAU Circ., 8095, 2
Markwardt C. B., Klein-Wolt M., Swank J. H., Wijnands R., 2007, ATel, 1068
Martí J., Mirabel I. F., Rodríguez L. F., Chaty S., 1998, A&A, 332, L45
Meers B. J., 1988, Phys. Rev. D, 38, 2317
Meinshausen N., Bickel P., Rice J., 2007, J. Appl. Stat., in press (arXiv:0712.1663)
Melatos A., Payne D. J. B., 2005, ApJ, 623, 1044
Méndez M., Belloni T., 2007, MNRAS, 381, 790
Méndez M., van der Klis M., 1999, ApJ, 517, L51
Méndez M., van der Klis M., 2000, MNRAS, 318, 938
Méndez M. et al., 1998a, ApJ, 494, L65
Méndez M., van der Klis M., Wijnands R., Ford E., van Paradijs J., Vaughan B., 1998b, ApJ, 505, L23
Méndez M., van der Klis M., van Paradijs J., 1998c, ApJ, 506, L117
Messenger C., Woan G., 2007, Class. Quantum Gravity, 24, 469
Middleditch J., Priedhorsky W., 1986, ApJ, 306, 230
Migliari S., Fender R. P., 2006, MNRAS, 366, 79
Migliari S., van der Klis M., Fender R., 2003, MNRAS, 345, L35
Migliari S., Fender R. P., Rupen M., Wachter S., Jonker P. G., Homan J., van der Klis M., 2004, MNRAS, 351, 186
Migliari S., Tomsick J. A., Maccarone T. J., Gallo E., Fender R. P., Nelemans G., Russell D. M., 2006, 643, L41
Mignani R. P., Chaty S., Mirabel I. F., Mereghetti S., 2002, A&A, 389, L11
Moore C. B., Rutledge R. E., Fox D. W., Guerriero R. A., Lewin W. H. G., Fender R., van Paradijs J., 2000, ApJ, 532, 1181
Motch C., Pedersen H., Beuermann K., Pakull M. W., Courvoisier T. J.-L., 1987, ApJ, 313, 792
Muno M. P., Fox D. W., Morgan E. H., Bildsten L., 2000, ApJ, 542, 1016
Muno M. P., Özel F., Chakrabarty D., 2002a, ApJ, 581, 550
Muno M. P., Remillard R. A., Chakrabarty D., 2002b, ApJ, 568, L35
Muno M. P., Baganoff F. K., Arabadijs J. S., 2003, ApJ, 598, 474
Murdin P., Jauncey D. L. L. I., Nicolson G. D., Kaluzienski L. J., Holt S. S., Haynes R. F., 1980, A&A, 87, 292
Natalucci L., Cornelisse R., Bazzano A., Cocchi M., Ubertini P., Heise J., in't Zand J., Kuulkers E., 1999, ApJ, 523, L45
Nayyar M., Owen B. J., 2006, Phys. Rev. D, 73, 084001
Nelemans G., Jonker P. G., Marsh T. R., van der Klis M., 2004, MNRAS, 348, L7
Nelemans G., Jonker P. G., Steeghs D., 2006, MNRAS, 370, 255
O'Neill P. M., Kuulkers E., Sood R. K., van der Klis M., 2002, MNRAS, 336, 217
Oosterbroek T., van der Klis M., Kuulkers E., van Paradijs J., Lewin W. H. G., 1995, A&A, 297, 141
Ooesterbroek T., Parmar A. N., Sidoli L., in't Zand J. J. M., Heise J., 2001, A&A, 376, 532
Orosz J. A., Kuulkers E., 1999, MNRAS, 305, 132
Owen B. J., 1996, Phys. Rev. D, 53, 6749
Owen B. J., Lindblom L., Cutler C., Schutz B. F., Vecchio A., Andersson N., 1998, Phys. Rev. D, 58, 084020
Paizis A., Nowak M. A., Wilms J., Courvoisier T. J.-L., Ebisawa K., Rodriguez J., Ubertini P., 2005, A&A, 444, 357
Papaloizou J., Pringle J. E., 1978, MNRAS, 184, 501
Papitto A., di Salvo T., Burderi L., Menna M. T., Lavagetto G., Riggio A., 2007, MNRAS, 375, 971
Papitto A., Menna M. T., Burderi L., di Salvo T., Riggio A., 2008, MNRAS, 383, 411
Parmar A. N., White N. E., Giommi P., Gottwald M., 1986, ApJ, 308, 199
Patruno A., Altamirano D., Hessels J. W. T., Casella P., Wijnands R., van der Klis M., 2008, ApJ, submitted (arXiv:0801.1031)
Payne D. J. B., Melatos A., 2006, ApJ, 641, 471
Penninx W., 1989, in Hunt J., Battrick B., eds, The 23rd ESLAB Symposium on Two Topics in X-ray Astronomy, Vol. 1. ESA Publications Division, Noordwijk, p. 185
Penninx W., Zwarthoed G. A. A., van Paradijs J., van der Klis M., Lewin W. H. G., Dotani T., 1993, A&A, 267, 92
Piro A. L., Bildsten L., 2005, ApJ, 629, 438
Podsiadlowski P., Rappaport S., Pfahl E. D., 2002, ApJ, 565, 1107
Pooley D. et al., 2002, ApJ, 573, 184
Prix R., 2007a, Class. Quantum Gravity, 24, S481
Prix R., 2007b, Phys. Rev. D, 75, 023004
Prix R., Itoh Y., 2005, Class. Quantum Gravity, 22, S1003
Ransom S. M., Cordes J. M., Eikenberry S. S., 2003, ApJ, 589, 911
Ransom S. M., Hessels J. W. T., Stairs I. H., Friere P. C. C., Camilo F., Kaspi V. M., Kaplan D. L., 2005, Sci, 307, 892
Rappaport S., Joss P. C., 1984, ApJ, 283, 232
Retter A., Chou Y., Bedding T. R., Naylor T., 2002, MNRAS, 330, L37
Revnivtsev M. G., Sunyaev R., 2002, Astron. Lett., 28, 19
Riggio A., di Salvo T., Burderi L., Iaria R., Papitto A., Menna M. T., Lavagetto G., 2007, MNRAS, 382, 1751
Riggio A., di Salvo T., Burderi L., Menna M. T., Papitto A., Iaria R., Lavagetto G., 2008, ApJ, 678, 1273
Rupen M. P., Dhawan V., Mioduszewski A. J., 2003, ATel, 210
Rupen M. P., Dhawan V., Mioduszewski A. J., 2004a, ATel, 364
Rupen M. P., Mioduszewski A. J., Dhawan V., 2004b, ATel, 286
Sathyaprakash B. S., Dhurandhar S. V., 1991, Phys. Rev. D., 44, 3819
Sathyaprakash B. S., Dhurandhar S. V., 1994, Phys. Rev. D., 49, 1707
Shabaz T., Zurita C., Casares J., Dubus G., Charles P. A., Wagner R. M., Ryan E., 2003, ApJ, 585, 443
Smale A. P., 1998, ApJ, 498, L141
Smale A. P., Wachter S., 1999, ApJ, 527, 341

Smale A. P., Mukai K., Rees Williams O., Jones M. H., Corbet R. H. D., 1992, ApJ, 400, 330
Smale A. P., Zhang W., White N. E., 1997, ApJ, 483, L119
Smith D., Morgan E., Bradt H., 1997, ApJ, 479, L137
Sosin C., King I. R., 1995, AJ, 109, 639
Southwell K. A., Casares J., Charles P. A., 1996, in Evans A., Wood J. H., eds, IAU Colloq. 158, Cataclysmic Variables and Related Objects. Kluwer, Dordrecht, p. 365
Steeghs D., Casares J., 2002, ApJ, 568, 273
Strohmayer T., Zhang W., Swank J., Smale A., Titarchuk L., Day C., Lee U., 1996, ApJ, 469, L9
Strohmayer T. E., Markwardt C. B., 2002, ApJ, 577, 345
Strohmayer T. E., Bildsten L., 2006, in Lewin, van der Klis, eds, Cambridge Astrophysics Series No. 39, Compact Stellar X-ray Sources. Cambridge Univ. Press, Cambridge, p. 113
Strohmayer T., Jahoda K., Giles A., Lee U., 1997, ApJ, 486, 355
Strohmayer T., Zhang W., Swank J. H., White N. E., Lapidus I., 1998a, ApJ, 498, L135
Strohmayer T. E., Zhang W., Swank J. H., Lapidus I., 1998b, ApJ, 503, L147
Strohmayer T. E., Markwardt C., Swank J., in't Zand J., 2003, ApJ, 596, L67
Strohmayer T. E., Markwardt C. B., Kuulkers E., 2008, ApJ, 672, L37
Taylor J. H., Weisberg J. M., 1989, ApJ, 345, 434
Tomsick J., Halpern J., Kemp J., Kaaret P., 1999, ApJ, 521, 341
Tomsick J. A., Heindl W. A., Chakrabarty D., Halpern J. P., Kaaret P., 2001, ApJ, 559, L123
Tomsick J. A., Heindl W. A., Chakrabarty D., Kaaret P., 2002, ApJ, 581, 570
Tomsick J. A., Gelino D. M., Halpern J. P., Kaaret P., 2004, ApJ, 610, 933
Torres M. A. P., McClinktock J. E., Garcia M. R., Murray S. S., 2004, ATel, 238
Torres M. A. P. et al., 2006, ATel, 784
Torres M. A. P. et al., 2008, ApJ, 672, 1079
Tout C. A., Pols O. R., Eggleton P. P., Han Z., 1996, MNRAS, 281, 257
Ushomirsky G., Cutler C., Bildsten L., 2000, MNRAS, 319, 902
Vacca W. D., Lewin W. H. G., van Paradijs J., 1986, MNRAS, 220, 339
van der Klis M., 2006, in Lewin, van der Klis, eds, Cambridge Astrophysics Series No. 39, Compact Stellar X-ray Sources. Cambridge Univ. Press, Cambridge, p. 39
van der Klis M., Swank J. H., Zhang W., Jahoda K., Morgan E. H., Lewin W. H. G., Vaughan B., van Paradijs J., 1996, ApJ, 469, L1
van der Klis M., Wijnands R. A. D., Horne K., Chen W., 1997, ApJ, 481, L97
Vanderlinde K. W., Levine A. M., Rappaport S. A., 2003, PASP, 115, 739.
van Straaten S., Ford E. C., van der Klis M., Méndez M., Kaaret P., 2000, ApJ, 540, 1049
van Straaten S., van der Klis M., di Salvo T., Belloni T., 2002, ApJ, 568, 912
van Straaten S., van der Klis M., Wijnands R., 2005, ApJ, 619, 455
Vaughan B. A. et al., 1994, ApJ, 435, 362
Verbunt F., van Kerkwijk M. H., in't Zand J. J. M., Heise J., 2000, A&A, 359, 960
Villarreal A., Strohmayer T. E., 2004, ApJ, 614, L121
Wachter S., 1997, ApJ, 490, 401
Wachter S., Margon B., 1996, AJ, 112, 2684
Wachter S., Smale A. P., 1998, ApJ, 496, L21
Wachter S., Smale A. P., Bailyn C., 2000, ApJ, 534, 367
Wachter S., Hoard D. W., Bailyn C. D., Corbel S., Kaaret P., 2002, ApJ, 568, 901
Wachter S., Wellhouse J. W., Patel S. K., Smale A. P., Alves J. F., Bouchet P., 2005, ApJ, 621, 393
Wade R. A., Quintana H., Horne K., Marsh T. R., 1985, PASP, 97, 1092
Wagoner R. V., 1984, ApJ, 278, 345
Wagoner R. V., 2002, ApJ, 578, L63
Watts A. L., Strohmayer T. E., 2006, MNRAS, 373, 769
Welsh W. F., Robinson E. L., Young P., 2000, AJ, 120, 943
Wen L., Levine A. M., Corbet R. H. D., Bradt H. V., 2006, ApJS, 163, 372
White N., Zhang W., 1997, ApJ, 490, L87
White N. E., Swank J. H., 1982, ApJ, 253, L61
Wijnands R., van der Klis M., 1997, ApJ, 482, L65
Wijnands R., van der Klis M., 1998, Nat, 394, 344
Wijnands R., van der Klis M., van Paradijs J., Lewin W. H. G., Lamb F. K., Vaughan B., Kuulkers E., 1997a, ApJ, 479, L141
Wijnands R. et al., 1997b, ApJ, 490, L157
Wijnands R. et al., 1998a, ApJ, 493, L87
Wijnands R., Méndez M., van der Klis M., Psaltis D., Kuulkers E., Lamb F. K., 1998b, ApJ, 504, L35
Wijnands R., Strohmayer T., Franco L., 2001a, ApJ, 549, L71
Wijnands R., Groot P. J., Miller J. J., Markwardt C., Lewin W. H. G., van der Klis M., 2001b, ATel, 72
Wijnands R., van der Klis M., Homan J., Chakrabarty D., Markwardt C., Morgan E., 2003, Nat, 424, 44
Wolff M. T., Hertz P., Wood K. S., Ray P. S., Bandyopadhyay R. M., 2002, ApJ, 575, 384
Wood K. S. et al., 1991, ApJ, 379, 295
Yin H. X., Zhang C. M., Zhao Y. H., Lei Y. J., Qu J. L., Song L. M., Zhang F., 2007, A&A, 471, 381
Zdziarski A. A., Wen L., Gierliński M., 2007, MNRAS, 377, 1006
Zhang W., Smale P., Strohmayer T., Swank J., 1998a, ApJ, 500, L171
Zhang W., Strohmayer T., Swank J., 1998b, ApJ, 500, L167
Zurita C. et al., 2000, MNRAS, 316, 137

This paper has been typeset from a TEX/LATEX file prepared by the author.